[American Journal of Science, Vol. 311, April, 2011, P. 261–314, DOI 10.2475/04.2011.01]

American Journal of Science

APRIL 2011

SYN-EXTENSIONAL PLUTONISM AND PEAK METAMORPHISM IN THE ALBION–RAFT RIVER–GROUSE CREEK METAMORPHIC CORE COMPLEX

ARIEL STRICKLAND*,†, ELIZABETH L. MILLER*, JOSEPH L. WOODEN**, REINHARD KOZDON***, and JOHN W. VALLEY***

ABSTRACT. The Cassia plutonic complex (CPC) is a group of variably deformed, Oligocene granitic plutons exposed in the lower plate of the Albion–Raft River–Grouse Creek (ARG) metamorphic core complex of Idaho and Utah. The plutons range from granodiorite to garnet-bearing, leucogranite, and during intrusion, sillimanite-grade peak metamorphism and ductile attenuation occurred in the country rocks and normal-sense, amphibolite-grade deformation took place along the Middle Mountain shear zone. U-Pb zircon geochronology from three variably deformed plutons exposed in the lower plate of the ARG metamorphic core complex revealed that each zircon is comprised of inherited cores (dominantly late Archean) and Oligocene igneous overgrowths. Within each pluton, a spread of concordant ages from the Oligocene zircon overgrowths is interpreted as zircon recycling within a long-lived magmatic system. The plutons of the CPC have very low negative whole rock εNd values of −26 to −35, and initial Sr values of 0.714 to 0.718, consistent with an ancient, crustal source. Oxygen isotope ratios of the Oligocene zircon overgrowths from the CPC have an average $\delta^{18}O$ value of 5.40 ± 0.63 permil (2SD, n = 65) with a slight trend towards higher $\delta^{18}O$ values through time. The $\delta^{18}O$ values of the inherited cores of the zircons are more variable at 5.93 ± 1.51 permil (2SD, n = 29). Therefore, we interpret the plutons of the CPC as derived, at least in part, from melting Archean crust based on the isotope geochemistry. *In situ* partial melting of the exposed Archean basement that was intruded by the Oligocene plutons of the CPC is excluded as the source for the CPC based on field relationships, age and geochemistry. Correlations between Ti and Hf concentrations in zircons from the CPC suggest that the magmatic system may have become hotter (higher Ti concentration in zircon) and less evolved (lower Hf in zircon concentration) through time. Therefore, the CPC represents prolonged or episodic magmatism system (32-25 Ma), and the intrusions were each accompanied by sillimanite-grade deformation and extension. The Oligocene magmatism and peak metamorphism preserved in the ARG metamorphic core complex are likely related to regional trends in mantle-derived magmatism that led to protracted heating, melting and mobilization of the deeper crust.

Key words: Zircon, U-Pb, pluton, Albion–Raft River–Grouse Creek, metamorphic core complex, Oligocene, zircon inheritance

* Department of Geological and Environmental Sciences, Stanford University, Stanford, California, 94305

** U.S. Geological Survey, Menlo Park, California, 94025

*** Department of Geoscience, University of Wisconsin, 1215 W Dayton Street, Madison, Wisconsin 53706

† Present address: Department of Geoscience, University of Wisconsin, 1215 W Dayton Street, Madison, Wisconsin 53706; stricklandariel@gmail.com

INTRODUCTION

Core complexes are extensional features that expose deep crustal metamorphic and igneous rocks in the lower plate that are juxtaposed with commonly unmetamorphosed supracrustal rocks along normal faults and detachment-style faults (Coney, 1980; Armstrong, 1982). Tertiary metamorphic core complexes of western North America occur in a sinuous, N/S-trending belt that lies approximately 100 km west of the Cretaceous Sevier/Laramide fold and thrust belt (fig. 1) (for example, Coney, 1980; Armstrong, 1982). Previous workers have linked the origin of metamorphic core complexes to partial melting and collapse of tectonically thickened crust following the end of shortening (Armstrong, 1982; Coney and Harms, 1984; Vanderhaeghe and others, 2003; Teyssier and others, 2005). In support of this idea, several studies of Cordilleran metamorphic core complexes in the northern United States and Canada have documented that the rocks exhumed in the lower plates of metamorphic core complexes represent the diapiric rise of partially molten crust that occurred *ca.* 60 to 50 Ma (for example, Teyssier and others, 2005; Gordon, and others, 2008).

The onset of crustal extension that formed Cordilleran metamorphic core complexes varies by more than 30 m.y. from north to south (Armstrong, 1982; Fayon and others, 2004), and was spatially and temporally linked to the migrating locus of voluminous magmatism that swept across western North America during the Tertiary (Coney, 1980; Gans and others, 1989; Armstrong and Ward, 1991; Christiansen and others, 1992; Foster and others, 2001). Metamorphic core complexes in the western United States (fig. 1) preserve a complex, multi-stage exhumation history that began with crustal melting and high grade, extensional deformation *ca.* 40 to 25 Ma, and ended with final exhumation along Basin and Range normal faults in the middle Miocene (Miller and others, 1999; Egger and others, 2003; Howard, 2003; Wagner and Johnson, 2006; Colgan and Metcalf, 2006; Colgan and Henry, 2009).

The deep crustal rocks exposed in Cordilleran metamorphic core complexes often contain a record of multiple periods of metamorphism and deformation that reflect earlier tectonic events. Mesozoic fabrics related to the Sevier/Laramide fold and thrust belt are common in many of the Cordilleran core complexes (for example, Miller and others, 1989; McGrew and others, 2000; Foster and others, 2001; Grice and others, 2005). Several studies have documented the survival of Precambrian tectonic fabrics in the core complexes of Arizona, despite Mesozoic and Cenozoic overprinting (Davis, 1980; Reynolds and DeWitt, 1991; Strickland and others, 2007). Since these rocks found in the lower plates of metamorphic core complexes are often highly deformed and metamorphosed by multiple events, the timing of growth of metamorphic index minerals can be difficult to discern such that a debate has developed regarding the age and tectonic significance of peak metamorphism in many metamorphic core complexes (for example, Miller and Gans, 1989; DeCelles, 2004; Sullivan and Snoke, 2007; Harris and others, 2007; Hoisch and others, 2008; Wells and Hoisch, 2008; Strickland and others, 2011).

The syn-extensional granitic intrusions that are common in most metamorphic core complexes provide some of the best age constraints on the timing of regional extension (Compton and others, 1977; Coney, 1980; Armstrong, 1982; Howard, 2003). Many of these intrusions have been interpreted as crustal melts based on their aluminous nature and radiogenic initial Sr isotope values (Armstrong, 1982). In the Albion–Raft River–Grouse Creek (ARG) metamorphic core complex of northern Utah and southern Idaho (fig. 1), syn-extensional, granitic plutons are exposed in both the upper and the lower plates. In the upper plate of the ARG metamorphic core complex, the 34 to 41 Ma Emigrant Pass plutonic complex ranges from hornblende granite to granodiorite in composition (Egger and others, 2003). These plutons overlap in age with 50 to 38 Ma volcanism in the Challis/Absaroka volcanic province of Idaho and

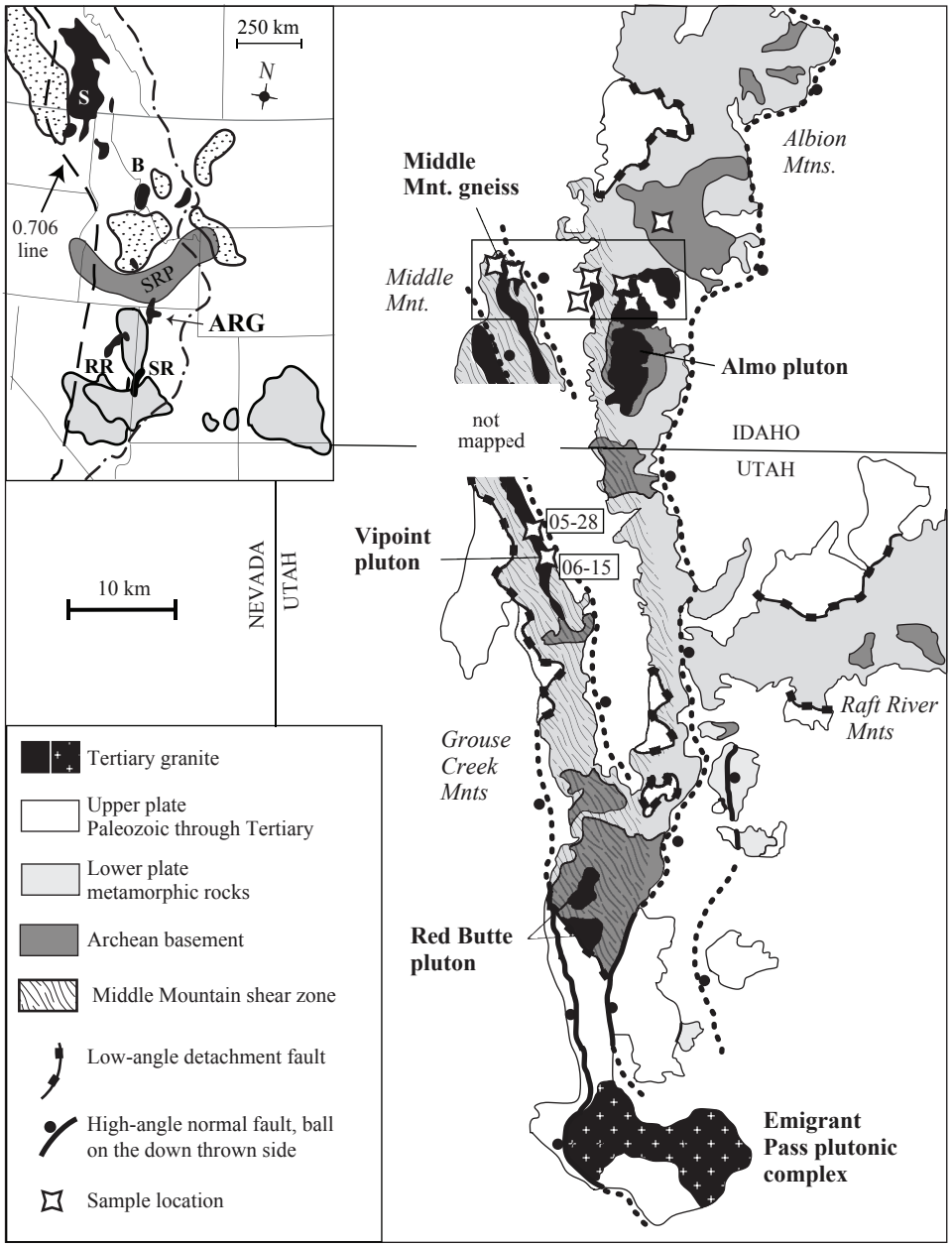

Fig. 1. Simplified geologic map of the Albion–Raft River–Grouse Creek metamorphic core complex after Armstrong (1968), Compton (1972, 1975), Compton and others (1977), Wells and others (2000) and Miller and others (2008). The Albion and Grouse Creek Mountains and Middle Mountain are bound by N/S-trending, Basin and Range-style normal faults. Earlier detachment-style faults place weakly to unmetamorphosed upper-plate rocks against gneisses and metamorphic rocks in the lower plate. Box shows location of figure 2. Inset shows the location of core complexes (black, after Armstrong, 1982) discussed in the text with respect to regional magmatism, the Laramide/Sevier fold and thrust belt (dashed and dotted line) and the $^{87}Sr/^{86}Sr$ = 0.706 line (heavy dashed line). S = Shuswap, B = Bitterroot, ARG = Albion–Raft River–Grouse Creek, RR = Ruby Range, SR = Snake Range. Stippled pattern is for Eocene volcanic fields (Dostal and others, 2003; Breitsprecher and others, 2003), solid gray is for Oligocene volcanic fields (Gans and others, 1989; Best and others, 1993), and dark gray is for Miocene volcanic rocks from the Snake River Plain (SRP).

Montana (Moye and others, 1988; Armstrong and Ward, 1991; fig. 1), as well as the nearby andesites, dacites, and rhyolitic ignimbrites of the 41 to 39 Ma Northeast Nevada Volcanic field (Brooks and others, 1995; Palmer and MacDonald, 2002; fig. 1).

Plutons exposed in the lower plate of the ARG metamorphic core complex, herein referred to as the Cassia plutonic complex (CPC; after Cassia county), were intruded at mid-crustal levels during the Oligocene (Armstrong and Hills, 1967; Compton and others, 1977; Todd, 1980; Egger and others, 2003; Strickland and others, 2011). These are variably deformed by the normal-sense Middle Mountain shear zone exposed along the western margin of the ARG metamorphic core complex (Compton and others, 1977; Todd, 1980; Saltzer and Hodges, 1988) (figs. 1 and 2). Where deformed, the fabrics in the Oligocene plutons are concordant with well-developed, amphibolite facies fabrics in the surrounding metasedimentary country rocks. This study focuses on the Middle Mountain gneiss, the Almo pluton and the Vipont pluton (fig. 1). Samples from these three plutons of varying composition and degree of deformation were chosen to evaluate the origin and evolution of the magmatic system through time, and to determine the relationship of magmatism to regional extension during the Oligocene. We combine geochronologic and geochemical data with structural and petrologic observations to demonstrate that the plutons of the CPC represent melting of Archean crust at depth, and were emplaced during ductile crustal thinning and peak metamorphism in the ARG metamorphic core complex.

GEOLOGIC SETTING

The lower plate of the ARG metamorphic core complex exposes late Archean crystalline basement and unconformably overlying, Neoproterozoic quartzites and schists, which have been metamorphosed and deformed to varying degrees across the core complex (Armstrong and Hills, 1967; Compton and others, 1977; Miller, 1980; Wells, 1997; Egger and others, 2003; Strickland and others, 2011). The contact between the late Archean basement and its overlying metasedimentary sequence is a clear stratigraphic and structural marker horizon that defines a broad, irregular dome bound by oppositely-dipping, normal sense shear zones (Wells and others, 2000). On the eastern side of the ARG metamorphic core complex, east-directed extension occurred along the Raft River shear zone during the Miocene (for detailed description of the Raft River shear zone see Wells and others, 2000 and Wells, 2001). The amphibolite facies, Middle Mountain shear zone is found along the western side of the ARG metamorphic core complex (fig. 1) where it deforms the Oligocene granites (Compton and others, 1977; Saltzer and Hodges, 1988; Egger and others, 2003; Strickland and others, 2011). Fabrics typically dip ~20 to 30° to the west with a gently plunging lineation that trends WNW.

The rocks exposed in the lower plate of the ARG metamorphic core complex include Late Archean augen gneiss with sparse wall rock of pelitic schist and amphibolite which together form the Green Creek Complex (Armstrong and Hills, 1967; Compton and others, 1977). The Green Creek augen gneiss is biotite + muscovite-bearing granite and is easily identified by its conspicuous alkali feldspar augen measuring up to 10 cm in length. Neoproterozoic quartzites and pelitic to psammitic schists unconformably overlie Archean basement and constitute a sequence of metamorphic rocks that is found throughout the lower plate (Compton, 1972, 1975; Compton and others, 1977; Wells and others, 1998; Link and Johnston, 2008; Strickland and others, 2011) (fig. 1). The metasedimentary rocks vary in thickness across the ARG metamorphic core complex, perhaps in part due to original facies changes, but more likely due to their attenuation by ductile deformation, as well as a missing section that has been omitted by faults (now deformed) that place younger rocks on older rocks (Compton, 1972, 1975; Compton, and others, 1977; Miller, 1980, 1983; Wells and others, 1990; Egger and others, 2003).

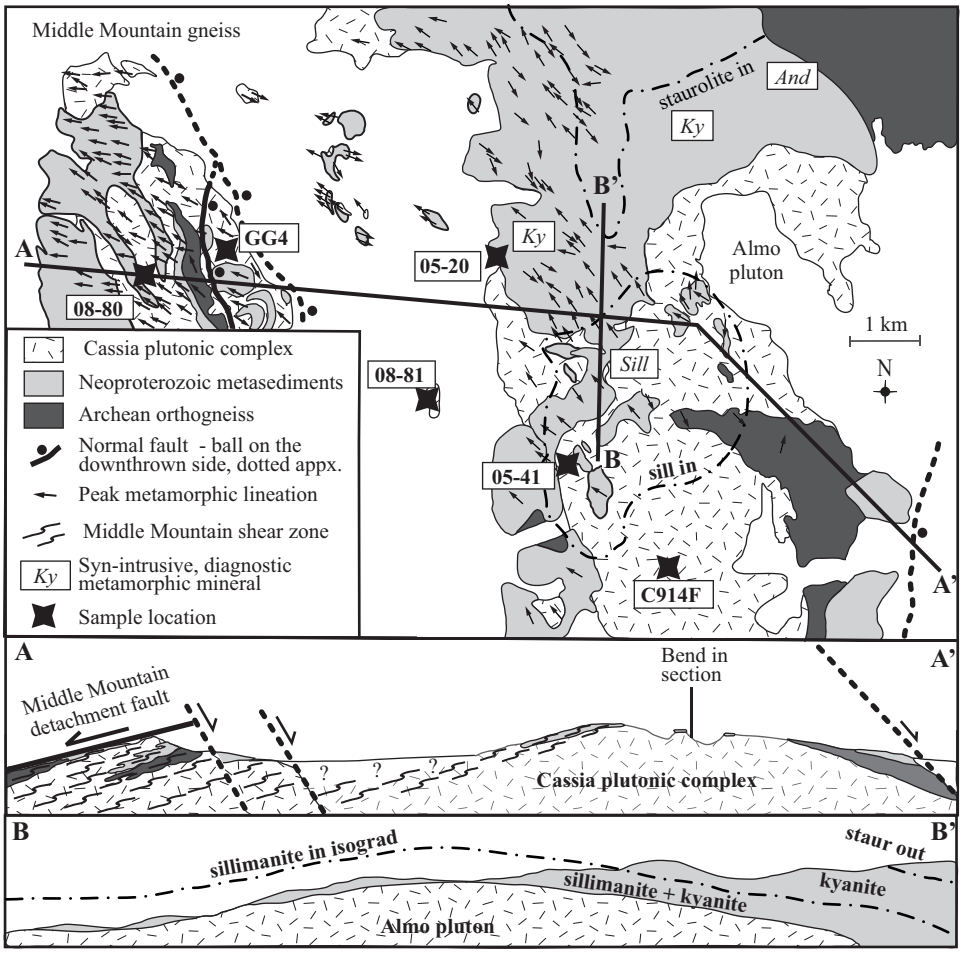

Fig. 2. Simplified geologic map and cross-section of the northern Cassia plutonic complex showing the location of samples discussed in the text. Complied from Armstrong (1968) and Miller and others (2008). Boxes indicate index minerals in Neoproterozoic metasedimentary rocks: Chl + Cltd = Chlorite + Chloritoid, And = andalusite, Sill = sillimanite, Ky = kyanite. Arrows represent mineral elongation lineations developed during peak metamorphic temperatures and show that strain increases from east to west. The cross-section A-A′ emphasizes deformation from the Middle Mountain shear zone (no vertical exaggeration). The sillimanite-in isograd after Armstrong (1968) refers to the presence of sillimanite in the roof rocks and country rocks to the Almo pluton (there is no sillimanite in the Almo pluton). The cross-section B-B′ shows the distribution of metamorphic minerals with respect to the Almo pluton (no vertical exaggeration). Sillimanite is found at structural levels closest to the Almo pluton. Above the sillimanite-in isograd, the assemblage garnet + staurolite + kyanite is found in pelitic rocks. At the highest structural levels, greenschist facies mineral assemblages are found after crossing the staurolite-out isograd.

The Green Creek complex and overlying metasedimentary rocks were intruded by Oligocene granitic plutons of the CPC (fig. 1) (Armstrong and Hills, 1967; Compton, 1972, 1975) Adjacent to the plutons, the country rocks were attenuated and deformed at sillimanite-grade metamorphic conditions, and evidence for older periods of metamorphism and deformation have been largely obliterated (Armstrong, 1968; Compton and others, 1977; Todd, 1980; Miller and Bedford, 1999; Egger and others, 2003; Strickland and others, 2011). Wall rocks and roof pendants to the plutons have gently west/northwest-plunging mineral elongation lineations, and where sillimanite

is present it is aligned with the lineation (Armstrong, 1968; Compton and others, 1977; Miller and Bedford, 1999; Egger and others, 2003; Strickland and others, 2011) (fig. 1). In the Albion and Grouse Creek Mountains (fig. 2), strain in the igneous and metamorphic rocks of the lower plate increases dramatically westward towards the down-to-the-west, normal-sense Middle Mountain shear zone (fig. 2).

The youngest known pluton within the CPC is the 25.3 ± 0.5 Ma, syn-extensional Red Butte pluton exposed in the Grouse Creek Mountains (fig. 1) (Compton and others, 1977; Egger and others, 2003). This pluton was intruded at a depth of 12 to 15 km based on wall rock assemblages of biotite + muscovite + garnet ± staurolite ± sillimanite ± kyanite ± andalusite (Compton and others, 1977; Todd, 1980; Egger and others, 2003). Todd (1980) suggested that only the top of the Red Butte pluton is currently exposed, and that it likely is a much larger body that underlies the Grouse Creek Mountains. The margins of the pluton have a subhorizontal foliation and W-trending lineation, and the pluton has been interpreted as late syn-deformational with respect to amphibolite-facies deformation along the Middle Mountain shear zone (Egger and others, 2003).

METHODS

The Middle Mountain gneiss, Almo pluton and Vipont plutons, and Green Creek gneiss were dated by U-Pb analyses with the SHRIMP-RG at the USGS/Stanford University facility. Geochronologic data are summarized in table 1, and the details are presented in Appendix 2. Analytical methods are described in detail in Appendix 1. Images of zircons in grain mounts were taken in cathodoluminescence (CL) before analysis, and show that the zircons from all samples have rounded cores with oscillatory zoning, indicative of igneous growth (fig. 3). The cores are surrounded by thick overgrowths of igneous zircon that grew in the evolving magmas of the CPC, and when analyzed these overgrowths produce generally concordant data (fig. 3). Therefore, the weighted mean average of the ^{207}Pb-corrected ^{206}Pb/^{238}U zircon ages from the overgrowths are reported below, and in general, the youngest group of concordant analyses is interpreted as the crystallization age for each sample. All uncertainties are given in the text as two sigma errors. A small number of analyses were excluded from the weighted mean average calculations based on their high U concentration (typically 3000 ppm or higher) or discordance due to high common Pb, and/or apparent Pb loss (Appendix 2). Problems with the high U zircons may be related to matrix differences compared to lower U standard zircons, or ion counting systems that have an inherent dead time such as that for high U zircons. Undercounting of the U and UO ions will produce an apparent Pb/U ratio that is too high and therefore an age that is too old (Williams, 1997). The errors of all ages are given at the two sigma level.

The same zircon mounts and individual grains were analyzed for trace element concentrations in separate sessions using the SHRIMP-RG. Trace element data are provided in Appendix 3. Ti and Hf concentrations were measured for the evaluation of petrologic processes (Claiborne and others, 2006, 2010; Wooden and others, 2007; Wooden and Barth, 2010). Quartz is present in all samples, indicating a SiO_2 activity of 1. No rutile is observed in any samples, and TiO_2 activities of 0.7 were assumed for all calculations. TiO_2 activities in silicic rocks are rarely below 0.6 (Hayden and Watson, 2007), will rarely underestimate zircon crystallization temperature by more than ~50 °C. The thermometer of Ferry and Watson (2007) uses an inherent pressure of 10 kb, which is likely an over estimate for the depth of intrusion of the CPC and therefore introduces addition uncertainty. We prefer to interpret the calculated Ti in zircon temperatures as model temperatures [see Fu and others (2008) for a discussion of the accuracy of the Ti in zircon thermometry]. Other trace element concentrations measured in zircon include Li, Na, Mg, Al, P, K, Ca, and Fe, which were used to identify micro inclusions or alteration of the zircon.

TABLE 1

Summary of geochronology and oxygen isotope data for plutons from the Cassia plutonic complex

Sample	Unit	UTM 12T; elevation	Minerals in decreasing abundances	Foliation Strike and dip	Lineation trend and plunge	Weighted mean of ^{207}Pb-corrected ^{206}Pb/^{238}U ages	δ^{18}O VSMOW zircon with 2SD uncertainty
Middle Mountain gneiss							
08-80	Middle Mnt gneiss	0265802, 4666432; 7854'	Plagioclase, quartz, biotite, epidote, apatite, zircon	175; 24W	17 to 285	**32.1 ± 0.6 Ma MSWD=2.1 (n=7)**	.
GG4	Middle Mnt gneiss	0266400, 4668946; 6722'	Plagioclase, quartz, biotite, hornblende, sphene, allanite, zircon	320; 24W	5 to 290	**31.8 ± 0.4 Ma MSWD=0.9 (n=14)**	**Rims: 5.47 ± 0.41 (n=12) Cores: 5.99 ± 0.48 (n=6)**
Almo pluton							
05-41	Almo pluton, western margin	0273102, 4664657, 7134'	Quartz, plagioclase, biotite (chloritized), muscovite, apatite, monazite, zircon	160; 30W	20 to 270	**30.4 ± 0.2 Ma MSWD=2.7 (n=22)**	**Rims: 5.30 ± 0.42 (n=15) Cores: 5.68 ± 0.83 (n=11)**
C914F	Almo pluton, center	0274463, 4663941, 6985'	Quartz, plagioclase, k-feldspar, muscovite, biotite, zircon	.	.	**30.6 ± 0.3 Ma MSWD=1.1 (n=10)**	**Rims: 5.20 ± 0.36 (n=10) Cores: 5.52 ± 1.44 (n=4)**
08-81	Almo pluton, deformed	0270889, 4665039, 6175'	Quartz, plagioclase, biotite (chloritized), muscovite, apatite, zircon	005, 17W	12 to 330	**28.9 ± 0.3 Ma MSWD=1.9 (n=21)**	
05-20	Boudinaged aplite sill in quartzite	0269224, 4668920, 5715'	Fine-grained quartz, feldspar, and white mica	017; 23W		**28.7 ± 0.5 Ma MSWD=2.8 (n=6)**	**Rims: 5.55 ± 0.72 (n=3) Cores: 5.42 ± 0.64 (n=2)**
Vipont pluton							
05-28	Vipoint granodiorite	0266985, 4646131 8212'	Quartz, plagioclase, biotite (chloritized), allanite, epidote, sphene, zircon	004, 32W	31 to 280	**28.9 ± 0.2 Ma MSWD=1.2 (n=17)**	**Rims: 5.30 ± 0.55 (n=12) Cores: 6.26 ± 0.53 (n=8)**
06-15	Vipoint granite	0265622, 4648836, 7998'	Plagioclase, quartz, muscovite, K-feldspar, garnet, monazite, zircon	010; 35 W		**28.2 ± 0.3 Ma MSWD=0.9 (n=9)**	**Rims: 5.74 ± 0.75 (n=13) Cores: 5.68 ± 0.43 (n=4)**
Green Creek Gneiss							
RR06-5 Raft River Mtns	medium-fine grained gneiss	0305084, 4646793; 27516'	Plagioclase, k-feldspar, quartz, biotite, epidote, zoisite, apatite, zircon	105; 35W		**2568 ± 8 Ma MSWD=1.3 (n=7)**	**5.71 ± 0.33 (n=3)**
AB06-9 Albion Mtns	coarse-grained augen gneiss	280540, 4675431; 4567'	Plagioclase, k-feldspar, quartz, biotite, muscovite, rutile, apatite, zircon	160, 30W	25 to 310	**2565 ± 16 Ma MSWD=5.9 (upper intercept)**	**5.77 ± 0.72 (n=3)**

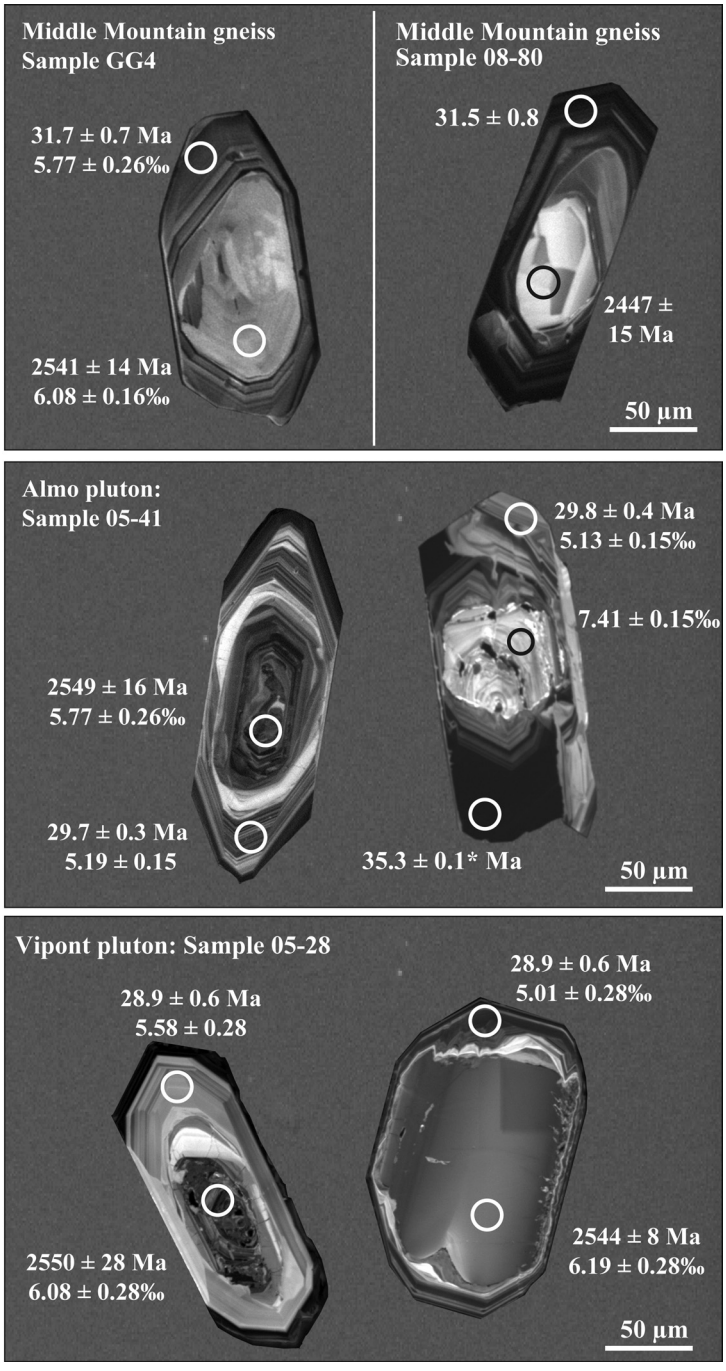

Fig. 3. Representative zircons from the Oligocene plutons in of the Cassia plutonic complex shown in cathodoluminescence. Tertiary overgrowths are given as ^{207}Pb-corrected ^{206}Pb/^{238}U ages, and Archean core ages are reported as ^{204}Pb-corrected ^{206}Pb/^{207}Pb ages (2σ errors). The asterisk on the 35 Ma age of the CL-dark zone on the zircon from the Almo pluton indicates that this analysis was high in U concentration (see discussion in text). Oxygen isotope ratios are given as δ^{18}O (VSMOW normalized) values with two standard deviation errors. δ^{18}O values of inherited zircon cores are higher than the zircon igneous overgrowths associated with Oligocene magmatism.

The zircon mounts were then top mounted with the KIM-5 oxygen isotope standard (Valley, 2003) inserted into the center of each mount and re-polished prior to oxygen isotope analyses using the Cameca ims-1280 at the WiscSIMS laboratory at the University of Wisconsin–Madison. Extra care was taken to achieve a smooth, flat, lower relief polish. Oxygen isotope ratios are given in Appendix 3. Sample preparation and analysis followed the procedures outlined by Kita and others (2009) and Valley and Kita (2009). All uncertainties are given as two standard deviations (2SD). Four consecutive measurements of KIM-5 zircon standard were done before and after each set of 10 to 20 sample analyses. The average precision (reproducibility) of the bracketing standards for this study ranged from ±0.07 to ±0.49 and averaged ±0.27 permil (2SD), and the results are summarized in table 1. The oxygen isotope ratios reported below were calculated using standard δ notation relative to the Vienna standard of mean ocean water, VSMOW. After oxygen isotope analysis, ion microprobe pits were imaged by secondary electron microscopy and pits that were located on obvious cracks or inclusions were excluded from the data set.

Representative rock samples from the Oligocene plutons and the Archean Green Creek gneiss were reduced to powders and analyzed for whole rock geochemistry at the Geoanalytical Laboratory at Washington State University (table 2).

U-Pb ages and oxygen isotope ratios of the Middle Mountain gneiss, the Almo pluton and the Vipont pluton

The Middle Mountain Gneiss

The Middle Mountain gneiss (fig. 2) is a deformed, biotite ± hornblende-bearing granodiorite exposed as sheet-like bodies interlayered and infolded with sillimanite-grade metasedimentary cover rocks and the Archean Green Creek gneiss (fig. 4A). The Middle Mountain gneiss is penetratively deformed and contains a well-developed, gently west-dipping foliation and W/NW-plunging mineral elongation lineations (fig. 4A). Foliation in the Middle Mountain gneiss is defined by biotite and recrystallized quartz. Plagioclase grains show subgrain development, embayed textures, and well-developed pressure shadows with asymmetric tails of quartz and biotite (fig. 4B). Quartz grains in the Middle Mountain gneiss appear strain free, but have a weak shape-preferred orientation that also helps to define the foliation. These textures are consistent with deformation at amphibolite-facies conditions (Hirth and Tullis, 1992; Passchier and Trouw, 1996). Leucocratic pegmatites within the gneiss and the country rocks are commonly folded and boudinaged (fig. 4A). Rare, less-deformed and crosscutting pegmatites can also be found. In pelitic horizons in the adjacent quartzite, sillimanite and biotite define the foliation and W/NW-trending lineation (figs. 5A and 5B). Aligned sillimanite occurs as both fibrous and prismatic forms indicating that the foliation developed during peak metamorphism. The high-grade fabrics define the Middle Mountain shear zone and are not strongly asymmetric in thin section (fig. 5B), but where found, shear sense indicators indicate top-to-the-west, extensional-sense deformation (fig. 5A).

Two samples of the deformed Middle Mountain gneiss were analyzed for U-Pb geochronology (fig. 2 and table 1). Sample 08-80 is a medium grained, foliated and lineated, biotite RR + epidote + sphene-bearing granite. The sample was obtained from a 10 to 15 m thick sheet-like body that intruded Neoproterozoic quartzite (fig. 4A). The zircons from sample 08-80 have inherited cores, with igneous overgrowths of high U zircon ranging from 275 to 8755 ppm U (fig. 3; Appendix 2). A U concentration versus age plot (inset in fig. 6A) was used to evaluate the effect of high uranium on the age determined, and analyses with U concentrations greater than 5200 ppm are considered unreliable and excluded (fig. 6A). A weighted mean $P^{206}PPb/P^{238}PU$ age of six concordant analyses gives an age of 32.1 ± 0.6 Ma with an MSWD of 2.1 (fig. 6A).

TABLE 2

Whole rock geochemical data for samples from the Cassia batholith and the Green Creek gneiss

Cassia plutonic complex	**06-15**	**08-52**	**05-28**	**GG-4**	**08-62**	**08-80**	**06-13**	**06-2**
pluton	Vipont -L	Vipont -L	Vipont -G	Middle Mtn	Middle Mtn	Middle Mtn	Almo	Almo
Age (ma)	**28.2 ± 0.3**		**28.9 ± 0.2**	**31.8 ± 0.4**		**32.1 ± 0.6**		
UTM 12T; elevation	0265622, 4648836; 7998'	0268568, 4640192; 6408'	0266985, 4646131; 8212'	0266400, 4668946; 6722'	0266458, 4669270; 6597'	0265802, 4666432; 7854'	0275968,4662800, 4661319 278200; ; 6277	6240'
Normalized Major Elements (Weight %):								
SiO_2	75.5	76.2	68.3	70.3	71.8	74.5	74.8	76.6
TiO_2	0.0	0.1	0.4	0.4	0.4	0.1	0.0	0.0
Al_2O_3	14.2	13.5	16.9	15.8	15.0	14.4	14.8	14.0
FeO*	0.5	1.3	3.3	2.8	2.8	1.3	0.5	0.5
MnO	0.1	0.0	0.1	0.0	0.0	0.0	0.1	0.1
MgO	0.1	0.2	1.0	0.8	0.8	0.3	0.0	0.1
CaO	1.0	1.1	3.9	3.1	3.0	1.6	0.5	0.7
Na_2O	4.2	4.0	4.4	4.1	4.0	4.3	4.4	3.3
K_2O	4.3	3.5	1.4	2.5	2.1	3.4	4.8	4.7
P_2O_5	0.0	0.1	0.3	0.2	0.1	0.1	0.1	0.0
Unnormalized Trace Elements (ppm):								
Ni	0.0	2.3	0.0	5.0	3.8	1.1	0.0	0.0
Cr	4.0	6.4	3.4	9.5	5.3	3.5	1.9	0.8
Sc	1.5	5.1	3.9	7.2	6.0	3.2	1.0	7.1
V	0.6	6.6	24.5	43.4	31.8	8.7	2.0	3.6
Ba	424.7	487.9	663.5	1892.1	1396.3	1852.7	8.8	30.1
Rb	126.9	191.5	137.6	85.2	91.0	174.8	339.9	150.8
Sr	125.8	122.0	509.1	499.8	403.3	304.9	4.4	27.7
Zr	36.1	107.3	257.7	216.7	347.4	161.8	24.2	31.1
Y	16.5	27.4	12.5	16.3	17.1	17.5	7.5	46.2
Nb	10.5	25.5	17.1	21.5	14.2	18.3	65.5	20.4
Ga	15.8	25.8	21.2	26.1	24.1	25.5	25.6	22.7
Cu	0.0	0.8	1.6	1.6	5.3	0.0	0.9	6.1
Zn	12.2	60.5	83.1	86.7	78.5	56.9	30.2	8.4
Pb	45.9	43.2	10.1	21.2	22.4	41.6	28.9	41.9
La	10.6	35.4	79.6	76.9	122.4	41.3	2.5	4.6
Ce	20.3	63.4	144.6	133.4	216.6	79.9	8.6	13.0
Th	5.0	22.2	17.9	17.0	27.5	15.0	4.0	12.0
Nd	8.2	22.3	45.5	42.7	62.8	27.8	6.9	7.3
U	1.4	5.2	1.3	1.8	2.1	1.1	3.4	3.6
Rb/Sr	1.0	1.6	0.3	0.2	0.2	0.6	77.3	5.4
Isotopic data								
$^{87}Sr/^{86}Sr$	**0.72**		**0.71**				**0.83**	
Sr_i (30 Ma)	**0.72**		**0.71**				**0.72**	
εNd (30 Ma)	**-36.46**	**-25.50**	**-35.10**	**-33.20**	**-34.20**	**-32.80**	**-34.23**	

TABLE 2
(continued)

Green Creek gneiss	**RR06-5**	**RR06-9**	**AB06-1**	**AB06-9**	**RR06-4**	**05-27**	**RR06-19**	**RR06-10**
Location	Raft River	Raft River	Albion	Albion	Raft River	Grouse Ck.	Raft River	Raft River
Age (Ma)	**2568 ± 8**			**2565 ± 16**				
UTM 12T; elevation	0305084, 4646793; 7516'	0282164, 4632992; 6204'	027790, 4663500; 6520'	280540, 4675431; 4567'	0305084, 4646793; 7516'	0268219, 4639907; 6371'	02936996, 4639583; 9206'	0282763, 4634876; 6359'
Normalized Major Elements (Weight %):								
SiO_2	74.4	74.7	72.1	76.5	75.8	73.7	74.5	73.8
TiO_2	0.2	0.2	0.3	0.1	0.1	0.2	0.2	0.2
Al_2O_3	13.8	14.0	15.0	13.2	13.6	14.4	14.1	14.8
FeO*	1.5	1.0	2.0	0.9	1.2	1.5	2.0	1.2
MnO	0.0	0.0	0.0	0.0	0.0	0.0	0.0	0.0
MgO	0.3	0.3	0.5	0.3	0.1	0.3	0.5	0.3
CaO	0.8	0.5	1.6	0.7	0.6	1.0	0.3	0.8
Na_2O	3.2	3.0	3.5	2.9	3.4	3.6	3.5	3.3
K_2O	5.6	6.4	4.8	5.4	5.1	5.2	4.8	5.5
P_2O_5	0.1	0.0	0.2	0.1	0.1	0.1	0.1	0.1
Unnormalized Trace Elements (ppm):								
Ni	0.0	0.0	0.0	0.0	0.0	0.0	0.0	0.0
Cr	6.2	3.9	8.3	4.0	1.8	4.6	4.4	4.9
Sc	4.0	2.3	3.2	2.4	2.9	4.5	5.0	2.6
V	9.7	10.3	18.4	5.7	4.6	8.6	10.4	11.5
Ba	689.4	990.6	1357.2	611.8	470.9	937.1	575.9	1123.9
Rb	273.6	226.1	195.1	187.3	266.2	176.8	256.0	180.8
Sr	72.5	85.4	163.5	77.0	57.6	100.0	66.6	133.9
Zr	157.8	134.9	226.8	77.3	108.5	162.6	199.9	183.1
Y	38.4	8.7	11.1	18.0	68.8	29.5	62.1	16.5
Nb	17.9	7.4	13.6	4.7	18.1	9.8	22.8	17.9
Ga	19.8	16.7	21.5	15.6	19.4	19.8	20.0	18.3
Cu	1.1	4.1	0.0	0.3	0.6	4.0	1.8	0.0
Zn	13.4	17.5	42.3	16.3	24.3	24.9	24.4	21.3
Pb	41.9	54.7	30.6	53.5	50.4	52.2	38.6	53.6
La	60.9	48.4	62.1	27.9	60.0	59.3	84.1	79.2
Ce	124.4	98.6	110.0	47.0	124.7	102.5	154.3	151.1
Th	51.7	39.6	33.8	21.5	46.2	46.4	73.5	53.8
Nd	44.9	34.6	38.9	19.0	46.6	39.7	60.9	56.4
U	8.0	2.3	3.3	3.3	2.8	4.7	7.8	4.3
Rb/Sr	3.8	2.6	1.2	2.4	4.6	1.8	3.8	1.4
Isotopic data								
$^{87}Sr/^{86}Sr$	**1.05**		**0.85**	**0.96**	**0.80**			
Sr_i (30 Ma)	**1.05**		**0.84**	**0.95**	**0.80**			
εNd (30 Ma)	**-36.09**		**-42.27**	**-28.64**	**-43.77**			

FeO* = total Fe. Vipont-L = leucocratic phase of the Vipont pluton, Vipont-G = the granodiorite phase of the Vipont pluton.

Samples were analyzed for major and trace element geochemistry at the Washington State Geoanalytical Facility. Sr and Nd isotopic analyses of Tertiary plutons and Archean basement were preformed by Bettina Weigand at Stanford University (fig. 15). Additional Nd isotopic analyses of Tertiary plutons were made by Wayne Premo at the U.S.G.S.

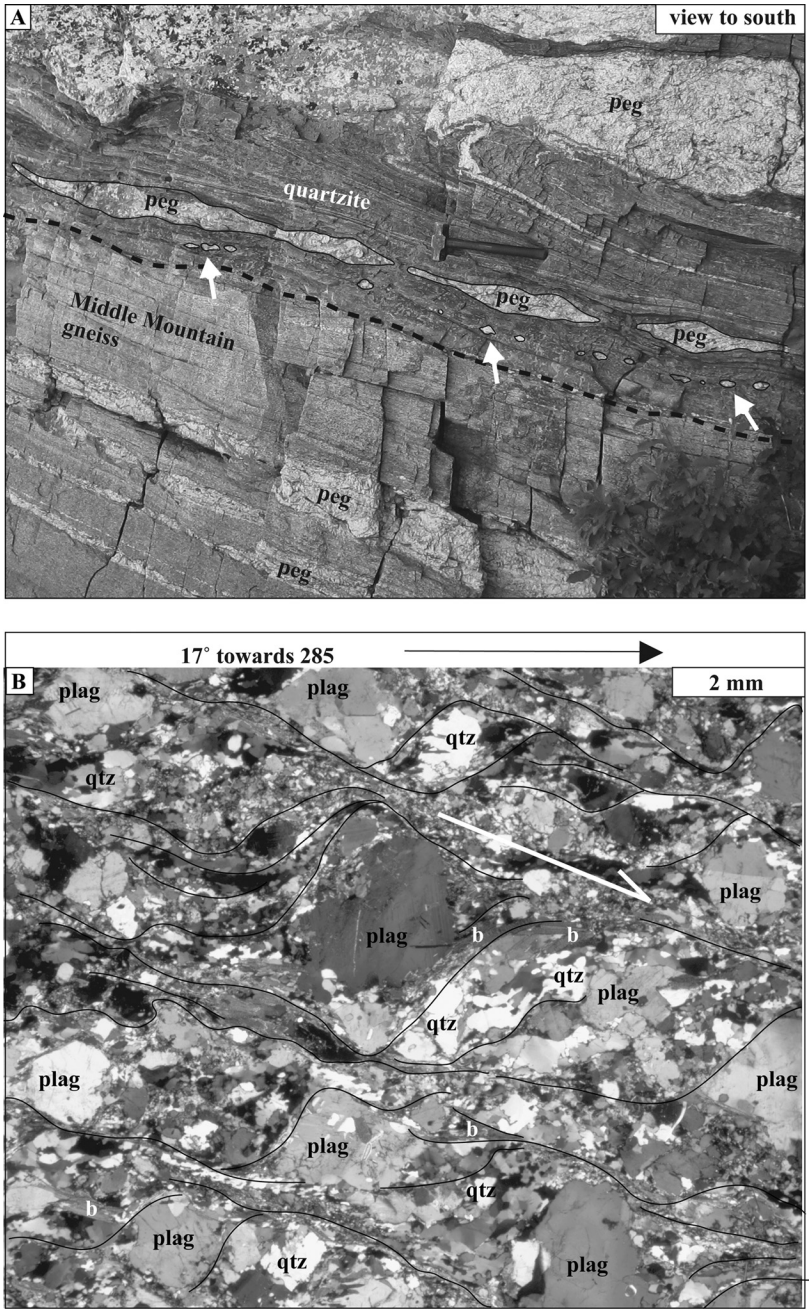

Fig. 4. The Middle Mountain gneiss. (A) Vertical cliff face showing contact between Middle Mountain gneiss and overlying quartzite; hammer for scale is 1 meter long. View to the south; the cliff face is roughly parallel to the gently west-dipping stretching lineation. Dashed line shows approximate contact between the Middle mountain gneiss and Neoproterozoic quartzite. Sample 08-80 comes from this location. The Middle Mountain gneiss and quartzite are intruded by pegmatites (peg) that are variably deformed. White arrows indicate tiny boundins of a pegmatite that has been highly attenuated within the foliation plane of the surrounding quartzite. (B) Sample 08-80 from the Middle Mountain gneiss in cross polarized light showing microstructures in quartz and feldspar consistent with amphibolite facies deformation. Field of view is ~10 × 8 mm. b = biotite, qtz = quartz, plag = plagioclase. The foliation defined by fine grained biotite has been traced in solid black lines. The white arrow indicates top-to-the-west sense of shear.

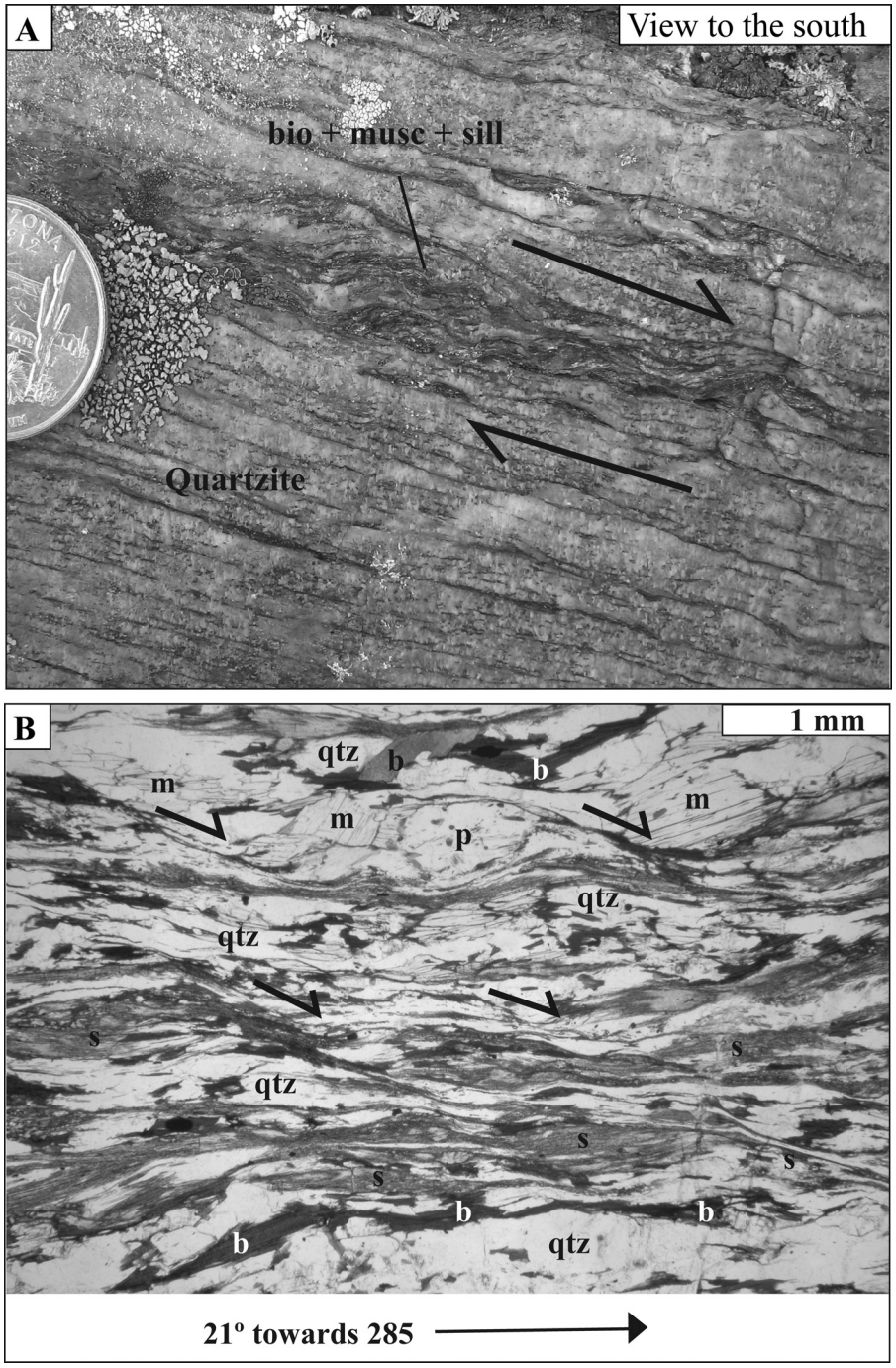

Fig. 5. High-grade fabrics in the country rock the Middle Mountain gneiss. (A) Vertical cliff face of quartzite with aluminous horizons. Edge of quarter for scale (field of view ~8 cm wide), view to the south; the cliff face is roughly parallel to the gently west-dipping stretching lineation. Asymmetry in fabric indicates down-to-the-west sense of shear. (B) The aluminous horizon in plain polarized light shows the fabric is defined by fibrolitic sillimanite (s; abundant fine gray fibrous), biotite (bio), muscovite (m), and quartz ribbons (qtz). Shear bands indicating top-to-the-west-sense of motion and indicated by black arrows.

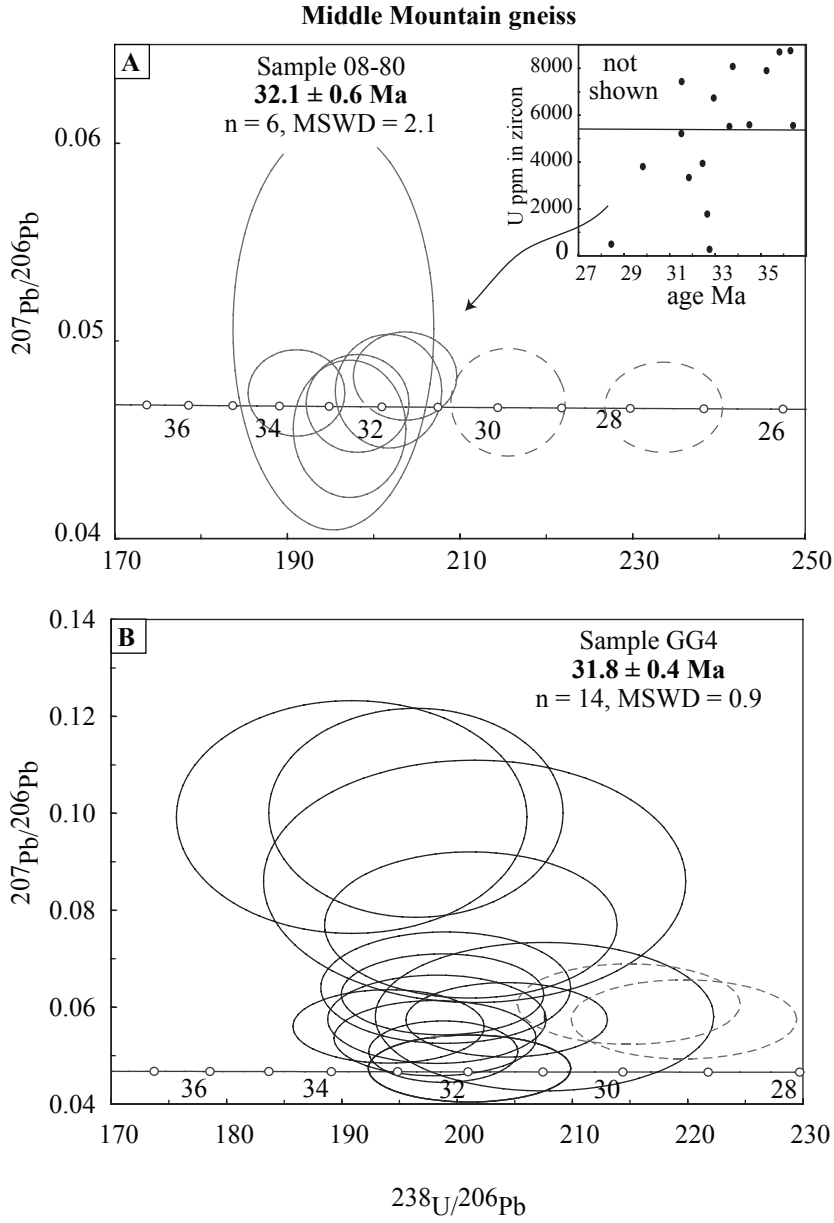

Fig. 6. Tera Waserburg concordia diagrams for two samples from the Middle Mountain gneiss. Dashed ellipses represent samples excluded suspected of Pb loss. (A) Sample 08-80. Inset shows age analyses that were considered unreliable because of high U concentrations (see text for details). (B) U/Pb concordia diagram for analyses of the zircons from sample GG4.

Two younger analyses gave ages of 27.5 ± 2 and 29.8 ± 2.4, and may have been affected by Pb loss. Twelve analyses of inherited cores with comparably lower U concentration (48 to 1419 ppm) yielded $^{207}Pb/^{206}Pb$ ages that range from 1786 ± 42 Ma to 2698 ± 18 (fig. 7; Appendix 2) (cores discussed in a separate section below).

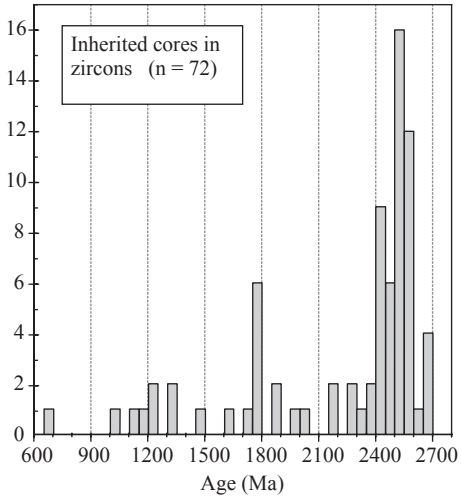

Fig. 7. Histogram of ^{204}Pb-corrected ^{207}Pb/^{206}Pb ages of inherited cores from the zircons of the Cassia plutonic complex including those reported for the Red Butte pluton by Egger and others (2003). The ages are dominantly 2.4–2.7 Ga. A second, smaller preak of ages near *ca.* 1.8 Ga may reflect known orogenic events, such as the Trans Hudson orogeny or Medicine Bow orogeny. The youngest core analyzed is 697 ± 7 Ma.

Sample GG4 is a deformed, hornblende + biotite + sphene + epidote-bearing granite collected near the base of Middle Mountain (fig. 2). Zircons are up to 100 μm long with dark, oscillatory zoning and metamict, inherited cores (fig. 3). Fifteen analyses of the igneous overgrowths define a weighted mean average P^{206}PPb/P^{238}PU age of 31.8 ± 0.4 Ma with a MSWD of 0.9 (fig. 6B). Two points with the youngest ages (dashed ellipses in fig. 6B) may be displaced due to minor Pb loss and are excluded from the main population. These analyses show a trend toward common Pb (fig. 6B), and the low precision of the most discordant analyses is due to modest U concentration (<50 ppm; Appendix 2). Eight analyses of inherited cores from this sample yielded ^{207}Pb/^{206}Pb ages that range from 697 ± 7 Ma to 2411 ± 63 Ma (fig. 7; Appendix 2).

Sample GG4 was selected for oxygen isotope ratio analysis in zircon (Appendix 3). Oxygen isotope analysis was done on the same zircons used for U-Pb analysis, and zircons that produced concordant U-Pb ages were targeted for oxygen isotope analyses for both magmatic overgrowths and inherited cores (fig. 8). The Oligocene overgrowths from zircons in sample GG4 have δ^{18}O values that average 5.47 ± 0.41 (n = 12; fig. 8), and the inherited cores have a slightly higher δ^{18}O value (although within uncertainty) of 5.99 ± 0.48 (n = 4).

The Almo Pluton

The Almo pluton is located in the southern Albion Mountains (fig. 1) and is a medium-grained, equigranular granite that typically contains magmatic biotite and muscovite. It is roughly compositionally zoned with a muscovite ± garnet phase concentrated in the center of the pluton and a biotite ± sphene phase found along the margins (Armstrong, 1968; Miller and Bedford, 1999; Miller and others, 2008). The upper contact between the Almo pluton and its country rocks is preserved in the Albion Mountains, and roof pendants are common in the Almo pluton, indicating that the uppermost levels of the pluton are exposed (Miller and Bedford, 1999). The Almo pluton is largely undeformed, except along its western-most exposures where it is deformed by the Middle Mountain shear zone (fig. 2). Strain increases to the west and

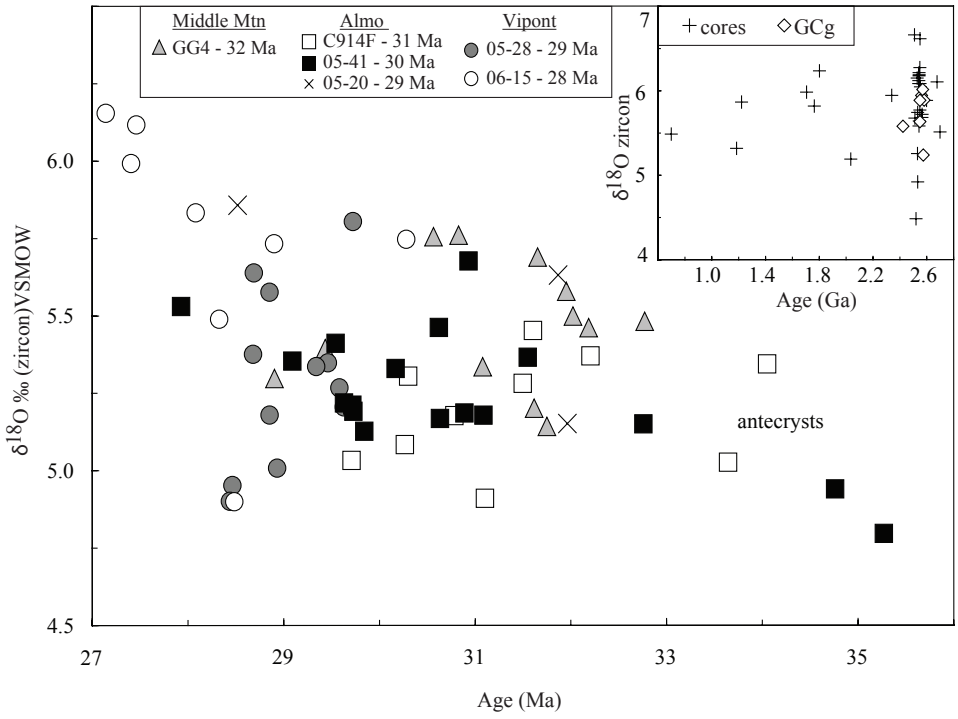

Fig. 8. Oxygen isotope ratios (VSMOW normalized) of zircons from the Cassia plutonic complex versus ^{207}Pb-corrected ^{206}Pb/^{238}U zircon age. The zircons have relatively primitive isotopic ratios and a fairly narrow range of values over several million years. Inset shows δ^{18}O (VSMOW) values versus age for the inherited zircon cores and for the Green Creek gneiss (GCg).

involves intrusive rocks of both the Almo granite and the granites of Middle Mountain. Lineations in the granite and the country rocks in the western Albion Mountains rotate from NW to E-W towards the Middle Mountain shear zone (fig. 2).

Neoproterozoic quartzites and pelitic schists that were intruded by the Almo pluton preserve amphibolite facies, horizontal stretching and vertical flattening fabrics as indicated by nearly symmetric deformational fabrics largely defined by shape preferred orientation of staurolite, biotite, and garnet (fig. 9A). Sillimanite is common in roof pendants and roof rocks to the Almo pluton, and Armstrong (1968) proposed a sillimanite isograd (fig. 2). Figure 9B shows sillimanite (fibrolite) on kyanite from an aluminous horizon in quartzite, suggesting that peak metamorphism occurred after kyanite growth. However, north of the sillimanite-in isograd, and within the staurolite zone, kyanite is commonly found within the sub-horizontal foliation (fig. 9C) and growing as sprays on foliation planes. One occurrence of andalusite was found in country rocks (fig. 2), but the significance is unknown. The presence of sillimanite, kyanite, and andalusite in the contact aureole of the Almo pluton could imply metamorphic pressures at or near the AlR_2RSiO_5 triple point at 3.6 to 4.5 kb (Holdaway, 1971). However, the extent of post-intrusive attenuation of the stratigraphic section is currently unknown. We regard the presence of sillimanite as the most reliable indicator for metamorphic conditions in the contact aureole of the Almo pluton because it is closely associated with all of the Oligocene plutons in the ARG metamorphic core complex (Armstrong, 1968; Egger and others, 2003; Strickland and others, 2011, this study). A more detailed study is needed to establish the detailed

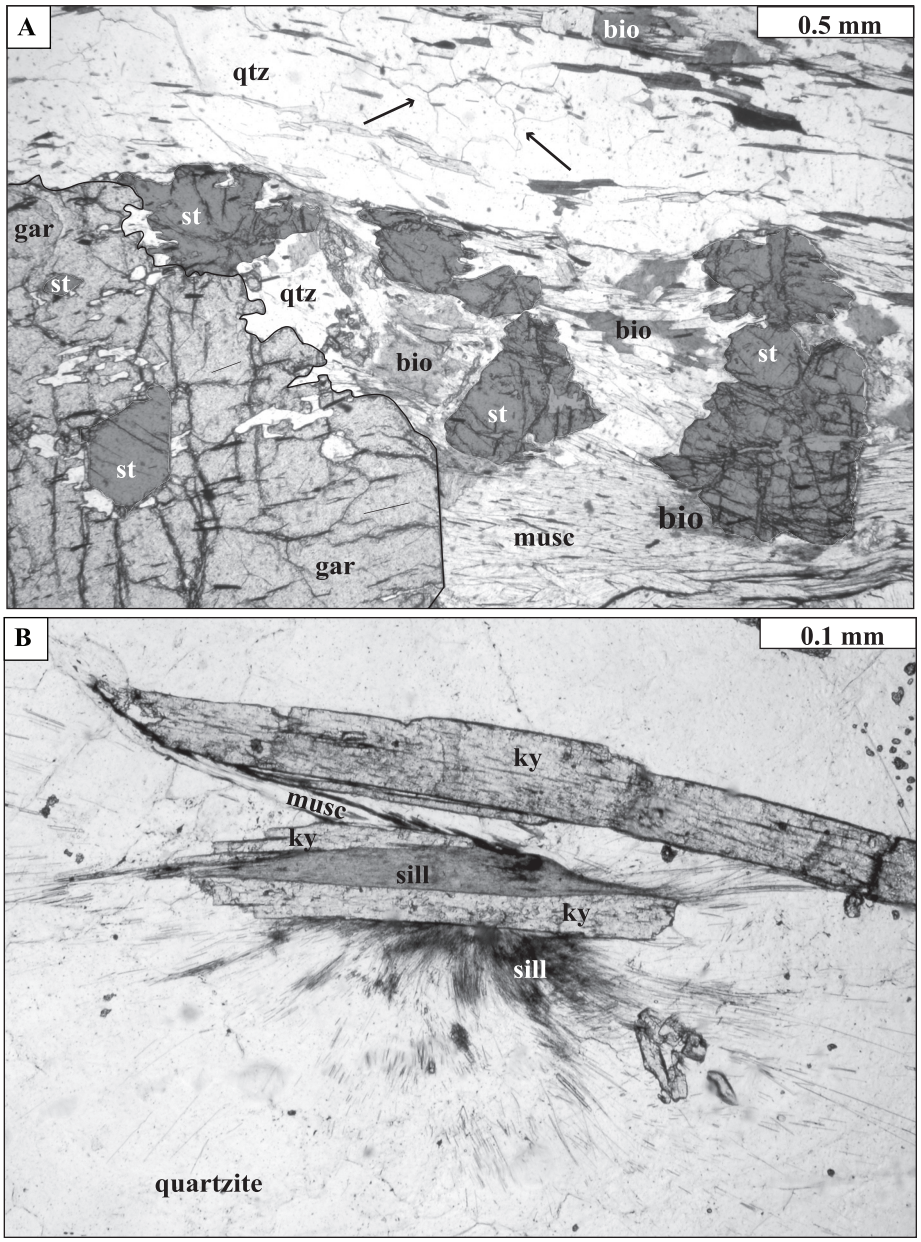

Fig. 9. The country rocks to the Almo pluton in thin section. (A) View in plain polarized light of metamorphic minerals in a pelitic schist in the contact aureole. The foliations largely defined by layers of muscovite (musc) and annealed quartz ribbons (qtz; black arrows point to triple junctions amongst quartz grains). A large garnet porphyroblast (gar; lower left) has inclusions of euhedral staurolite (st; staurolite shaded to distinguish from garnet). Staurolite is also found as large porphyroblasts in the pressure shadow of the garnet, but is corroded and fringed with biotite. We interpret this to indicate that garnet and staurolite were initially coeval, but with increasing metamorphic conditions the staurolite became unstable. (B) Sillimanite (sill) on kyanite (ky) in an aluminous horizon in quartzite from the contact aureole of the Almo pluton. Muscovite (musc) is also present, but may be secondary.

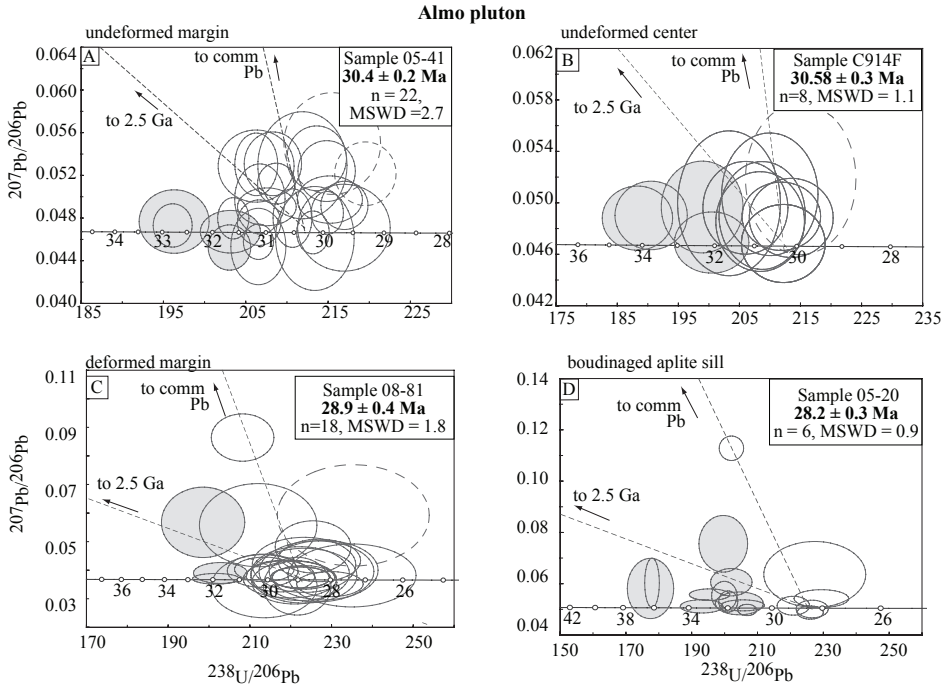

Fig. 10. Concordia diagrams for four samples from the Almo pluton. Analyses of zircon cores are not shown. Age determinations listed are the weighted mean averages of the ^{207}Pb-corrected, ^{206}Pb/^{238}U ages (open ellipses), not intercept ages. Diagrams are shown to illustrate the real spread in zircon ages. Shaded ellipses are interpreted as antecrystic, or inherited from earlier phases of magmatism related to the Cassia plutonic complex. Dashed ellipses represent samples excluded due to suspected Pb loss. The dashed line labeled "to 2.5 Ga" was calculated using an upper intercept of 2.5 Ga and can be used to evaluate any component of ancient, inherited zircon within the analyses. The dashed line labeled "to comm. Pb" was calculated using an upper intercept ^{207}Pb/^{206}Pb value of the Red Butte pluton determined by Wright and Wooden (1991) to evaluate any contribution of common Pb to the spread in ages. (A) Sample 05-41, the undeformed, biotite + muscovite-bearing Almo pluton collected near the western margin. (B) Sample C194F from the central Almo pluton. (C) Sample 08-81, a deformed, two mica granite exposed along the western Almo pluton. (D) 05-20, a boudinaged aplite dike.

relationships between the alumino-silicate minerals to deformation near the Almo pluton, but the depth of intrusion of the pluton was most likely at least or greater than ~3.5 kb based on the presence of magmatic muscovite (Thompson and Connolly, 1995).

Three samples from the Almo granite (05-41, C194F, and 08-81) and one pegmatite (05-20) (fig. 2) were analyzed for U-Pb zircon geochronology. Sample 05-41 was collected from the northwestern margin of the Almo pluton (fig. 2). It is an undeformed, biotite + muscovite bearing granite representative of the main phase of the pluton. Zircons from the sample are large (>100 microns) and euhedral (fig. 3). In cathodoluminescence, they have distinct, rounded cores and euhedral overgrowths, both of which have oscillatory zoning indicative of igneous growth (fig. 3).

U-Pb analyses of zircon overgrowths from sample 05-41 are shown on a concordia diagram in figure 10A. They form a cluster of points on or near concordia that range in P^{206}PPb/P^{238}PU ages from 29.5 to 31.5 Ma, with a small subpopulation of analyses at 32 to 33 Ma (fig. 10A and Appendix 2). Two slightly younger and discordant analyses are considered to have Pb loss and were excluded from age determinations (dashed ellipses in fig. 10A). A weighted mean P^{206}PPb/P^{238}PPb age of 30.4 ± 0.2 (n = 22,

MSWD = 2.7) is determined for this sample. Fifteen zircon cores were also dated using U-Pb, and $^{207}Pb/^{206}Pb$ ages of the inherited cores ranged from 1185 ± 28 to 2699 ± 41 Ma (fig. 7, Appendix 2).

The spread in ages in the sample 05-41 and the corresponding high MSWD from these 22 analyses can be evaluated in several ways. Both inheritance of older zircon (for example from the Archean basement) and differing components of common Pb can cause scatter of data in a concordia diagram (represented by the two dashed lines in fig. 10A). While it appears that the data may have a minor common Pb component, a trend towards Archean inheritance is not strongly indicated despite abundant Archean cores in these zircons. We consider the possibility that the spread of ages in this sample could represent two distinct age populations, both with a minor trend toward common Pb (fig. 10A). The youngest population, 29.9 ± 0.2 Ma (MSWD = 0.2), would represent the time of crystallization of the Almo pluton. A slightly older population of zircon at 30.9 ± 0.25 (MSWD = 0.6) could represent antecrystic zircons inherited from a pre-existing phase of the magmatic system (terminology after Miller and others, 2007). However, since many of the errors of the individual analyses overlap, we favor a conservative treatment of the data and interpret the weighted mean average $P^{206}PPb/P^{238}PU$ age of all 22 analyses (30.4 ± 0.3) to be the crystallization age, despite an MSWD of 2.7.

The five analyses that are older than the main population (gray ellipses on fig. 10A) are interpreted as antecrystic zircons from an earlier phase that were recycled into the younger batch of melt that formed the Almo pluton. This interpretation of magma system inheritance is supported by the complex zoning in CL images; one grain from the Almo pluton appeared to have a core with two overgrowths (fig. 3). U-Pb analyses of the two overgrowths yielded an age of 29.8 ± 0.4 Ma whereas the inner rim is ~35 Ma (high U content precludes a robust age determination). This high U overgrowth is identical to the zircons in sample 08-80 from the slightly older Middle Mountain pluton.

A second undeformed sample from the Almo pluton, also a biotite + muscovite-bearing granite, was collected near the center of the pluton. Sample C914F yielded very similar results to sample 05-41. Fourteen analyses of igneous overgrowths of zircons from sample C914F (fig. 2) produced a spread along concordia (fig. 10B). Ten analyses define a single population with a weighted mean $P^{206}PPb/P^{238}PU$ age of 30.5 ± 0.4 Ma, while four analyses are 32 Ma to 34 Ma. As with sample 05-41, the older population of ages is concordant, and interpreted as inherited from earlier phases of the Cassia plutonic complex magmatic system (antecrysts). Five inherited cores were dated from this sample and gave a range of $^{207}Pb/^{206}Pb$ ages of 2437 ± 30 to 2566 ± 18 Ma (fig. 7, Appendix 2).

Sample 08-81 is deformed biotite-muscovite-bearing granite that is exposed in a road cut between the Albion Mountains and Middle Mountain (fig. 2). It is interpreted as part of the Almo pluton based on sparse but semi-continuous exposure of the Almo granite to the east and on the presence of abundant igneous muscovite that is not found in the Middle Mountain gneiss. However, sample 08-81 is younger than the other two samples from the Almo pluton, and may be correlative to the Vipont pluton (see below).

Eighteen analyses of zircon overgrowths from sample 08-81 form a cluster on concordia with a weighted mean average $P^{206}PPb/P^{238}PU$ age of 28.9 ± 0.4 with an MSWD of 1.8 (fig. 10C and Appendix 2). As with the other samples from the Almo pluton, a subpopulation of analyses at 32 Ma (fig. 10C) is taken to represent an earlier phase of zircon growth inherited from the magmatic system. Eight inherited cores were dated from this sample and gave a range of $^{207}Pb/^{206}Pb$ ages of 1044 ± 32 to 2566 ± 14 Ma (fig. 7, Appendix 2).

Sample 05-20 is from an aplite sill that intruded the metasedimentary country rocks along the western margin of the Almo pluton (figs. 2 and 10D). It is internally undeformed, but boudinaged within the deformed quartzite that surrounds it. Similar to the Almo pluton, 17 analyses of these grains range from ~36 Ma to 28 Ma (fig. 10D, Appendix 2). A subpopulation of 6 analyses that form the youngest coherent group is interpreted as the crystallization age at 28.7 ± 0.5 Ma with an MSWD of 0.9 (fig. 10D). The youngest ages come from the outermost edges of the grains. This sample contained the most inheritance from slightly older, Tertiary zircons (fig. 10D). Zircons from this sample also contained inherited cores (Appendix 2) that gave a range of $^{207}Pb/^{206}Pb$ ages of 1347 ± 44 to 2545 ± 22 Ma (fig. 7, Appendix 2). We interpret the majority of the Tertiary zircon in the aplite sill to be antecrystic, and that it therefore represents a small volume of melt generated from (re)melting of pre-existing granites, perhaps already at subsolidus temperatures. Because the aplite sill is boudinaged within the foliation plane of the enclosing metasedimentary rocks, ductile deformation was still ongoing after 28.7 ± 0.5 Ma.

Two samples of the main phase of the Almo pluton, samples 05-41, C914F, were selected for oxygen isotope analyses. Oxygen isotope ratios in zircons from the main phase of the Almo pluton are similar to those of the Middle Mountain gneiss. Zircons from sample 05-41 have an average $\delta^{18}O$ value of 5.30 ± 0.42 permil (n = 15) for the Oligocene overgrowths and an average value of 5.68 ± 0.83 permil (n = 11) for the Precambrian cores (fig. 8, Appendix 3). Results from sample C914F are nearly identical; the Oligocene zircon overgrowths yield a $\delta^{18}O$ average of 5.20 ± 0.36 permil (n = 10) and core analyses average 5.52 ± 1.44 permil (n = 4). In addition, a small number of oxygen isotope analyses were performed on zircons from the boudinaged aplite sill, sample 05-20 because of the small grains and the narrow nature of the zircon overgrowths. $\delta^{18}O$ (VSMOW) for the zircon overgrowths from the aplite average 5.55 ± 0.72 permil (n = 3), and inherited cores yielded 5.42 ± 0.64 permil (n = 2).

The Vipont Pluton

To the south of Middle Mountain (fig. 1), the two-phase Vipont pluton is exposed in the northern Grouse Creek Mountains along a N-S-trending, fault-bound ridge (fig. 1). The spatial relationship between the Vipont pluton and the Middle Mountain gneiss has not been mapped (fig. 1). In the Vipont pluton, an early biotite + sphene-bearing granodiorite phase is cut by abundant dikes and sills of medium to coarse-grained, muscovite + garnet-bearing leucogranite granite. From north to south, the garnet + muscovite-bearing sills and pegmatites become more abundant until a medium to coarse-grained, leucocratic garnet-bearing granite becomes the dominant phase. The Vipont was originally dated by U-Pb monazite as 27 ± 2 Ma (Wells and others, 1997).

Compton and others (1977) were the first to study the Vipont pluton and its country rocks, and subsequent studies in the area have been done by Hoisch and others (2002, 2008), and Strickland and others (2011). Compton and others (1977) reported that highly deformed garnet and pyroxene-bearing marbles and sillimanite-bearing pelitic schists are present in the contact aureole of the Vipont pluton (for an alternative interpretation of the age of peak metamorphism see Hoisch and others, 2002, 2008; Wells and others, 2008). Figure 11A shows an example of pelitic schist collected ~1.5 km from the exposed Vipont pluton in Basin Creek, Utah, in an area riddled with stocks and pegmatites that are associated with the pluton. This sillimanite-bearing schist is referred to as the "lower horizon" in Hoisch and others (2002, 2008), and as "sample 08-55" in Strickland and others (2011).

The foliation in sample 08-55 is defined by fibrolitic sillimanite, biotite and bands of muscovite + quartz. Large porphyroblasts (>5 mm) of garnet, plagioclase, and staurolite often contain crenulated inclusion trails of ilmenite and quartz that are at

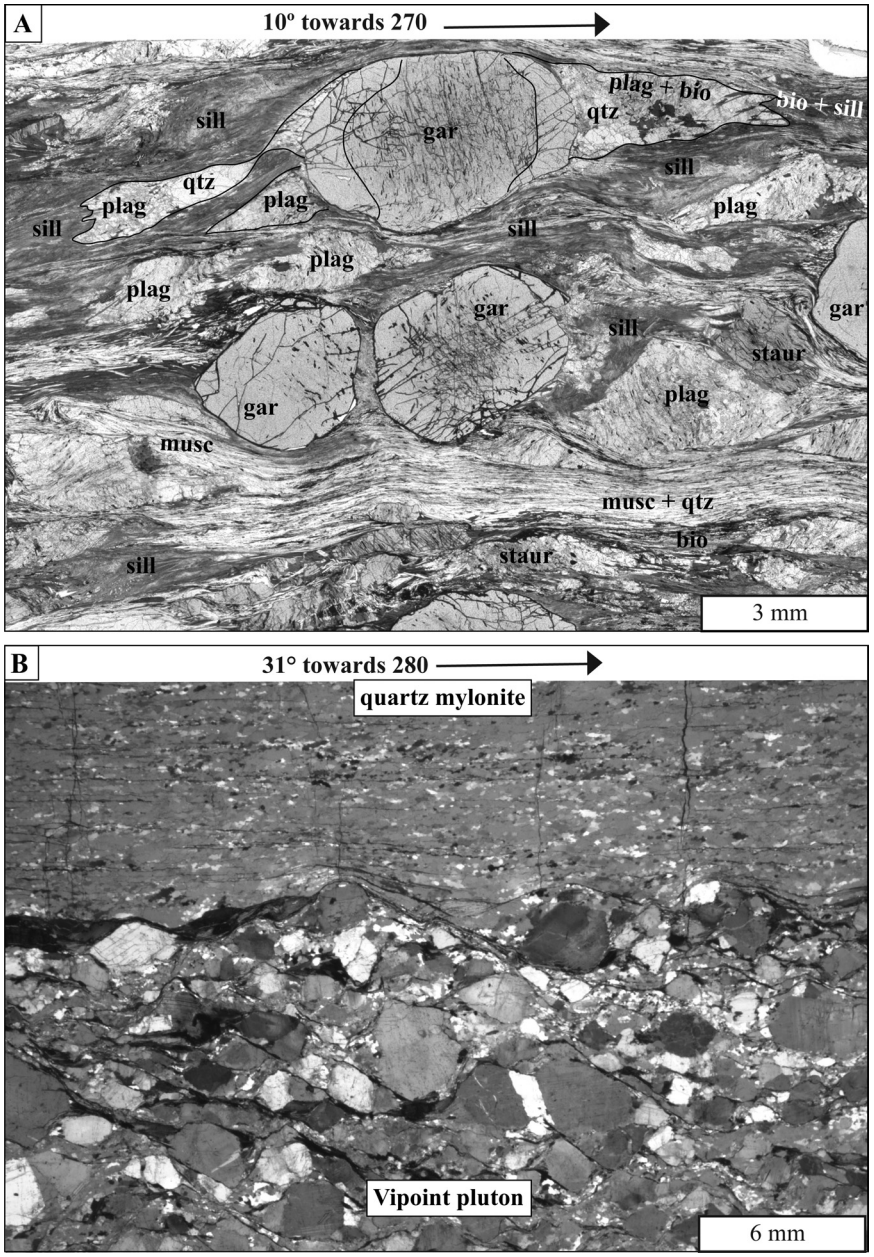

Fig. 11. Photomicrographs of the country rocks to the Vipont pluton. (A) Sillimanite (sill) schist with large porphyroblasts of garnet (gar), plagioclase (plag) and staurolite (staur). Abundant fibrolitic sillimanite and biotite define the foliation, with parallel horizons of muscovite (musc) + quartz (qtz). Large porphyroblasts have inclusion trails that are at high angles to the external foliation. Garnet at top has strain free caps that are elongate in the stretching directions, and well-developed strain shadows of plagioclase, quartz and sillimanite. (B) The mylonitized intrusive contact between the Vipont pluton and its overlying quartzite. Field of view is ~30 × 16mm. The quartz mylonite has a well-developed lattice preferred orientation indicated by the uniform gray color. The feldspars in the Vipont pluton have weak undulose extinction, but remained relatively undeformed.

high angles to the external foliation (fig. 11A). The large garnets, in particular, have inclusion rich interiors and asymmetric, inclusion-free overgrowths (caps) that are elongate in the stretching direction (fig. 11A). Well-developed strain shadows of plagioclase and quartz are present on the edges of garnets, and the fabric appears to be gently deflected around the garnet and plagioclase porphyroblasts (fig. 11A). Staurolite in this sample commonly has ragged grain boundaries and is fringed with biotite and sillimanite, which may indicate that the peak metamorphic conditions surpassed the field of stability for staurolite along the reaction staurolite = garnet + biotite + alluminosilicate + H_2O (Spear and Cheney, 1989 and references therein) Because sillimanite is found adjacent to the Almo pluton, Middle Mountain gneiss, and Red Butte pluton (Armstrong, 1968; Egger and others, 2003; Strickland and others, 2011) but has not been found away from the Oligocene plutons, we interpret the sillimanite in the contact aureole of the Vipont pluton as related to the intrusion of the Oligocene Vipont pluton. Strickland and others (2011) dated monazite associated with the sillimanite grade metamorphism as *ca.* 32 to 27 Ma, and found evidence (in structurally higher rocks) for monazite growth during an earlier, 140 Ma event. However, based on Th-Pb ages of monazite inclusions in garnet, Hoisch and others (2008) proposed that the garnets in this unit grew during peak metamorphism and a period of increasing pressure (thrusting) between 37 and 62 Ma.

Pelitic rocks near the Vipont pluton have a foliation and lineation defined by biotite and fibrolitic sillimanite indicating that ductile deformation was associated with peak metamorphism (fig. 11A). At structurally higher levels, the ductile fabrics are overprinted by a mylonitic, gently west-dipping foliation and a W-NW-plunging mineral lineation that is parallel to higher-grade ductile fabrics (fig. 11B). Figure 11B shows a deformed intrusive contact between the granodiorite phase of the Vipont pluton and the overlying quartz mylonite. The feldspar grains in the granodiorite remained relatively intact whereas the quartz grains have been grain sized reduced (fig. 11B). The quartzite is strongly mylonitized with pervasive grain size reduction with a well-developed lattice preferred orientation consistent with development at greenschist-facies conditions (Hirth and Tullis, 1992). Shear sense indicators in both the high grade fabrics and the mylonites show down to the west, extensional sense deformation. The presence of sillimanite-grade fabrics overprinted by mylonites with the same orientation and sense of shear is interpreted as strain localization under decreasing metamorphic conditions during exhumation after crystallization of the pluton, which is common to metamorphic core complexes (Davis, 1980; Armstrong, 1982). At the structurally highest levels, all units are truncated by the Middle Mountain detachment fault, which also has top to the west sense of motion.

Both phases of the Vipont pluton were dated by U-Pb zircon techniques. Fifteen igneous overgrowths were analyzed on zircon separated from the granodiorite, (sample 05-28), and resulted in a coherent population of ages with a weighted mean average of the $P^{206}PPb/P^{238}PU$ age of 29.0 ± 0.3 Ma (fig. 12A). Like the Almo pluton, slightly older analyses are interpreted as antecrystic zircons that were inherited from earlier phases within the same magmatic system. Two analyses were excluded due to suspected Pb loss. These analyses of igneous overgrowths show a very minor trend towards common Pb, but no discernable component of Archean inheritance. Inherited cores in the zircons from sample 05-28 range from 1990 ± 10 Ma to 2620 ± 12 Ma (n = 12; fig. 7, Appendix 2).

Sample 06-15 represents the garnet-muscovite-bearing leucogranite phase of the Vipont pluton (fig. 1). Like all other samples from the CPC, zircons from sample 06-15 have the characteristic core and overgrowth textures in CL. Eleven analyses of zircon overgrowths are shown on a concordia diagram in figure 12B, and nine analyses define a single population with a trend towards common Pb, and a lower intercept age of

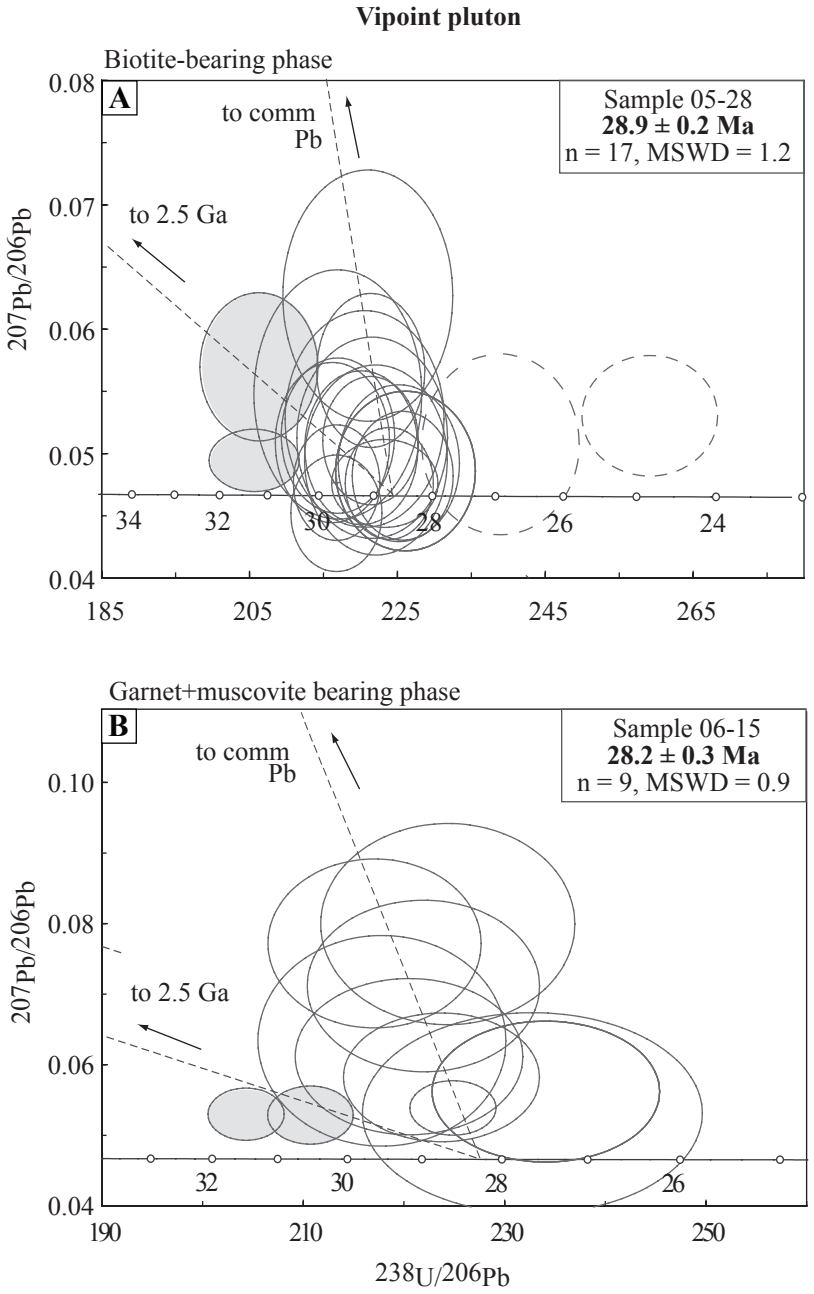

Fig. 12. Concordia diagrams for two samples from the Vipont pluton. Analyses of zircon cores are not shown. Age determinations listed are the weighted mean averages of the ^{207}Pb-corrected, ^{206}Pb/^{238}U ages (open ellipses), not the concordia intercept ages. Shaded ellipses are interpreted as antecrystic, or inherited from earlier phases of magmatism related to the Cassia plutonic complex. Dashed ellipses represent samples excluded due to suspected Pb loss. The dashed line labeled "to 2.5 Ga" was calculated using an upper intercept of 2.5 Ga and can be used to evaluate any component of ancient, inherited zircon within the analyses. The dashed line labeled "to comm. Pb" was calculated using an upper intercept ^{207}Pb/^{206}Pb value of the Red Butte pluton determined by Wright and Wooden (1991) to evaluate any contribution of common Pb to the spread in ages. (A) Concordia diagram showing ages of zircons from sample 05-28, the biotite-bearing phase of the Vipont pluton. (B) U/Pb concordia diagram for analyses of zircon overgrowths from sample 06-15, the garnet + muscovite-bearing phase of the Vipont pluton. A minor trend towards a component of common Pb is indicated by both samples.

28.2 ± 0.6 Ma. Two slightly older analyses are taken to be inherited from a pervious magmatic phase. Six analyses of inherited cores from this sample yielded $^{207}Pb/^{206}Pb$ ages of 697 ± 7 Ma to 2568 ± 44 Ma.

Oxygen isotope ratios for zircons from the two phases of the Vipont pluton are not significantly different from each other (fig. 8B, Appendix 3). Zircons from the slightly older, granodiorite (sample 05-28) has an average $\delta^{18}O$ value of 5.30 ± 0.55 permil (n = 12) for Oligocene overgrowths and 6.26 ± 0.53 (n = 8) for inherited cores. The garnet + muscovite-bearing phase (sample 06-15) has slightly higher $\delta^{18}O$ zircon ratio of 5.74 ± 0.75 permil (n = 13) for Oligocene overgrowths and $\delta^{18}O$ average ratio of 5.68 ± 0.431 (n = 4) for the inherited cores.

The Green Creek Gneiss

Because of the abundance of inherited Archean zircon in the Tertiary granites of the CPC, two samples from the Green Creek gneiss were investigated as a possible source for Tertiary melts. The muscovite and biotite-bearing Green Creek augen gneiss was originally dated by Armstrong and Hills (1967) by a Rb/Sr 6 point isochron age of 2.46 ± 0.3 Ga. Zircons from the Green Creek gneiss are metamict, although patches of oscillatory zoning are still preserved in CL, (fig. 13). In sample RR06-5 from the eastern Raft River Mountains, seven concordant analyses yielded a weighted mean average $P^{207}PPb/P^{206}PPb$ age of 2568 ± 8 Ma (MSWD = 1.3; fig. 13). Other analyses from this sample are discordant, and fall along a line that is interpreted to indicate a Pb loss event in the Cretaceous; although a precise lower intercept can not be determined. Sample AB06-9, from the northern Albion Mountains, produced a similar array on concordia (fig. 13), and yielded an upper intercept age of 2565 ± 16 Ma and a lower intercept of 99 ± 25 Ma (MSWD = 5.9). Despite significant Pb loss, these two samples yielded nearly identical ages of 2.56 Ga, which is taken as the crystallization age for the Green Creek gneiss.

Oxygen isotope SIMS analysis of zircons from the Archean Green Creek gneiss was challenging due to the extensive metamictization and altered nature of the grains (fig. 13) and robust analysis is sensitive to both matrix effects and to the surface condition of the zircon (Kita and others, 2009). Seven analyses from spots that gave concordant U-Pb ages from the two samples of the Green Creek gneiss give an average $\delta^{18}O$ value of 5.77 ± 0.72 permil (fig. 8; Appendix 3). This is consistent with Archean $\delta^{18}O$ values worldwide (Valley and others, 2005).

GEOCHEMISTRY

Ti and Hf Concentrations in Zircon

Zircons from each pluton of the CPC have a range of Ti and Hf concentrations (fig. 14, Appendix 3). The Ti in zircon thermometer of Ferry and Watson (2007) was used to calculate model temperatures for comparative purposes using a SiO_2 activity of 1, a TiO_2 activity of 0.7 and no pressure correction. In general, the inherited cores have higher Ti concentrations (average = 16.4 ± 14.8 ppm, 2SD) than the Oligocene overgrowths (average = 7.1 ± 13.7 ppm, 2SD).

In zircons from sample GG4 of the 32 Ma Middle Mountain gneiss, Ti concentrations in Oligocene overgrowths ranged from 1.2 to 13.5 ppm, which corresponds to model temperatures that range from 603 to 812 °C (n = 8) (Appendix 3, fig. 14). Hf concentration also varies from 8416 to 17950 ppm, and a trend of increasing Hf concentration with decreasing Ti concentration is consistent with zircon growth during cooling and fractionation of a melt (Claiborne and others, 2006, 2010; Wooden and Barth, 2010) (fig. 14, Appendix 3). Ti concentrations from the Precambrian cores from sample GG4 have higher Ti concentrations of 8.5 to 31.7 ppm and model temperatures of 765 to 911 °C (Appendix 3).

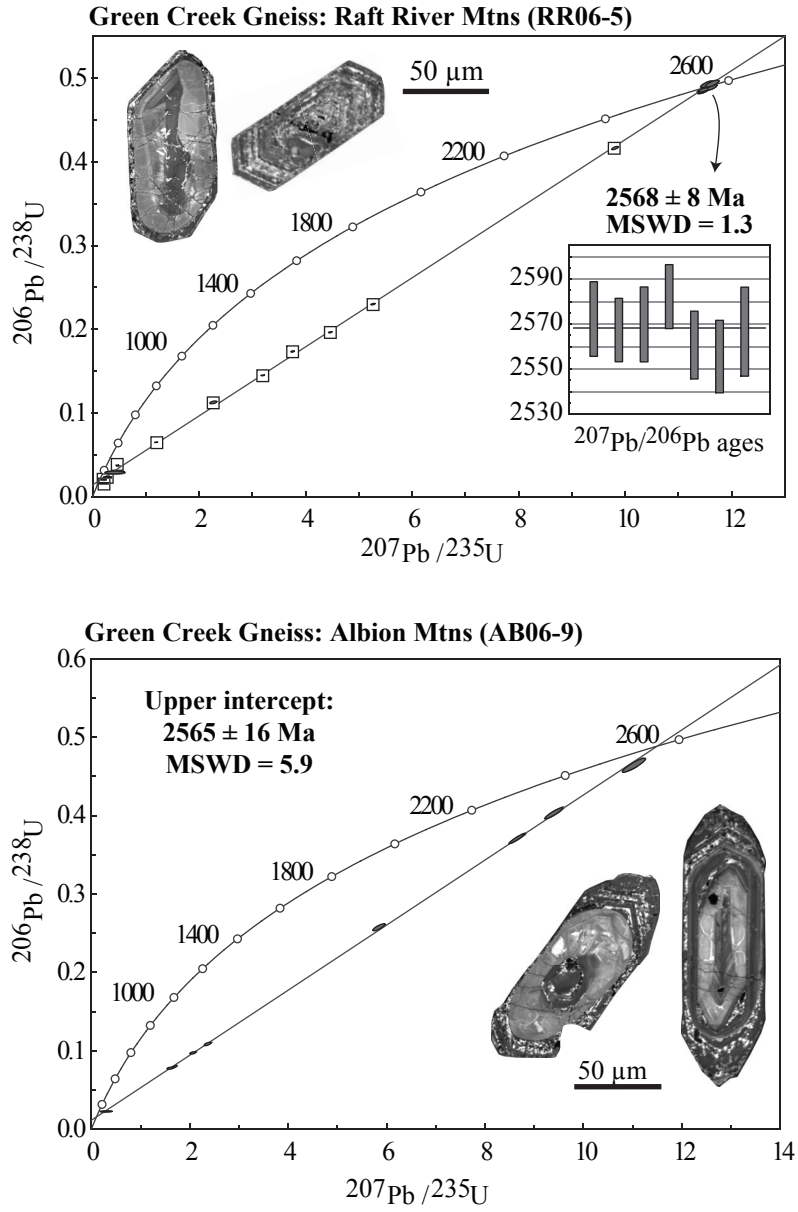

Fig. 13. Concordia diagrams for two samples from the Green Creek gneiss. Cathodoluminescence images of representative zircons from each sample are shown. Top shows sample from the Raft River Mountains, with boxes around small error ellipses to make them more visible, and the weighted mean average diagram for the $^{206}Pb/^{207}Pb$ ages of concordant analyses. Bottom shows a sample from the northern Albion Mountains, and the age determination is taken from the upper intercept.

Zircons from the Almo pluton have Ti concentrations that range from 2.4 to 4.1 for sample 05-41 and 2.2 to 14.9 ppm for sample C914F, which corresponds to lower model temperatures of 618 to 753 °C (fig. 14, Appendix 3). Given the more evolved composition of the two mica Almo pluton when compared to the hornblende, biotite,

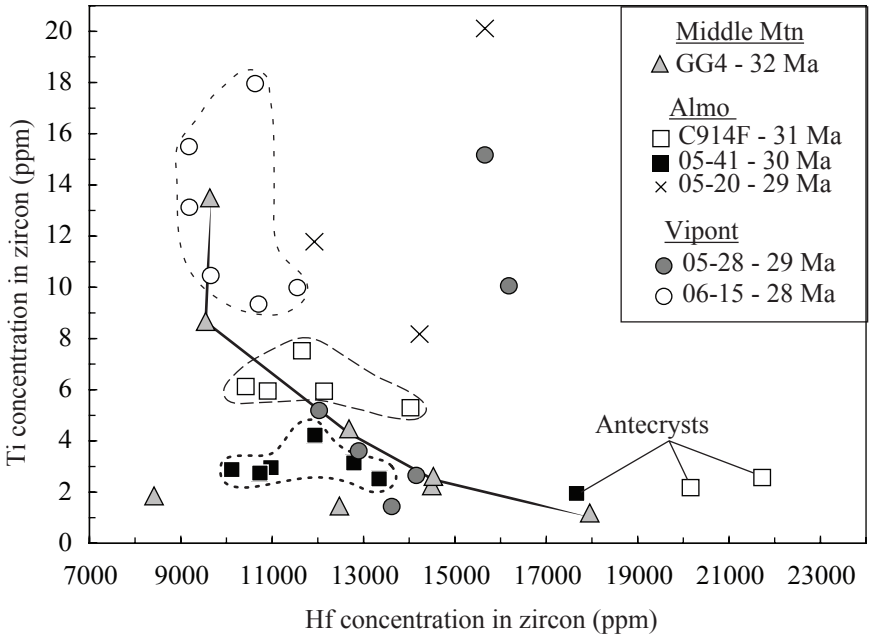

Fig. 14. Ti concentration plotted against Hf concentration to evaluate fractionation trends. Only the sample GG4 from the Middle Mountain gneiss shows a trend. Both samples from the Almo pluton show little range in Ti or Hf. The youngest, most compositionally evolved sample 06-15 has the highest Ti and lowest Hf concentrations.

and sphene-bearing Middle Mountain gneiss, lower model Ti in zircon temperatures are not surprising. No trends in the Ti and Hf concentrations are observed for the Almo pluton (fig. 14). Ti concentration from the inherited cores in the zircons from the Almo pluton have a larger range (1.5-33 ppm) and correspond to model temperatures of 699 to 916 °C (Appendix 3).

The Ti and Hf concentrations for Oligocene zircon overgrowths from the two phases of the Vipont pluton show an interesting relationship. Zircons from sample 05-28, the 28.9 ± 0.2 Ma granodiorite, have Ti concentration of 4.4 to 17.1 ppm (model temperatures of 616-824 °C) and Hf concentrations of 12030 to 16184 ppm (fig. 14, Appendix 3). In contrast, despite being a compositionally leucogranite, the 28.2 ± 0.3 Ma garnet-muscovite-bearing phase (sample 06-15), has consistently higher Ti concentrations of 9.3 to 18 ppm (excluding two analyses of antecrystic zircon) with a corresponding narrow range of model temperatures of 774 to 826 °C. Sample 06-15 also has lower Hf concentration (9190-11550 ppm) than the older granodiorite phase (fig. 14, Appendix 3). This shift may reflect renewed or increased magmatism in the source area.

Whole Rock Chemistry

Geochemical data from the CPC and adjacent Archean Green Creek gneiss help to assess the evolution of the Tertiary granitoids through time, the contribution of crustal versus primitive melts in the formation of the these plutons, and the possibility that the exposed Archean basement was a source rock for the Tertiary melts. Geochemical data from eight samples each of Oligocene plutons and Archean basement (table 2) were combined with geochemical data from the Emigrant Pass plutonic complex and the Red Butte pluton reported by Egger and others (2003) to construct the Harker

diagrams shown in figure 15. Although this data set is illustrative and helps us interpret the evolution of the CPC as a whole, a larger data set that includes multiple geochemical samples per pluton is required for a more detailed petrologic analysis.

Figure 15 shows the Rb/Sr ratios of Tertiary plutons with the Rb/Sr ratios of the Archean Green Creek gneiss. With the exception of one sample from the Almo pluton with a Rb/Sr of 77 (not shown), the Rb/Sr ratios of the Tertiary plutons averages 0.766 ± 1.22 (2SD), whereas the Rb/Sr ratios of the Green Creek gneiss average 2.70 ± 2.53 (2SD). The initial Sr ratios (at 30 Ma) of samples 06-15 and 05-28 from the Vipont pluton and an undated sample of the Almo pluton range from 0.7297 to 0.7183 (table 2 and fig. 15). The εNd values from these samples, also calculated for 30 Ma, are −36.5 to −25.5 (fig. 15, table 2). For the Green Creek gneiss, initial Sr and εNd values have been calculated for 30 Ma rather than the age of the gneiss (2.5 Ga) for a direct comparison with the Oligocene plutons (fig. 15). At 30 Ma, the Green Creek gneiss had a Sr composition of 0.798 to 1.046, which is higher than the initial Sr of the Oligocene plutons. The εNd values of the Archean gneiss range from −28.5 to −43.9, which are similar to εNd values from the Tertiary plutons (table 2 and fig. 15).

The Tertiary plutons generally become more siliceous through time. One sample of the 29 Ma granodiorite phase of the Vipont pluton, ("g" in fig. 15), is the exception and is the most mafic at 68 percent SiO_2. It falls along the same trends as the other plutons, and may therefore represent a higher degree of partial melting in the source area or a larger component of mantle-derived magmas mixed with crustal melts. Major element chemistry from the 32 Ma Middle Mountain gneiss is similar to the older granodiorites from the Emigrant Pass plutonic complex (Egger and others, 2003). The 30 Ma Almo pluton, the 28 Ma garnet-bearing phase of the Vipont pluton, and the 25 Ma Red Butte pluton have more evolved chemistry than the Middle Mountain gneiss and the Emigrant Pass plutonic complex (fig. 15). Whole rock geochemical data for the Archean Green Creek gneiss are also shown on figure 15. Samples of the exposed biotite + muscovite-bearing Archean basement (Green Creek gneiss) have less variation in major element chemistry than do the Tertiary plutons, particularly in Ca and K (fig. 15). The Green Creek gneiss is more aluminous, more potassic and has a higher silica content that the 32 Ma Middle Mountain gneiss and the 28 Ma granodiorite phase of the Vipont pluton (fig. 15).

The Nd isotopic data alone would permit the Tertiary magmas to represent melts of the Green Creek gneiss, but the Sr_i values of the CPC were lower than the Sr_i of the Green Creek gneiss at 30 Ma (fig. 15). Additionally the Rb/Sr ratios of the Tertiary plutons are typically lower than the Green Creek gneiss (fig. 15). If the CPC was a melt of the exposed Green Creek gneiss, or any ~2.5 Ga rock with a Rb/Sr ratio similar to that of the exposed Green Creek gneiss, the Oligocene plutons would have a much higher initial Sr values (>0.8). The low, negative εNd values for the CPC require an Archean crustal source with a long-term low Rb/Sr of ~0.15. No late Archean rocks with similar Rb/Sr ratios are exposed in the region of the ARG metamorphic core complex, but examples of such rocks can be found in the late Archean trondhjemite-tonalite-granodiorite rocks exposed in the Beartooth and Bighorn Mountains of Wyoming (Mueller and others, 1985; Wooden and Mueller, 1988). The implication is the CPC could represent melting of the Archean lower crust at depth, possibly with limited contribution from juvenile magmas.

DISCUSSION

Geochronology

In summary, three plutons from the Cassia plutonic complex that are exposed in the lower plate of the ARG metamorphic core complex were intruded between 32.1 ± 0.5 and 28.2 ± 0.6 Ma. Figure 16 shows histograms of $P^{206}PPb/P^{238}PU$ ages for the

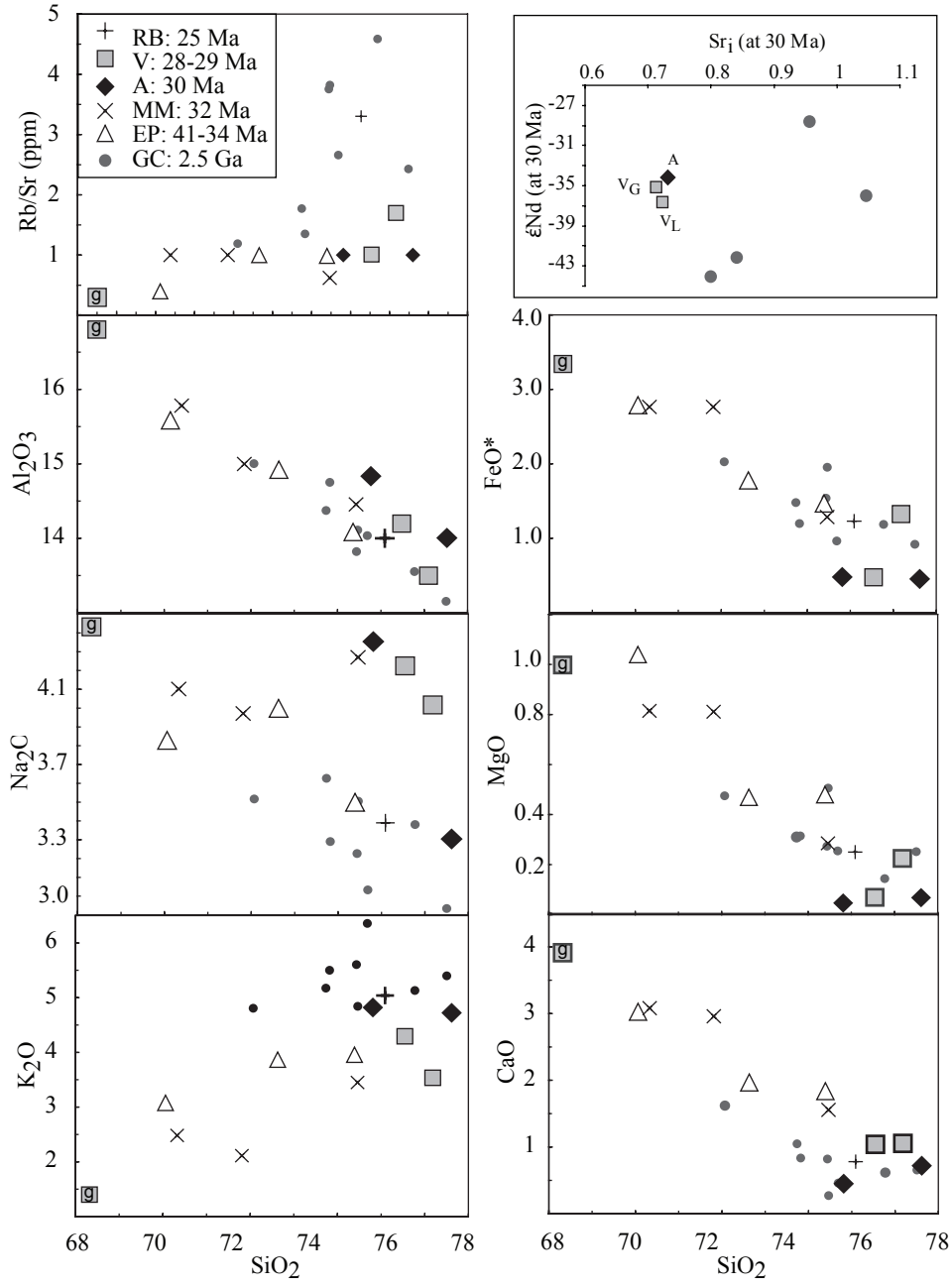

Fig. 15. Harker variation diagrams for whole rock geochemical data from the Cassia plutonic complex and the Green Creek gneiss. Data from this study combined with Egger and others (2003). Upper right shows Sr and Nd isotopes for the Oligocene plutons and the Archean Green Creek gneiss (A = Almo pluton, VG = granodiorite phase of the Vipont pluton, VL = leucocratic phase of the Vipont pluton, circles = Green Creek gneiss). Isotopic values shown are calculated for 30 Ma to evaluate the Green Creek gneiss as a source for the Cassia plutonic complex. For all other plots, "g," indicates the granodiorite phase of the Vipont pluton.

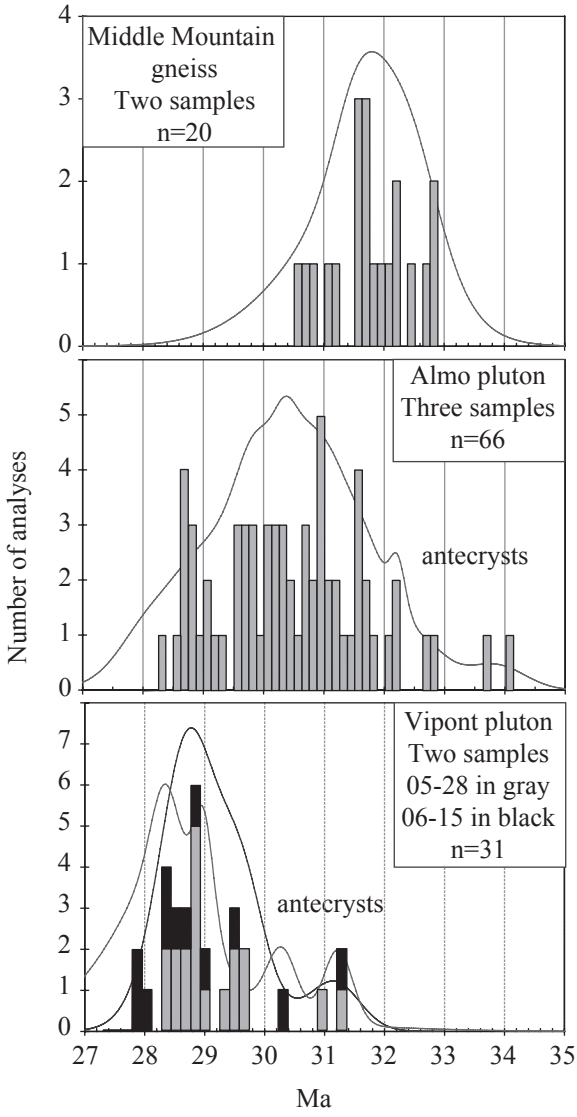

Fig. 16. Histograms and probability density curves for ^{207}Pb-corrected $^{206}Pb/^{238}U$ zircon ages from the Middle Mountain gneiss, the Almo pluton, and the Vipont pluton including analyses interpreted as antecrystic. Each pluton contains zircons with a range in ages that is interpreted as recycling within a long-lived magmatic event.

Middle Mountain gneiss, the Almo and Vipont plutons, including ages that are interpreted to be antecrystic. Each sample contains zircons with a range of ages that, to some extent, overlap each other. The 32.1 ± 0.5 Ma, biotite ± hornblende-bearing Middle Mountain gneiss is the oldest known pluton from the lower plate of the ARG metamorphic core complex, and was penetratively deformed at amphibolite facies conditions by the Middle Mountain shear zone. The Almo pluton is a two-mica granite, and largely undeformed, but demonstrably syn-tectonic with country rock and roof rock deformation. Three samples of the Almo pluton range in age from 30.6 ± 0.3 Ma

to 28.9 ± 0.3 Ma. The Vipont pluton contains a 28.9 ± 0.2 Ma granodiorite phase and a 28.2 ± 0.3 Ma (MSWD = 0.9) leucocratic, garnet-muscovite bearing granite phase, both of which have been deformed by the Middle Mountain shear zone. Country rocks to all three plutons contain sillimanite, which also occurs in the aureole of the 25.3 ± 0.5 Ma Red Butte pluton (Egger and others, 2003), indicating that peak metamorphism in the Green Creek gneiss and Neoproterozoic metasedimentary rocks occurred over a time range *ca.* 32 to 25 Ma. Zircons from all of the Oligocene plutons contain inherited cores with ages between 697 ± 7 to 2698 ± 18 Ma, and are dominantly late Archean (fig. 7).

The ages of two samples of Archean Green Creek gneiss exposed in the lower plate of the ARG metamorphic core complex are 2565 ± 16 Ma (northern Albion Mountains) and 2568 ± 8 Ma (Raft River Mountains), which are within error of the U-Pb zircon age of 2532 ± 33 Ma reported for the Green Creek gneiss in the northern Grouse Creek Mountains (Strickland and others, 2011). These ages are all consistent with a Rb-Sr whole rock isochron age of 2.51 ± 0.17 Ga from the southern Grouse Creek Mountains (Compton and others, 1977). The similarity in ages across the ARG metamorphic core complex and the evolved chemistry of the Green Creek gneiss (fig. 15) implies that the exposures of the Green Creek gneiss are windows into a late Archean, crustally-derived, granite batholith.

Deformation in the Country Rocks to the CPC

The timing and significance of peak metamorphism and deformation in the metasedimentary rocks of the ARG metamorphic core complex are still controversial, largely because of the multiple tectonic events that are preserved and there is variability in degrees of overprinting by the Oligocene events across the ARG metamorphic core complex. Armstrong (1968), Compton and others (1977) and Todd (1980) initially interpreted field relations and geochronologic data to suggest that peak metamorphism (indicated by the presence of sillimanite) was syn-plutonic and therefore middle Tertiary in age. These authors also noted that away from the Tertiary plutons, in the Raft River range and northern Albion Mountains, multiple sets of lineations were present and possibly suggested a Mesozoic history for the garnet + staurolite-bearing fabrics there. More recent studies have suggested that the sillimanite-grade metamorphism preserved in the western ARG metamorphic core complex is Cretaceous to early Tertiary based on detailed petrologic studies and Th-Pb ages of monazite inclusions in garnet from a pelitic schist that range from 37 to 72 Ma (Hoisch and others, 2002; Hoisch and others, 2008).

We favor the interpretation that the occurrence of sillimanite in the lower plate of the ARG metamorphic core complex is directly related to the intrusion of the CPC based on the observation that sillimanite is only found adjacent to the Oligocene plutons, and that the sillimanite is commonly aligned with the lineations in the Middle Mountain shear zone (figs. 2, 5, 9 and 11). Country rocks to the Oligocene plutons display sillimanite-bearing deformational fabrics that developed during ductile thinning of their cover rocks and NW/SE-directed stretching (figs. 5 and 11). The exact timing of peak metamorphism and deformation within the Middle Mountain shear zone is the subject of a companion paper (Strickland and others, 2011), which describes Oligocene monazite growth in the contact aureole of the Vipont pluton.

Source for Oligocene Plutons

The source for the Oligocene plutons of the CPC must have included a significant contribution from Archean crustal material based on the ages of inherited cores and the Sr and Nd isotopic chemistry of the plutons. The plutons of the CPC intrude the 2.56 Ga Green Creek gneiss and a suite of metasedimentary rocks that have detrital zircon populations that are similar in age to the inherited zircon cores in the plutons.

However, the Green Creek gneiss has significantly higher Rb/Sr ratios than the CPC (fig. 15), and detrital zircons older than 2.7 Ga are common in the metasediments and have not yet been identified in the inherited zircons in the plutons (Link and Johnston, 2008; Strickland and others, 2011). In the field, it is evident that metamorphic conditions in the country rocks to the CPC did not reach partial melting conditions during the intrusion, and therefore the melts that formed the CPC were generated at some depth below the level of intrusion. The oxygen isotope ratios measured on Oligocene overgrowths on zircons from all of the plutons are relatively primitive (average = 5.40 ± 0.63‰, n = 65), which is consistent with both mantle zircons (5.3 ± 0.6‰ (2SD); Valley and others, 1998) and Archean zircons worldwide (summarized in Valley and others, 2005). Significant digestion of wall rock during pluton emplacement is not likely and the $\delta^{18}O$ zircon values from sample 05-41 from the western margin of the Almo pluton are essentially identical to the $\delta^{18}O$ zircon values from sample C914F that was collected from the center of the Almo pluton (table 1). Furthermore, the zircons from the CPC consistently have primitive $\delta^{18}O$ zircon values from the three plutons studied regardless of age or chemistry (table 1) consistent with a large, long-lived magmatic system. The average $\delta^{18}O$ values for all of the inherited cores in the zircons from the CPC are higher and more variable than the Oligocene overgrowths, with an average of 5.93 ± 1.51 permil (2SD, n = 29) (fig. 8, Appendix 3). This indicates that the source rocks from which the cores were inherited can not be the only source for the melts of the CPC, and that a component with lower and less variable $\delta^{18}O$ values (for example, mantle-derived melt) is required. The distinct differences in $\delta^{18}O$ values between the cores and rims also documents that original $\delta^{18}O$ zircon values can be preserved in zircons even after melting of the host rock and being incorporated into new melts. Based on whole rock Rb/Sr ratios, the low negative εNd values, the consistently primitive $\delta^{18}O$ Oligocene zircon values, and late Archean inherited zircons found in all the plutons of the CPC, we propose that these plutons are the product of melting of the late Archean crust of TTG affinity that underlies the region (for example Wright and Wooden, 1991) caused by mantle-derived magmatism.

Although Ti concentration in zircon was analyzed in this study, recent work has shown that the uncertainties associated with Ti in zircon thermometry can be significant and difficult to constrain (for example, Fu and others, 2008; Ferriss and others, 2008; Hofmann and others, 2009). However, Ti concentrations in zircon can be used as an indicator of magmatic processes, particularly when considered with the Hf concentration of the zircon (Claiborne and others, 2006, 2010; Wooden and others, 2007; fig. 15). Zircons that grow from a fractionating melt should often show a predicted trend towards lower Ti concentrations and higher Hf concentrations through time (Claiborne and others, 2006, 2010; Wooden and Barth, 2010). The zircons from the CPC have a range of Ti and Hf concentrations within each sample (fig. 15), but only the zircons from the Middle Mountain gneiss show a fractionation trend, although more data are needed from the individual plutons. Considering the magmatic system as a whole, the Ti and Hf concentrations from three antecrystic zircons from the Almo pluton are lower in concentration than the slightly younger zircons, suggesting that the magmatic system was getting hotter and more primitive through time. Similarly, the 28.2 ± 0.3 Ma leucogranite from the Vipont pluton (sample 06-15) appears to have the highest average Ti in zircon concentration and lowest Hf concentrations, despite it's evolved garnet + muscovite chemistry. Therefore, this sample does not represent a fractionated melt of the slightly older granodiorite that it intrudes (sample 05-28), and this could instead indicate a renewed pulse of magmatism in the source area.

Thermal relaxation of geotherms and/or the collapse of gravitationally unstable, thickened crust have been suggested as the source for migmatites and syn-extentional granitic melts in metamorphic core complexes (for example, Teyssier and others, 2005; Gordon and others, 2008). Models have been proposed wherein dehydration melting of muscovite and biotite in tectonically buried sediments can produce crustally-derived melts. Patiño-Douce (1999) and Thompson (1999) both suggested that only migmatites and small volumes of peraluminous leucogranite could be produced by pure crustal melting, and that other granitoids with crustal affinity are actually the products of mixing between crustal melt and fractionating melts of mafic intrusions into the lower crust. For the plutons from the CPC, which do have a wide range in composition from granodiorite to leucogranite, magma mixing must have occurred well below the current exposure level due to the overall homogeneity of the granites (few mafic enclaves or schlieren). The abundant inherited zircon, the low negative εNd values, and the present day Rb/Sr ratios are consistent with melting of Archean crust likely of TTG affinity. However, the temperatures required to melt an Archean lower crust of TTG affinity are likely higher than the biotite dehydration melting which is commonly used in models that generate crustal melts (Patiño-Douce, 1999; Thompson, 1999; Petford and Gallagher, 2001; Annen and others, 2006). Hydration of the lower crust may have occurred during Laramide flat-slab subduction that may have facilitated melting of what might have otherwise been a relatively dry rock assemblage during the Tertiary (Humphreys and others, 2003; Dixon and others, 2004; Lee, 2005).

Previous authors have linked extension and magmatism in metamorphic core complexes to voluminous magmatism that swept from north to south in the Cordillera (for example, Armstrong and Ward, 1991; Humpreys, 1995). The ARG metamorphic core complex overlaps both spatially and temporally with two large, Eocene volcanic provinces: The widespread, mantle-derived Challis-Absoroka volcanic province north of the ARG metamorphic core complex was active from *ca.* 51 to 38 Ma. To the south and west of the ARG metamorphic core complex, extensive volcanism in the Northeast Nevada volcanic field erupted intermediate composition rocks from 42.6 to 38 Ma (Brooks and others, 1995; Palmer and MacDonald, 2002). The Challis-Absaroka province is made up of early more mafic lavas (basalt to dacite) whose eruption was followed by explosive, rhyodacite to rhyolite volcanism (Moye and others, 1988). Recent workers (for example, Dostal and others, 2003; Breitsprecher and others, 2003; Ickert and others, 2009) suggest that volcanism, extension and core complex development in the northern Cordillera may have been triggered by asthenospheric upwelling in a slab window between the Kula and Farallon subducting slabs in the Eocene. In the ARG metamorphic core complex, the 41.3 ± 0.3 to 34.3 ± 0.3 Ma granodiorite and biotite granite plutons of the Emigrant Pass plutonic complex in the southern Grouse Creek Mountains (fig. 1), are described in detail by Egger and others (2003). The Emigrant Pass plutonic complex cuts several pre-existing normal faults and is syn-extensional with respect to a map-scale recumbent fold of steeply tilted strata (Egger and others, 2003). Compton (1983) reported remnants of an early Eocene/Oligocene (36.4 ± 1.1 and 32.9 ± 1 Ma, K/Ar on biotite) crystal-rich tuff in the eastern Grouse Creek Mountains that may represent an eruptive counterpart of the Emigrant Pass plutonic complex.

To the south and west of the ARG metamorphic core complex, 42.6 to 38 Ma magmas erupted in northern Nevada (Brooks and others, 1995; Palmer and MacDonald, 2002) and at about 35 Ma in east central Nevada (Best and others, 1993). The Nevada volcanic fields have been interpreted to be the product of basaltic magma mixed with crustal melts based on geochemistry and Sr and Nd isotopic data (for example, Gans and others, 1989). In west central Utah, the Marysvale volcanic field erupted calc-alkaline, intermediate composition rocks between 34 to 22 Ma (Cunning-

ham and others, 1998), while the Indian Peak volcanic field erupted multiple sheets of dacite and rhyolite ash flows between 32 and 27 Ma (Best and others, 1989). At the same time, large plagioclase-hornblende porphyries were intruded as laccoliths in southern Utah (for example, the Henry, Abajo and La Sal Mountains). These shallow intrusions are interpreted as mantle-derived magmas that assimilated amphibolitic, Proterozoic crust based on their geochemistry and Sr and Nd isotopic data (Nelson and Davidson, 1998).

All of these volcanic fields form part of the southern younging ignimbrite flare-up across Idaho, Nevada, Utah and southern Colorado from *ca.* 40 to 25 Ma (for example, Best and others, 1989; Gans and others, 1989; Humphreys and others, 1995; du Bray, 2007). Thus, the Late Eocene and Oligocene was a major period of magmatic activity in the western U.S. that involved mantle-derived magmas, melting and mixing with a heterogeneous crust over a broad region. Many workers have ascribed the evolution of these magmatic systems to the foundering of the shallow Laramide slab beneath what was to become the Basin and Range, with concomitant upwelling of hot asthenosphere closer to the base of the crust (for example, Humphreys, 1995). As suggested by previous studies (for example Armstrong and Ward, 1991; Humphreys, 1995), we interpret the Oligocene extension, crustal melting and plutonism in the ARG metamorphic core complex to be associated with, and ultimately driven by the trends in regional, mantle-derived magmatism that greatly affected western North America in the Tertiary.

Implications for Metamorphic Core Complex Development

Tertiary magmatism preserved in the upper and lower plates of the ARG metamorphic core complex spans ~16 m.y. (41-25 Ma). The initial shallow level, granodioritic intrusions of the Emigrant Pass plutonic complex of the Grouse Creek Mountains occurs at ~41 to 34 Ma (Egger and others, 2003). An Eocene period of extension along the Middle Mountain shear zone has been suggested based on $^{40}Ar/^{39}Ar$ cooling ages (Saltzer and Hodges, 1988; Wells and others, 2000; Wells, 2001). A period of Late Cretaceous to early Tertiary extension has also been documented in the upper plate rocks of the ARG metamorphic complex (Wells and others, 1990, 1998, 2008).

Plutons exposed in the lower plate of the ARG metamorphic core complex were emplaced between 32 to 25 Ma. Over this ~7 Ma interval, magmatism occurred at least four times to produce the 32 Ma Middle Mountain gneiss, the 30 Ma Almo pluton, the 29 to 28 Ma Vipont pluton, and the 25 Ma Red Butte pluton (fig. 16). These plutons were emplaced concomitant with ductile thinning of overlying metamorphic rocks and amphibolite-facies metamorphism as well as extensional-sense motion along the Middle Mountain shear zone. Prolonged and/or episodic magmatism likely caused thermal weakening of the crust and may have facilitated continued deformation. Dipairic ascent and emplacement of the plutons is likely given their cross-cutting margins and essentially flat tops after Teyessier and Whitney (2002).

Apatite fission track ages from the western margin of the ARG metamorphic core complex indicate that cooling through ~60 to 100 °C occurred at 13.4 Ma for the Albion and Grouse Creek Mountains (weighted mean age of Egger and others, 2003). Therefore, the Oligocene emplacement of the CPC and the high-grade metamorphism and deformation recorded in the lower plate of the ARG metamorphic core complex significantly predated its exhumation by the bounding Miocene normal faults (fig. 1).

The data presented here support the proposition that the lower and middle crust beneath the Basin and Range was at sufficiently high temperatures to undergo partial melting and flow during the emplacement of the CPC. Direct evidence for large-scale mobility of the middle and lower crust beneath the Basin and Range was first described in detail by Gans (1987) who suggested that the extreme differences in supracrustal

strain across the Basin and Range together with a uniformly flat Moho (Klemperer and others, 1986) could only be explained by crustal flow and/or magmatic addition at depth. The physical processes driving such "channel flow" beneath the Basin and Range were elaborated by Block and Royden (1990) and McKenzie and others (2000). Whitney and others (2004) discuss lower crustal flow in relation to the formation of northern metamorphic core complexes and revive the diapiric gneiss dome models for these complexes, first proposed by the earliest workers in the area (Armstrong and Hills, 1967; Compton and others, 1977). The composition, chemical and isotopic characteristics and emplacement mechanism of the syn-extensional, Oligocene plutons in the ARG metamorphic core complex provide solid support for both crustal melting and flow as well as for vertical, diapiric rise of plutonic complexes and their overlying and entrained roof and wall rocks.

Beginning with Wells and others (1990) and Hodges and Walker (1992), as well as similar views by others as summarized in DeCelles (2004), it has been proposed that extensional deformation of the crust was widespread during the Sevier Orogeny both at deep and shallow levels across the Sevier hinterland, prior to the Tertiary magmatic pulse and ignimbrite flare-up (for example, Wells and others, 1990; Hodges and Walker, 1992; Wells, 1997; DeCelles, 2004). A late Cretaceous early Tertiary history of extension in the ARG metamorphic core complex has also been suggested by crosscutting relationships of the Emmigrant Pass plutonic complex, (Armstrong and Hills, 1967; Egger and others, 2003) and by $^{40}Ar/^{39}Ar$ cooling ages (Wells and others, 1990, 1998, 2008), although all of these studies have focused on the upper plate. In contrast, this paper describes events in the lower plate and outlines evidence for crustal melting and significant mobility of the crust beneath the ARG metamorphic core complex in the Oligocene (32-25 Ma), during which time a component of vertical uplift of deeper rocks occurred by ductile thinning of cover rocks and normal-sense movement along the Middle Mountain shear zone. Given the extensive new data on the timing of events in the lower plate of the ARG metamorphic core complex, we propose that ductile flow of the crust and peak metamorphism is associated with the CPC and is linked with the onset of the Oligocene ignimbrite flare-up.

CONCLUSIONS

In the ARG metamorphic core complex of southern Idaho and northern Utah, the 32 Ma Middle Mountain gneiss, the 30 Ma Almo pluton and the 29 to 28 Ma Vipont pluton were emplaced during regional extension, as was the 25 Ma Red Butte pluton described by Compton and others (1977) and Egger and others (2003). Taken together, these plutons record a long-lived period of magmatism that was synchronous with top-to-the-west extension along the amphibolite-facies, Middle Mountain shear zone, and sillimanite-grade ductile attenuation in roof and country rocks to the plutons. This is consistent with the results from Strickland and others, 2011, who documented monazite growth in the Middle Mountain shear zone in samples collected near the Vipont intrusion at ~35 to 27 Ma. Throughout the lower plate of the ARG metamorphic core complex, sillimanite has only been found in the contact aureoles of the Oligocene plutons, indicating that peak metamorphic temperatures were achieved in the Oligocene. The Middle Mountain gneiss and the Vipont granodiorite are both penetratively deformed by the Middle Mountain shear zone, whereas the Almo pluton is only deformed along its western margin. The relationships documented here among intrusion, deformation, and peak metamorphic temperatures in the country rocks suggest that thermal weakening facilitated ductile deformation.

Zircon inheritance is ubiquitous in the plutons of the CPC in the form of antecrysts (zircon recycled from an earlier phase of the magmatic system) and inheritance from the source area. Nearly every zircon contains a Precambrian inherited core that is mantled by igneous overgrowths that are Oligocene (fig. 3). Antecrys-

tic zircons are present in every sample and are typically two to four million years younger than the crystallization age of the sample (fig. 3), suggesting a long-lived magmatic system. The Oligocene zircon overgrowths have $\delta^{18}O$ values that are remarkably consistent regardless of age and chemistry that average $=5.40 \pm 0.63$ permil, ($n = 65$). The presence of abundant Archean inherited zircons in the CPC suggests a late Archean crust source for the CPC, which is consistent with the whole rock Nd and Sr isotopic compositions of the plutons. As the inherited cores typically have higher $\delta^{18}O$ zircon values than the Oligocene overgrowths, mantle-derived heat and fluids may also be a significant component to the melts. Based on age and geochemistry, the exposed Archean Green Creek gneiss is excluded as a significant source for the plutons of the CPC. Due to the large volume of granitic melt generated, the long-lived nature of the magmatic system, the presence of intermediate composition plutons, and the primitive $\delta^{18}O$ zircon values in the Oligocene zircons, we propose the heat and/or melts derived from the mantle caused melting in the Archean crust beneath the ARG metamorphic core complex. Intrusion of the CPC and peak metamorphism in the Albion–Raft River–Grouse Creek metamorphic core complex overlapped in time with and is likely related to, widespread, mantle-derived magmatism of the Eocene-Oligocene ignimbrite flare-up.

ACKNOWLEDGMENTS

The authors would like to thank Andrew Barth and Trevor Dumitru for thoughtful discussions and reviews of earlier manuscripts. Technical support for analyses using the SHRIMP-RG was graciously provided by Brad Ito. We are also grateful to Calvin Miller and an anonymous reviewer for very helpful reviews. The authors also gratefully acknowledge support for this study from the U.S. Geological Survey, and partial funding from two National Science Foundation grants awarded to Elizabeth Miller (EAR-0809226, EAR-0229854). The WiscSims lab is partially funded by grants from the National Science Foundation (EAR-0319230, EAR-0744079), and this research was also supported by a grant from the National Science Foundation awarded to John Valley (EAR-0838058).

Appendix 1

Zircon U-Th-Pb analyses were conducted on the SHRIMP-RG (reverse geometry) co-operated by U.S. Geological Survey and Stanford University in the SUMAC facility at Stanford University. Zircons, concentrated by standard heavy mineral separation processes and hand picked for final purity, were mounted on double stick tape on glass slides in 1×6 mm rows, cast in epoxy, ground and polished to a 1 micron finish on a 25 mm diameter by 4 mm thick disc. All grains were imaged with transmitted light and reflected light (and incident light if needed) on a petrographic microscope, and with cathodoluminescence on a JEOL 5600 SEM to identify internal structure, inclusions and physical defects. The mounted grains were washed with a saturated EDTA solution and thoroughly rinsed in distilled water, dried in a vacuum oven, and coated with Au. Mounts typically sat in a loading chamber at high pressure ($10P^{-7}P$ torr) for several hours before being moved into the source chamber of the SHRIMP-RG.

Secondary ions were generated from the target spot with an $OR_2RP^{-}P$ primary ion beam varying from 4 to 6 nA. The primary ion beam typically produced a spot with a diameter of 20 to 40 microns and a depth of 1 to 2 microns for an analysis time of 9 to 12 minutes. The basic acquisition routine begins with a high mass normalizing species ($P^{90}PZrR_2RP^{16}POP^{+}P$) followed by $P^{204}PPbP^{+}P$, a background measured at 0.050 mass units above $P^{204}PPbP^{+}P$, $P^{206}PPbP^{+}P$, $P^{207}PPbP^{+}P$, $P^{208}PPbP^{+}P$, $P^{238}PUP^{+}P$, $P^{232}PThP^{16}POP^{+}P$ and $P^{238}PUP^{16}POP^{+}P$ and $P^{232}PThP^{+}P$. Selected sets of trace elements are also included for each analyses and are measured briefly (typically 1 sec/mass) immediately following the geochronology peaks. For zircon, these extra masses include a limited set of REE, Y and Hf. Peak centering on both ubiquitous species and on guide peaks adjacent to low-abundance or interference-prone species is used to eliminate any potential effects of magnet drift or peak wandering. The number of scans through the mass sequence and counting times on each peak are varied according to the sample age and the U and Th concentrations to improve counting statistics and age precision. Measurements are made at mass resolutions of $M/\Delta M = \sim 8500$ (10% peak height), which eliminates all interfering molecular species, particularly for the REE. The SHRIMP-RG

was designed to provide higher mass resolution than the standard forward geometry of the SHRIMP I and II (Clement and Compston, 1994). This design also provides very clean backgrounds and combined with the high mass resolution, the EDTA washing of the mount, and rastering the primary beam for 90 to 120 seconds over the area to be analyzed before data is collected, assures that any counts found at mass of $P^{204}PPbP^{+}P$ are actually from Pb in the zircon and not surface contamination. In practice greater than 95 percent of the spots analyzed have no common Pb.

For zircon, concentration data for U, Th and all of the measured trace elements are standardized against well-characterized, homogeneous zircon standard MAD-green (4196 ppm U). Age data for zircons were standardized against R33 (419 Ma, quartz diorite of Braintree complex, Vermont; Black and others, 2004), which were analyzed repeatedly throughout the duration of the analytical session. Data reduction for geochronology follows the methods described by Williams (1997), and Ireland and Williams (2003), and use the MS Excel add-in Squid and Isoplot programs of Ludwig (2001, 2003). Data reduction for the trace element concentrations are also done in MS Excel. Average count rates of each element of interest are ratioed to the appropriate high mass normalizing species (see above) to account for any primary current drift, and the derived ratios for the unknowns are compared to an average of those for the standards to determine concentrations. Spot to spot precisions (as measured on the standards) vary according to elemental ionization efficiency and concentration. For the MAD-green zircon, precisions generally range from about ±3 percent for Hf, ±5 percent for the HREE, ±10 to 15 percent for P, Sc, Y and the MREE, and up to ±40 percent for La (all values at 2σ).

Analyses of Ti concentration in zircon were done in separate sessions from the geochronology. However, Ti analyses were preformed on the same zones from the same grains (in some cases the same spot) as the geochronology. The titanium in zircon technique has the advantage of being paired with U-Pb, Hf, and other trace element analyses of single spots on zircon grains. Analyses with high Fe concentrations (>50 ppm), were culled from the data set as they are commonly associated with elevated concentrations of Ca, Al, and F, and may contain excess Ti from a non-zircon component (Wooden and others, 2007) (Appendix 3). We used an estimate of TiO_2 activity of 0.7 and SiO_2 activity of 1, which introduces an uncertainty of likely <50 °C (see discussions by Harrison and others, 2007; Ferry and Watson, 2007; Ferriss and others, 2008; Fu and others, 2008).

Oxygen isotope analysis was performed at the University of Wisconsin WiscSims laboratory using a CAMECA ims-1280 ion microprobe following the procedures outlined in Kita and others (2009). Data were acquired over four separate sessions. A focused Cs^{+} primary beam was used for analysis at 1.9 to 2.2 nA and a corresponding spot size of 10 to 12 μm. A normal incident electron gun was used for charge compensation. Oxygen ions were detected with two separate Faraday cups, simultaneously, using a mass resolving power of ~2200. Zircon standard KIM-5 was analyzed at the beginning and end of each session, and every 10 to 15 unknowns throughout each session. Data were corrected for instrumental bias using the bracketing analysis of standards. The average values of the standard analyses that bracket each set of unknowns was used to correct for instrumental bias. The average precision of the bracketing standards for this study is ±0.27 permil (2SD). After analyses for oxygen isotopes were made, each individual ion probe spot was imaged using secondary electron microscopy to inspect the spot location with respect to core and rim domains, cracks, inclusions and overlap onto epoxy.

Appendix 2

Data U-Pb geochronology

Spot Name	% common ^{206}Pb	U (ppm)	Th (ppm)	$^{232}Th/^{238}U$	^{204}Pb corrected $^{206}Pb/^{238}U$ Age	1 sigma error	**Preferred age***	**1 sigma error**	Total $^{238}U/^{206}Pb$	% error	Total $^{207}Pb/^{206}Pb$	% error	^{204}Pb corrected $^{207}Pb/^{206}Pb$	% error	Reason to exclude
Sample 08-80 from the Middle Mountain gneiss. 32.1 ± 0.6 Ma MSWD=2.1															
08-80-22	*11.03*	*3608*	*52*	*0.01*	*25.2*	*1.2*	*27.3*	*0.8*	*226.94*	*1.4*	*.0757*	*23.8*			1
08-80-20R	0.00	4276	334	0.08	27.5	0.3	27.5	0.3	233.60	1.2	.0466	2.0	.0466	2.0	2
08-80-23	*80.19*	*493*	*241*	*0.50*	*19.7*	*10.0*	*28.4*	*6.4*	*64.86*	*2.1*	*.6094*	*8.2*			1
08-80-7R	0.00	3806	556	0.15	29.8	0.4	29.8	0.4	215.57	1.3	.0469	2.4	.0469	2.4	2
08-80-4R	0.28	5266	1331	0.26	31.5	0.4	**31.5**	**0.4**	203.65	1.2	.0482	1.9	.0460	3.1	
08-80-8R	*0.11*	*7435*	*130*	*0.02*	*31.5*	*0.4*	*31.5*	*0.4*	*203.73*	*1.2*	*.0475*	*1.6*	*.0467*	*1.9*	3
08-80-17R	0.22	3340	395	0.12	31.8	0.4	**31.8**	**0.4**	201.73	1.2	.0475	2.5	.0457	3.5	
08-80-2R	0.00	3942	862	0.23	32.5	0.4	**32.4**	**0.4**	198.14	1.2	.0468	2.2	.0468	2.2	
08-80-12.1R	0.40	1778	332	0.19	32.5	0.5	**32.7**	**0.4**	197.22	1.4	.0456	3.1	.0423	7.2	
08-80-13C	5.98	275	180	0.68	31.0	1.1	**32.8**	**0.8**	195.34	2.4	.0506	8.2			
08-80-5R	*0.00*	*6736*	*127*	*0.02*	*33.0*	*0.4*	*32.9*	*0.4*	*195.05*	*1.2*	*.0474*	*1.7*	*.0474*	*1.7*	3
08-80-10R	*0.11*	*5417*	*1013*	*0.19*	*33.6*	*0.4*	*33.6*	*0.4*	*191.06*	*1.2*	*.0474*	*1.9*	*.0465*	*2.1*	3
08-80-3R	*0.19*	*8080*	*149*	*0.02*	*33.7*	*0.4*	*33.8*	*0.4*	*190.29*	*1.2*	*.0471*	*1.5*	*.0456*	*2.2*	3
08-80-19.3	*0.46*	*5590*	*1095*	*0.20*	*34.5*	*0.4*	*34.5*	*0.4*	*185.74*	*1.1*	*.0493*	*2.1*	*.0457*	*3.6*	3
08-80-8RR	*0.39*	*7903*	*833*	*0.11*	*35.2*	*0.4*	*35.3*	*0.4*	*181.77*	*1.2*	*.0493*	*1.6*	*.0462*	*2.9*	3
08-80-21	*-0.09*	*8703*	*575*	*0.07*	*35.9*	*0.4*	*35.8*	*0.4*	*179.10*	*1.1*	*.0484*	*1.1*	*.0490*	*1.4*	3
08-80-14R	*0.11*	*8755*	*2771*	*0.33*	*36.3*	*0.4*	*36.3*	*0.4*	*176.81*	*1.1*	*.0479*	*1.3*	*.0470*	*2.0*	3
08-80-24.1R	*0.08*	*5558*	*522*	*0.10*	*36.4*	*0.4*	*36.4*	*0.4*	*176.41*	*1.1*	*.0472*	*1.2*	*.0466*	*1.4*	3
08-80-3C	0.21	39	57	1.52	1678.8	29.0	**1786.3**	**41.9**	3.35	2.0	.1110	1.9	.1092	2.3	
08-80-9R	0.00	131	94	0.74	1768.0	21.6	**2455.4**	**15.1**	3.17	1.4	.1600	0.9	.1600	0.9	
08-80-11C	0.00	299	118	0.41	1748.6	18.8	**1851.8**	**11.5**	3.21	1.2	.1132	0.6	.1132	0.6	
08-80-20C	-0.33	48	37	0.79	1856.8	27.0	**1786.8**	**34.2**	3.01	1.7	.1063	1.4	.1092	1.9	
08-80-6	0.00	277	169	0.63	1993.8	21.3	**2434.1**	**9.5**	2.76	1.2	.1580	0.6	.1580	0.6	
08-80-8C	0.00	106	112	1.09	2188.3	27.0	**2447.0**	**15.3**	2.47	1.5	.1592	0.9	.1592	0.9	
08-80-15	0.13	100	105	1.09	2186.3	27.4	**2429.3**	**16.3**	2.47	1.5	.1587	0.9	.1575	1.0	
08-80-1C	0.01	365	544	1.54	2333.8	23.9	**2553.5**	**7.9**	2.29	1.2	.1697	0.5	.1696	0.5	
08-80-16	0.03	351	196	0.58	2354.1	23.7	**2451.3**	**7.5**	2.27	1.2	.1599	0.4	.1596	0.4	
08-80-18R	0.00	280	79	0.29	2559.8	26.0	**2542.1**	**19.3**	2.05	1.2	.1684	1.2	.1684	1.2	
08-80-19IC	0.04	143	113	0.82	2760.8	29.8	**2698.1**	**8.8**	1.87	1.3	.1853	0.5	.1850	0.5	
08-80-19C	0.00	1419	376	0.27	2760.8	25.3	**2583.6**	**12.3**	1.87	1.1	.1727	0.7	.1727	0.7	
Sample GG4 from the Middle Mountain gneiss. 31.8 ± 0.4 Ma MSWD=0.9															
GG4-3.1R	1.28	352	57	0.17	28.6	0.6	28.9	0.5	219.68	1.8	.0575	5.8	.0387	27.0	2
GG4-14.1R	1.64	338	39	0.12	29.5	0.6	29.4	0.6	214.91	1.8	.0606	5.6	.0472	16.5	2
GG4-1.1	4.61	73	66	0.94	30.3	1.6	**30.4**	**1.2**	201.52	3.7	.0860	11.9	.0416	80.3	
GG4-7.1	6.27	108	69	0.66	24.2	3.3	**30.7**	**0.9**	196.43	2.7	.1001	8.8			

Appendix 2
(continued)

Spot Name	% common ^{206}Pb	U (ppm)	Th (ppm)	$^{232}Th/^{238}U$	^{204}Pb corrected $^{206}Pb/^{238}U$ Age	1 sigma error	**Preferred age***	**1 sigma error**	Total $^{238}U/^{206}Pb$	% error	Total $^{207}Pb/^{206}Pb$	% error	^{204}Pb corrected $^{207}Pb/^{206}Pb$	% error	Reason to exclude
Sample GG4 from the Middle Mountain gneiss. 31.8 ± 0.4 Ma MSWD=0.9															
GG4-17.1	1.34	91	74	0.84	29.4	1.2	**30.6**	**0.9**	207.58	2.9	.0581	10.8			
GG4-13.1	3.55	128	57	0.46	26.0	2.6	**30.8**	**0.8**	201.20	2.6	.0770	8.0			
GG4-12.1R	1.26	421	30	0.07	30.4	0.8	**31.1**	**0.6**	204.31	1.7	.0574	5.5	.0285	58.4	
GG4-8.1	13.49	129	73	0.59	32.9	2.0	**31.7**	**1.0**	175.30	2.5	.1618	8.8	.0764	62.1	
GG4-5.1	6.16	69	63	0.94	31.0	2.2	**31.6**	**1.1**	190.86	3.3	.0992	9.9			
GG4-15.1	2.04	186	50	0.28	28.5	1.8	**31.7**	**0.7**	199.01	2.2	.0640	7.3			
GG4-10.1	1.88	339	32	0.10	31.7	0.6	**31.7**	**0.6**	198.74	1.8	.0627	5.4	.0462	18.3	
GG4-16.2R	0.08	336	45	0.14	32.0	0.6	**32.0**	**0.6**	201.08	1.8	.0474	6.0	.0474	6.0	
GG4-4.1R	1.27	269	31	0.12	29.7	1.2	**32.0**	**0.6**	198.25	2.0	.0575	6.5			
GG4-9.1	0.49	1304	173	0.14	32.2	0.4	**32.2**	**0.4**	198.81	1.3	.0508	5.1	.0469	7.0	
GG4-18.1	0.82	338	7	0.02	32.1	0.6	**32.2**	**0.6**	198.10	1.8	.0536	5.9	.0443	16.1	
GG4-11.1R	1.10	357	24	0.07	32.5	0.7	**32.8**	**0.6**	194.05	1.7	.0560	5.5	.0393	23.6	
GG4-16.1C	2.63	113	70	0.64	1354.2	17.5	**1325.5**	**18.3**	4.27	1.4	.1078	1.1	.1054	1.4	
GG4-2.1	0.65	59	21	0.37	1715.1	24.9	**1705.3**	**27.6**	3.28	1.7	.1101	1.3	.1101	1.3	
GG4-11.2C	4.35	101	63	0.64	1925.2	25.9	**1856.2**	**30.6**	2.87	1.5	.1514	3.5	.1495	3.6	
GG4-6.1C	9.43	1188	533	0.46	1327.7	13.8	**1213.8**	**13.6**	4.37	1.1	.1604	0.3	.1602	0.3	
GG4-9.2C	8.69	330	104	0.33	1578.7	17.2	**1457.0**	**17.5**	3.60	1.2	.1658	0.5	.1652	0.6	
GG4-4.2C	2.52	565	92	0.17	2317.8	23.0	**2269.2**	**27.6**	2.31	1.2	.1657	0.3	.1654	0.3	
GG4-14.2C	1.41	290	243	0.86	2440.0	25.1	**2411.6**	**31.5**	2.17	1.2	.1684	0.4	.1683	0.4	
Almo pluton, sample 05-41. 30.4 ± 0.2 Ma MSWD=2.7															
05-41-19.1	*9.15*	*30*	*48*	*1.62*	*30.7*	*1.9*	*27.9*	*1.9*	*209.22*	*6.3*	*.1190*	*15.2*	*.1190*	*15.2*	1
05-41-12.1	0.70	748	181	0.25	28.9	0.5	29.1	0.4	219.53	1.4	.0522	4.7	.0406	19.7	2
05-41-1.2	*-1.87*	*99*	*81*	*0.84*	*33.7*	*2.7*	*29.3*	*1.0*	*223.38*	*3.3*	*.0318*	*23.6*	*.1824*	*34.2*	4
05-41-6.1	1.06	226	79	0.36	29.8	0.7	29.5	0.7	215.51	2.2	.0550	7.1	.0550	7.1	2
05-41-5.1	0.32	989	227	0.24	29.4	0.3	**29.5**	**0.3**	216.98	1.1	.0492	3.8	.0425	9.1	
05-41-1.1	0.06	285	68	0.25	29.1	0.7	**29.6**	**0.6**	216.92	2.1	.0471	7.1	.0322	31.3	
05-41-17.1	0.73	694	233	0.35	29.9	0.4	**29.7**	**0.4**	214.83	1.3	.0524	4.4	.0524	4.4	
05-41-9.1	-0.51	1141	450	0.41	30.0	0.3	**29.7**	**0.3**	217.45	0.9	.0426	4.3	.0561	10.3	
05-41-4.1	0.39	1043	463	0.46	29.7	0.5	**29.8**	**0.5**	215.21	1.5	.0497	3.6	.0454	6.2	
05-41-18.1	0.88	620	237	0.39	29.6	0.5	**29.8**	**0.4**	213.61	1.4	.0536	4.6	.0409	17.0	
05-41-12.1	0.24	1625	283	0.18	29.9	0.2	**29.9**	**0.2**	214.91	0.7	.0485	3.4	.0508	3.4	
05-41-11.1	0.80	273	220	0.83	30.4	0.6	**30.1**	**0.6**	211.88	2.1	.0529	7.7	.0661	7.7	
05-41-1.1	-0.07	321	248	0.80	29.7	0.6	**30.2**	**0.6**	213.40	1.8	.0461	8.6	.0486	24.5	
05-41-11.2	0.00	1545	489	0.33	30.2	0.2	**30.2**	**0.2**	213.16	0.8	.0467	3.5	.0491	3.5	
05-41-4.1	-0.28	3188	238	0.08	30.3	0.2	**30.4**	**0.2**	212.42	0.6	.0444	3.0	.0460	3.0	
05-41-14.2	0.17	1047	330	0.33	30.3	0.3	**30.5**	**0.3**	210.68	0.9	.0480	4.7	.0461	7.8	

Appendix 2
(continued)

Spot Name	% common ^{206}Pb	U (ppm)	Th (ppm)	$^{232}Th/^{238}U$	^{204}Pb corrected $^{206}Pb/^{238}U$ Age	1 sigma error	**Preferred age***	**1 sigma error**	Total $^{238}U/^{206}Pb$	% error	Total $^{207}Pb/^{206}Pb$	% error	^{204}Pb corrected $^{207}Pb/^{206}Pb$	% error	Reason to exclude
Almo pluton, sample 05-41. 30.4 ± 0.2 Ma MSWD=2.7															
05-41-16.1	0.82	600	154	0.26	30.7	0.4	**30.6**	**0.4**	208.29	1.4	.0531	4.6	.0476	9.0	
05-41-8.1	0.58	1594	269	0.17	30.6	0.3	**30.6**	**0.3**	208.71	0.9	.0512	3.1	.0454	8.1	
05-41-7.1	-0.36	1076	255	0.25	30.7	0.3	**30.8**	**0.3**	209.74	0.9	.0438	4.4	.0472	4.4	
05-41-3.1	0.31	1559	230	0.15	31.0	0.4	**30.9**	**0.4**	207.56	1.4	.0491	2.9	.0491	2.9	
05-41-8.1	0.81	821	339	0.43	30.6	0.4	**30.9**	**0.3**	206.27	1.0	.0530	4.5	.0427	19.0	
05-41-5.1	0.79	400	107	0.28	31.0	0.6	**30.9**	**0.6**	206.26	1.8	.0529	5.2	.0478	8.9	
05-41-16.2	0.40	535	281	0.54	31.1	0.4	**31.0**	**0.4**	206.71	1.2	.0498	5.4	.0561	5.4	
05-41-7.1	0.12	1115	439	0.41	31.0	0.3	**31.1**	**0.3**	206.62	1.0	.0476	3.7	.0432	6.4	
05-41-1.1	-0.11	3453	260	0.08	31.2	0.2	**31.2**	**0.2**	206.54	0.7	.0458	3.0	.0482	3.8	
05-41-5.1	-0.17	411	91	0.23	30.4	0.5	**31.2**	**0.4**	206.53	1.3	.0453	6.5	.0336	38.0	
05-41-11.2	*2.48*	*211*	*86*	*0.42*	*31.1*	*0.9*	*31.4*	*0.8*	*200.02*	*2.4*	*.0663*	*7.1*	*.0412*	*33.5*	1
05-41-2.1	0.17	2777	400	0.15	31.5	0.2	31.6	0.2	203.48	0.8	.0480	3.3	.0459	4.0	5
05-41-8.1	0.01	977	388	0.41	31.7	0.5	31.7	0.5	203.14	1.5	.0467	3.5	.0467	3.5	5
05-41-3.1	-0.18	1107	167	0.16	32.1	0.4	31.7	0.3	203.02	1.0	.0452	3.8	.0553	9.5	5
05-41-16.1	*-0.07*	*6672*	*5910*	*0.92*	*32.2*	*0.1*	*32.2*	*0.1*	*199.67*	*0.4*	*.0462*	*2.0*	*.0467*	*2.0*	3
05-41-2.1	0.13	486	126	0.27	31.9	0.6	32.7	0.6	196.30	1.8	.0477	5.1	.0276	31.8	5
05-41-14.1	0.08	1265	432	0.35	32.9	0.3	32.8	0.3	196.12	1.0	.0473	3.5	.0503	4.6	5
05-41-6.1	*0.01*	*7757*	*286*	*0.04*	*33.5*	*0.1*	*33.5*	*0.1*	*192.10*	*0.3*	*.0468*	*1.5*	*.0473*	*1.5*	3
05-41-10.1	*-0.03*	*8631*	*197*	*0.02*	*34.8*	*0.1*	*34.8*	*0.1*	*184.99*	*0.4*	*.0465*	*1.3*	*.0465*	*1.3*	3
05-41-18.2	*0.08*	*11329*	*3510*	*0.32*	*35.3*	*0.1*	*35.3*	*0.1*	*182.12*	*0.3*	*.0474*	*1.0*	*.0469*	*1.2*	3
05-41-14.1	*0.03*	*20450*	*6533*	*0.33*	*38.0*	*0.1*	*38.0*	*0.1*	*169.13*	*0.2*	*.0470*	*0.9*	*.0470*	*0.9*	3
05-41-4.1C	*10.21*	*1071*	*134*	*0.13*	*190.7*	*1.1*	**2067.8**	**24.2**	*33.15*	*0.5*	*.1309*	*0.9*	*.1278*	*1.4*	
05-41-3.2	9.67	3006	994	0.34	1222.7	2.5	**2430.9**	**4.0**	4.79	0.2	.1581	0.2	.1577	0.2	
05-41-10.1	-0.18	179	242	1.39	1228.1	6.5	**1184.8**	**27.6**	4.76	0.6	.0799	1.4	.0799	1.4	
05-41-13.1	-0.04	218	340	1.61	1247.1	8.1	**1221.6**	**23.3**	4.68	0.7	.0818	1.0	.0810	1.2	
05-41-11.1	1.60	1004	198	0.20	1533.9	4.4	**1763.4**	**6.7**	3.72	0.3	.1079	0.4	.1078	0.4	
05-41-6.1C	7.37	1614	1460	0.94	1746.1	5.7	**2494.7**	**4.6**	3.21	0.4	.1642	0.3	.1637	0.3	
05-41-6.2	0.49	760	328	0.45	1700.8	4.1	**1766.3**	**8.0**	3.31	0.3	.1081	0.4	.1081	0.4	
05-41-2.1	2.56	132	84	0.66	1893.3	17.2	**2160.0**	**50.7**	2.93	1.0	.1357	2.8	.1351	2.9	
05-41-3.1	3.83	681	79	0.12	2218.2	7.9	**2533.0**	**7.3**	2.44	0.4	.1674	0.4	.1676	0.4	
05-41-15.1	3.20	1082	5925	5.66	2278.7	14.4	**2531.7**	**7.8**	2.36	0.8	.1676	0.5	.1674	0.5	
05-41-13.1	2.28	166	374	2.33	2373.1	11.2	**2538.6**	**15.7**	2.24	0.6	.1688	0.9	.1683	0.9	
05-41-9.1	1.51	1582	661	0.43	2440.6	5.7	**2549.3**	**8.3**	2.17	0.3	.1692	0.5	.1692	0.5	
05-41-3.2	2.97	316	81	0.26	2475.9	25.9	**2676.3**	**66.8**	2.14	1.3	.1826	4.0	.1826	4.0	
05-41-12.2	1.03	493	489	1.02	2481.8	9.0	**2553.6**	**5.5**	2.13	0.4	.1697	0.3	.1696	0.3	

Appendix 2
(continued)

Spot Name	% common ^{206}Pb	U (ppm)	Th (ppm)	$\frac{^{232}Th}{^{238}U}$	^{204}Pb corrected $^{206}Pb/^{238}U$ Age	1 sigma error	**Preferred age***	**1 sigma error**	Total $^{238}U/^{206}Pb$	% error	Total $^{207}Pb/^{206}Pb$	% error	^{204}Pb corrected $^{207}Pb/^{206}Pb$	% error	Reason to exclude
Almo pluton, sample 05-41. 30.4 ± 0.2 Ma MSWD=2.7															
05-41-15.1	0.30	493	319	0.67	2523.0	6.7	**2543.1**	**12.6**	2.09	0.3	.1686	0.8	.1686	0.8	
05-41-8.2	0.95	488	107	0.23	2642.2	10.9	**2698.9**	**40.6**	1.97	0.5	.1851	2.5	.1851	2.5	
05-41-7.1	-1.08	441	256	0.60	2738.7	27.5	**2677.6**	**4.7**	1.89	1.2	.1827	0.3	.1827	0.3	
Almo pluton, sample C914F. 30.6 ± 0.3 Ma MSWD=1.1															
C914F-11.1	0.66	603	182	0.31	29.9	0.5	29.7	0.5	215.04	1.7	.0519	4.6	.0519	4.6	2
C914F-1.1	0.28	2156	1730	0.83	29.9	0.4	**30.0**	0.4	213.48	1.3	.0488	2.6	.0430	6.3	
C914F-7.1	0.29	3234	1315	0.42	30.3	0.4	**30.3**	0.4	211.86	1.2	.0490	2.2	.0465	3.5	
C914F-9.1	0.03	2215	1409	0.66	30.2	0.4	**30.3**	0.4	212.18	1.3	.0468	2.6	.0452	3.6	
C914F-8.1	0.51	952	292	0.32	30.6	0.5	**30.5**	0.5	209.98	1.5	.0507	3.8	.0507	3.8	
C914F-2.1	0.30	1769	418	0.24	30.6	0.4	**30.7**	0.4	208.72	1.4	.0490	3.5	.0434	8.4	
C914F-12.1	0.24	1311	387	0.31	30.6	0.5	**30.8**	0.4	208.40	1.4	.0485	3.3	.0431	11.6	
C914F-4.1	0.38	1488	775	0.54	31.1	0.4	**31.1**	0.4	205.98	1.4	.0496	3.0	.0463	4.8	
C914F-5.1	0.42	598	238	0.41	31.1	0.6	**31.5**	0.5	203.30	1.7	.0500	4.6	.0363	18.3	
C914F-6.2C	*0.58*	*203*	*285*	*1.45*	*30.2*	*1.1*	*31.6*	*0.8*	*202.29*	*2.5*	*.0512*	*8.3*			5
C914F-6.1	0.03	3366	1150	0.35	32.1	0.4	32.1	0.4	200.46	1.2	.0469	2.1	.0469	2.1	5
C914F-16.1	0.38	1497	815	0.56	32.3	0.4	32.2	0.4	198.90	1.4	.0497	2.9	.0497	2.9	5
C914F-17.1	0.29	2561	428	0.17	33.7	0.4	33.6	0.4	190.55	1.3	.0490	2.2	.0490	2.2	5
C914F-14.1	0.27	2880	628	0.23	33.9	0.4	34.1	0.4	188.31	1.2	.0488	2.1	.0437	5.3	5
C914F-3.1	13.07	683	289	0.44	871.8	9.6	**2565.7**	**8.8**	6.89	1.2	.1725	0.5	.1708	0.5	
C914F-10.1C	10.80	2603	189	0.07	992.5	11.5	**2437.4**	**15.3**	6.01	1.2	.1585	0.9	.1583	0.9	
C914F-18.1	8.38	715	91	0.13	1646.0	17.2	**2520.4**	**14.7**	3.44	1.2	.1667	0.9	.1663	0.9	
C914F-13.1	7.46	418	362	0.89	1821.5	19.1	**2532.9**	**7.6**	3.06	1.2	.1690	0.4	.1675	0.5	
C914F-15.1C	0.86	746	483	0.67	2469.3	23.9	**2529.4**	**4.3**	2.14	1.2	.1673	0.3	.1672	0.3	
Almo pluton, sample 08-81. 28.9 ± 0.3 Ma MSWD=1.9															
08-81-31R	7.87	106	57	0.56	25.2	1.2	26.6	0.9	235.33	3.2	.0692	10.5			2 and 1
08-81-17R	-6.04	236	450	1.97	28.7	1.1	27.1	0.6	237.29	2.3	.0458	8.8	.0980	25.3	2
08-81-1C	0.00	215	280	1.34	27.4	0.7	**27.3**	**0.8**	235.01	2.7	.0482	9.3	.0482	9.3	
08-81-18R	0.42	942	543	0.60	27.9	0.4	**28.1**	**0.4**	229.60	1.4	.0451	4.0	.0418	6.7	
08-81-25R	4.68	199	136	0.71	26.9	0.9	**28.1**	**0.7**	228.05	2.4	.0500	8.5			
08-81-15R	3.95	420	292	0.72	27.2	0.7	**28.1**	**0.5**	226.98	1.8	.0534	5.7	.0213	78.8	
08-81-23R	5.47	785	101	0.13	27.0	0.7	**28.1**	**0.5**	225.48	1.7	.0581	6.4			
08-81-4OSC	0.00	244	366	1.55	28.4	0.7	**28.3**	**0.7**	226.32	2.5	.0496	8.8	.0496	8.8	
08-81-2R	1.77	303	414	1.41	28.3	0.7	**28.6**	**0.7**	223.27	2.3	.0519	7.6	.0378	29.4	
08-81-3OSC	0.00	279	581	2.15	28.8	0.7	**28.8**	**0.7**	223.23	2.4	.0481	8.1	.0481	8.1	
08-81-28R	0.51	1063	744	0.72	28.7	0.4	**28.8**	**0.4**	223.14	1.4	.0475	3.6	.0434	6.1	
08-81-21C	3.60	214	339	1.63	27.9	0.8	**28.9**	**0.7**	222.32	2.2	.0488	7.9	.0194	80.6	

Appendix 2
(continued)

Spot Name	% common ^{206}Pb	U (ppm)	Th (ppm)	$^{232}Th/^{238}U$	^{204}Pb corrected $^{206}Pb/^{238}U$ Age	1 sigma error	**Preferred age***	**1 sigma error**	Total $^{238}U/^{206}Pb$	% error	Total $^{207}Pb/^{206}Pb$	% error	^{204}Pb corrected $^{207}Pb/^{206}Pb$	% error	Reason to exclude
Almo pluton, sample 08-81. 28.9 ± 0.3 Ma MSWD=1.9															
08-81-24R	0.00	1346	533	0.41	28.9	0.4	**28.9**	**0.4**	222.39	1.3	.0474	3.2	.0474	3.2	
08-81-10R	3.95	743	200	0.28	29.7	0.6	**29.1**	**0.5**	208.22	1.5	.0964	3.5	.0639	18.6	
08-81-29R	0.49	676	1269	1.94	28.9	0.4	**29.1**	**0.5**	221.60	1.5	.0444	9.3	.0405	12.0	
08-81-9	2.91	348	819	2.43	28.3	0.7	**29.1**	**0.6**	220.91	1.9	.0457	6.7	.0220	57.2	
08-81-32C	2.31	354	439	1.28	28.6	0.7	**29.3**	**0.6**	219.81	2.1	.0469	5.7	.0282	35.1	
08-81-12R	-0.99	758	159	0.22	29.9	0.5	**29.5**	**0.5**	217.53	1.6	.0479	4.7	.0559	8.1	
08-81-27R	11.05	119	69	0.60	27.0	1.8	**29.6**	**0.9**	212.04	2.8	.0658	9.0			
08-81-14R	0.08	1103	463	0.43	30.1	0.4	**30.0**	**0.4**	213.53	1.4	.0503	3.5	.0497	3.7	
08-81-1R	0.00	940	244	0.27	30.2	0.5	**30.1**	**0.5**	213.13	1.7	.0498	4.8	.0498	4.8	
08-81-13R	-7.21	155	187	1.25	32.3	1.5	**30.2**	**0.8**	213.53	2.5	.0444	10.2	.1072	27.4	
08-81-5OSC	1.87	181	302	1.73	30.1	0.9	**30.7**	**0.9**	209.72	2.7	.0455	11.6	.0304	37.1	
08-81-6OSC	0.89	333	118	0.37	32.1	0.7	31.6	0.7	198.56	2.1	.0667	7.5	.0595	11.6	5
08-81-11R	0.31	1289	679	0.54	31.6	0.4	31.6	0.4	202.78	1.3	.0490	3.0	.0466	5.0	5
08-81-8RDARK	0.30	5647	1253	0.23	31.8	0.4	31.9	0.4	201.70	1.2	.0470	1.6	.0446	2.7	5
08-81-19C	0.05	377	132	0.36	1048.6	11.6	**1043.6**	**17.2**	5.66	1.2	.0745	0.8	.0741	0.9	
08-81-26C	0.06	178	92	0.54	1307.3	15.3	**1327.4**	**19.2**	4.45	1.3	.0860	0.9	.0855	1.0	
08-81-20C	0.02	400	265	0.68	1410.9	14.9	**1822.2**	**9.7**	4.09	1.2	.1116	0.5	.1114	0.5	
08-81-22C	0.01	426	74	0.18	1549.3	16.3	**1755.9**	**9.5**	3.68	1.2	.1075	0.5	.1074	0.5	
08-81-7C	0.02	245	133	0.56	1559.0	17.2	**1781.6**	**12.5**	3.65	1.2	.1091	0.7	.1089	0.7	
08-81-30C	0.00	520	106	0.21	1648.9	16.8	**1783.1**	**10.0**	3.43	1.2	.1090	0.5	.1090	0.5	
08-81-16C	0.00	1056	477	0.47	2432.2	23.1	**2559.6**	**13.1**	2.18	1.1	.1702	0.8	.1702	0.8	
08-81-25C	0.00	964	195	0.21	2550.4	23.9	**2566.1**	**7.1**	2.06	1.1	.1709	0.4	.1709	0.4	
Almo pluton, sample 05-20. 28.7 ± 0.5 Ma MSWD=2.8															
05-20-8.1	*2.85*	*73*	*25*	*0.36*	*24.5*	*1.2*	*25.4*	*1.0*	*246.49*	*3.9*	*.0691*	*12.2*			2 and 1
05-20-4.2	1.74	150	148	1.03	27.7	0.8	**27.8**	**0.8**	227.41	2.8	.0603	9.1	.0438	27.5	
05-20-1.2	0.50	1768	413	0.24	27.5	0.4	**27.9**	**0.4**	229.42	1.5	.0505	2.9	.0344	14.5	
05-20-7.1R	-0.04	2116	862	0.42	27.9	0.3	**28.4**	**0.3**	226.62	0.9	.0463	3.2	.0328	14.8	
05-20-2.1R	-0.22	4150	945	0.24	28.6	0.2	**28.5**	**0.2**	226.03	0.7	.0448	2.5	.0500	6.4	
05-20-8.1R	0.13	2044	601	0.30	28.5	0.3	**29.1**	**0.3**	220.88	0.9	.0476	3.3	.0315	19.0	
05-20-6.1R	8.22	2699	1105	0.42	28.5	0.5	**29.2**	**0.2**	202.07	0.7	.1116	1.8	.0272	44.6	
05-20-9.1R	-0.10	4646	2034	0.45	31.0	0.2	31.1	0.2	206.86	0.6	.0459	2.0	.0424	4.1	5
05-20-10.1	3.31	2951	1404	0.49	31.4	0.5	31.2	0.5	199.59	1.5	.0728	6.5	.0526	14.2	5
05-20-2.1	0.14	3934	2215	0.58	31.2	0.4	31.2	0.4	205.50	1.3	.0477	1.9	.0458	2.8	5
05-20-5.1	0.24	2019	59	0.03	30.7	0.5	31.4	0.5	204.48	1.5	.0485	3.9	.0288	24.3	5

Appendix 2
(continued)

Spot Name	% common ^{206}Pb	U (ppm)	Th (ppm)	$\frac{^{232}Th}{^{238}U}$	^{204}Pb corrected $^{206}Pb/^{238}U$ Age	1 sigma error	**Preferred age***	**1 sigma error**	Total $^{238}U/^{206}Pb$	% error	Total $^{207}Pb/^{206}Pb$	% error	^{204}Pb corrected $^{207}Pb/^{206}Pb$	% error	Reason to exclude
Almo pluton, sample 05-20. 28.7 ± 0.5 Ma MSWD=2.8															
05-20-1.1	1.33	4593	2943	0.66	31.5	0.4	31.4	0.4	202.03	1.3	.0572	4.0	.0487	6.3	5
05-20-4.1R	0.33	2644	640	0.25	31.8	0.2	31.9	0.2	201.11	0.6	.0493	3.6	.0458	8.3	5
05-20-1.1R	0.63	2926	1196	0.42	32.2	0.3	32.0	0.3	199.92	0.8	.0516	4.6	.0519	4.6	5
05-20-7.1	0.69	4235	1391	0.34	32.6	0.4	32.7	0.4	195.40	1.3	.0521	1.8	.0444	4.7	5
05-20-4.1	0.08	4480	1640	0.38	33.0	0.5	33.3	0.5	193.02	1.4	.0473	2.3	.0390	7.4	5
05-20-5.1R	0.27	7769	3205	0.43	34.1	0.1	34.2	0.1	187.29	0.4	.0489	1.4	.0443	3.5	5
05-20-3.1R	1.29	4231	1959	0.48	35.6	0.2	35.7	0.3	177.94	0.5	.0569	7.2	.0463	10.7	5
05-20-9.1	0.99	1614	221	0.14	34.3	0.8	35.9	0.6	177.46	1.6	.0546	9.2			5
05-20-6.1	10.01	893	21	0.02	142.9	2.2	142.6	2.1	40.22	1.3	.1285	3.5	.0503	17.1	
05-20-3.1	2.29	290	108	0.39	946.4	11.4	**1346.5**	**22.4**	6.30	1.3	.0891	0.8	.0864	1.2	
05-20-2.3W	10.33	94	88	0.96	1390.8	14.0	**2544.7**	**21.8**	4.14	1.1	.1703	1.1	.1687	1.3	
05-20-1.2C	0.32	252	133	0.55	2003.8	11.0	**2034.9**	**11.1**	2.74	0.6	.1257	0.6	.1254	0.6	
05-20-2.2C	-0.31	1585	62	0.04	2565.6	6.5	**2544.7**	**11.2**	2.05	0.3	.1687	0.7	.1687	0.7	
Vipont pluton, granodiorite phase, sample 05-28. 28.9 ± 0.2 Ma MSWD=1.2															
05-28-9R	3.17	747	426	0.59	24.0	0.4	24.4	0.4	259.14	1.4	.0530	3.7	.0274	30.0	2
05-28-7R	0.00	351	64	0.19	26.9	0.5	26.9	0.5	238.94	1.8	.0507	5.9	.0507	5.9	2
05-28-4R	1.09	437	105	0.25	28.1	0.5	**28.4**	**0.5**	226.10	1.7	.0486	5.4	.0399	12.8	
05-28-19.1R	0.21	1048	489	0.48	28.3	0.4	**28.4**	**0.4**	225.72	1.2	.0482	4.4	.0430	7.8	
05-28-6.1R	0.33	690	144	0.22	27.9	0.5	**28.5**	**0.4**	225.21	1.5	.0492	5.2	.0312	30.2	
05-28-4.1R	2.04	392	92	0.24	27.1	1.0	**28.5**	**0.6**	221.00	2.1	.0627	6.6			
05-28-5.2R	1.27	890	341	0.40	28.9	0.4	**28.7**	**0.4**	221.40	1.3	.0567	4.5	.0523	7.4	
05-28-16.1C	0.13	1310	1124	0.89	28.3	0.4	**28.7**	**0.3**	223.91	1.1	.0476	3.9	.0351	17.1	
05-28-6R	0.18	1188	582	0.51	28.8	0.4	**28.8**	**0.4**	223.30	1.3	.0476	3.0	.0462	4.4	
05-28-9.1R	0.59	465	201	0.45	28.4	0.6	**28.9**	**0.6**	221.60	1.9	.0513	6.4	.0352	32.1	
05-28-12.1R	0.36	461	87	0.20	29.0	0.5	**28.9**	**0.5**	222.10	1.8	.0495	6.3	.0506	6.3	
05-28-3.1	0.56	1144	447	0.40	28.6	0.4	**28.9**	**0.4**	221.38	1.2	.0510	4.1	.0383	14.8	
05-28-7.1R	0.78	363	82	0.23	28.1	0.7	**28.9**	**0.6**	220.57	2.0	.0528	6.7	.0242	56.8	
05-28-13.3R	0.49	868	243	0.29	28.8	0.5	**29.1**	**0.4**	220.13	1.4	.0505	5.0	.0383	22.7	
05-28-17.1R	1.03	343	23	0.07	29.9	0.6	**29.3**	**0.6**	216.95	2.1	.0548	7.5	.0607	8.8	
05-28-10.1R	0.61	833	175	0.22	29.6	0.4	**29.5**	**0.4**	216.96	1.4	.0514	5.0	.0514	5.0	
05-28-15.1R	0.54	826	48	0.06	28.9	0.9	**29.6**	**0.4**	216.22	1.5	.0509	5.2	.0289	77.5	
05-28-8.1R	0.13	1267	233	0.19	29.0	0.4	**29.6**	**0.3**	216.78	1.1	.0477	4.0	.0297	26.0	
05-28-1.1	-0.18	1092	421	0.40	29.5	0.4	**29.7**	**0.4**	216.75	1.2	.0452	4.2	.0394	11.3	

Appendix 2
(continued)

Spot Name	% common ^{206}Pb	U (ppm)	Th (ppm)	$^{232}Th/^{238}U$	^{204}Pb corrected $^{206}Pb/^{238}U$ Age	1 sigma error	**Preferred age***	**1 sigma error**	Total $^{238}U/^{206}Pb$	% error	Total $^{207}Pb/^{206}Pb$	% error	^{204}Pb corrected $^{207}Pb/^{206}Pb$	% error	Reason to exclude
Vipont pluton, granodiorite phase, sample 05-28. 28.9 ± 0.2 Ma MSWD=1.2															
05-28-3R	3.23	462	105	0.23	30.2	0.6	31.0	0.5	206.27	1.6	.0570	4.3	.0310	36.2	5
05-28-8R	0.40	2454	126	0.05	31.1	0.4	31.2	0.4	205.63	1.2	.0494	2.1	.0463	4.1	5
05-28-13.1R	*4.04*	*624*	*137*	*0.23*	*37.7*	*0.7*	*37.1*	*0.5*	*166.47*	*1.4*	*.0788*	*4.2*	*.0606*	*14.8*	*1*
05-28-13.2C	4.90	3699	427	0.12	2077.3	3.7	**1989.8**	**4.8**	2.63	0.2	.1653	0.4	.1652	0.4	
05-28-9.2C	1.68	2257	1307	0.60	2429.5	4.6	**2395.6**	**5.8**	2.18	0.2	.1693	0.2	.1693	0.2	
05-28-7.2C	1.24	3452	174	0.05	2456.0	3.5	**2430.7**	**4.6**	2.16	0.2	.1687	0.3	.1687	0.3	
05-28-2.1	1.13	672	224	0.35	2461.3	8.2	**2438.2**	**10.5**	2.15	0.4	.1684	0.3	.1684	0.3	
05-28-01	0.00	151	96	0.65	2434.7	27.0	**2449.3**	**29.2**	2.18	1.3	.1710	0.9	.1710	0.9	
05-28-5.1C	0.98	671	343	0.53	2474.7	8.4	**2454.7**	**11.0**	2.14	0.4	.1686	0.6	.1685	0.6	
05-28-18.1C	0.84	905	112	0.13	2493.2	7.3	**2476.1**	**9.6**	2.12	0.4	.1694	0.4	.1693	0.4	
05-28-5R	0.01	960	210	0.23	2502.9	23.2	**2501.5**	**23.8**	2.11	1.1	.1686	0.3	.1685	0.3	
05-28-02	0.01	563	134	0.25	2504.4	23.7	**2504.1**	**24.4**	2.11	1.1	.1711	0.6	.1710	0.6	
05-28-2.2R	0.07	87	273	3.23	2556.2	23.8	**2558.3**	**31.5**	2.05	1.1	.1707	0.8	.1692	0.9	
05-28-11.1C	0.13	560	496	0.92	2577.7	9.8	**2575.3**	**13.2**	2.03	0.5	.1730	0.5	.1728	0.5	
05-28-14.1C	-0.24	4049	1342	0.34	2614.5	4.0	**2619.8**	**5.9**	2.00	0.2	.1743	0.4	.1742	0.4	
Vipont pluton, leucocratic phase phase, sample 06-15. 28.2 ± 0.3 Ma MSWD=0.9															
06-15-18.1	*5.79*	*240*	*99*	*0.43*	*26.6*	*0.8*	*26.2*	*0.6*	*231.69*	*2.2*	*.0923*	*6.3*	*.0573*	*30.5*	*1*
06-15-16.2	*44.68*	*27*	*37*	*1.39*	*36.3*	*6.4*	*26.3*	*2.4*	*135.21*	*5.0*	*.3999*	*8.1*	*.2587*	*43.5*	*1*
06-15-17.1	*12.18*	*74*	*75*	*1.04*	*26.7*	*2.0*	*26.9*	*1.1*	*209.92*	*3.7*	*.1429*	*9.0*			
06-15-8.1	1.22	315	444	1.46	26.9	0.6	**27.1**	**0.6**	234.10	2.0	.0562	7.3	.0399	23.4	
06-15-1.1	0.83	143	275	1.99	25.1	1.3	**27.4**	**0.8**	232.76	3.0	.0531	11.0			
06-15-21.1	4.22	200	124	0.64	27.3	0.9	**27.5**	**0.7**	224.35	2.3	.0799	7.3	.0414	46.1	
06-15-14.1	3.11	242	243	1.04	28.0	0.8	**28.1**	**0.6**	221.94	2.1	.0712	7.0	.0428	34.6	
06-15-20.1	1.47	333	187	0.58	28.7	0.5	**28.3**	**0.5**	223.72	1.8	.0582	6.4	.0582	6.4	
06-15-16.3	0.92	1733	8	0.00	28.4	0.2	**28.3**	**0.2**	224.87	0.8	.0539	2.9	.0481	5.9	
06-15-3.1	3.87	271	274	1.05	27.1	1.1	**28.5**	**0.6**	217.08	2.0	.0772	6.3			
06-15-5.1	1.84	256	328	1.33	28.3	0.7	**28.6**	**0.6**	220.50	2.1	.0611	7.4	.0371	32.3	
06-15-15.1	2.12	201	175	0.90	28.9	0.7	**28.9**	**0.7**	217.81	2.3	.0634	9.6	.0472	21.9	
06-15-4.2	0.20	3999	956	0.25	29.0	0.2	29.0	0.2	221.50	0.6	.0482	2.2	.0468	2.7	
06-15-16.1	*19.09*	*27*	*32*	*1.23*	*17.5*	*7.4*	*29.6*	*2.0*	*175.90*	*5.7*	*.1976*	*12.1*			*1*
06-15-13.1	0.79	1651	11	0.01	29.7	0.3	30.3	0.3	210.70	0.8	.0529	3.2	.0308	22.0	5
06-15-6.1	0.80	2168	40	0.02	31.3	0.2	31.2	0.2	204.31	0.8	.0530	2.9	.0495	4.5	5
06-15-10.1	*0.25*	*6185*	*45*	*0.01*	*36.1*	*0.2*	*36.2*	*0.1*	*176.95*	*0.4*	*.0487*	*1.5*	*.0447*	*3.0*	*3*
06-15-9.1	*0.22*	*6739*	*209*	*0.03*	*36.4*	*0.2*	*36.5*	*0.1*	*175.92*	*0.4*	*.0485*	*1.4*	*.0457*	*2.6*	*3*

Appendix 2
(continued)

Spot Name	% common ^{206}Pb	U (ppm)	Th (ppm)	$\frac{^{232}Th}{^{238}U}$	^{204}Pb corrected $^{206}Pb/^{238}U$ Age	1 sigma error	**Preferred age***	**1 sigma error**	Total $^{238}U/^{206}Pb$	% error	Total $^{207}Pb/^{206}Pb$	% error	^{204}Pb corrected $^{207}Pb/^{206}Pb$	% error	Reason to exclude
Vipont pluton, leucocratic phase phase, sample 06-15. 28.2 ± 0.3 Ma MSWD=0.9															
06-15-12.1	-0.04	390	259	0.69	697.2	3.2	**697.1**	**3.4**	8.76	0.5	.0624	1.1	.0627	1.2	
06-15-2.1	0.24	70	23	0.34	1138.7	11.4	**1140.6**	**12.0**	5.15	1.1	.0798	2.1	.0764	3.0	
06-15-11.1	0.73	407	103	0.26	1609.5	6.6	**1600.0**	**7.3**	3.52	0.5	.1050	0.6	.1045	0.6	
06-15-4.1	3.77	663	34	0.05	2240.2	6.3	**2168.7**	**7.6**	2.41	0.3	.1687	0.3	.1685	0.3	
06-15-19.1	0.38	229	253	1.14	2525.7	11.5	**2516.8**	**15.8**	2.09	0.6	.1693	1.0	.1696	1.0	
06-15-7.1	-0.11	125	290	2.40	2567.7	16.7	**2568.0**	**22.4**	2.05	0.8	.1701	0.7	.1707	0.7	
The Green Creek gneiss, sample 06-9 from the Albion Mountains. 2565 ± 16 Ma MSWD=5.9															
06-9-1.1R	14.39	1734	77	0.05	522.9	7.9	2342.9	26.1	11.45	1.6	.1730	0.6	.1497	1.5	
06-9-2.1C	4.53	400	264	0.68	2186.0	27.4	2550.5	9.8	2.47	1.5	.1704	0.5	.1693	0.6	
06-9-3.1C	5.89	574	318	0.57	2035.9	25.0	2552.4	7.4	2.69	1.4	.1700	0.4	.1695	0.4	
06-9-4.1R	9.43	716	219	0.32	1478.5	18.8	2512.1	15.1	3.87	1.4	.1670	0.9	.1654	0.9	
06-9-5.1R	14.35	1101	90	0.08	599.0	8.4	2428.4	36.0	10.02	1.4	.1747	1.1	.1574	2.1	
06-9-6.1R	13.91	2130	654	0.32	511.8	7.1	2285.6	53.9	11.70	1.4	.1689	2.4	.1448	3.1	
06-9-7.1C	1.76	171	131	0.79	2461.5	32.9	2581.0	12.7	2.15	1.6	.1729	0.7	.1724	0.8	
06-9-8.1	14.90	1101	34	0.03	665.6	9.9	2464.5	25.9	8.93	1.5	.1812	1.0	.1608	1.5	
06-9-9.1R	28.01	1694	15	0.01	144.1	4.8	1867.3	497.2	34.96	1.5	.2715	6.4	.1146	27.6	
The Green Creek gneiss, sample RR06-5 from the Raft River Mountains. 2568 ± 8 Ma MSWD=1.3 (weighted mean average of 7 concordant analyses shown in bold)															
RR06-5-11.1	25.17	761	41	0.06	98.4	2.9	1663.4	619.3	52.58	2.1	.2477	9.9	.1025	33.5	
RR06-5-6.1	13.76	1667	80	0.05	125.5	1.6	1162.2	283.3	45.72	0.4	.1578	3.1	.0787	14.3	
RR06-5-13.1	38.20	2689	148	0.06	129.5	5.4			30.10	3.8	.3526	11.8			
RR06-5-10.1	13.45	1319	227	0.18	142.8	1.8	1400.5	262.6	40.79	0.5	.1558	4.9	.0889	13.7	
RR06-5-9.1	22.28	2316	598	0.27	145.2	2.7	1450.7	394.1	36.24	0.9	.2261	5.1	.0914	20.7	
RR06-5-12.1	25.32	1945	90	0.05	180.8	8.1	1781.5	641.6	28.54	2.2	.2513	7.7	.1092	35.2	
RR06-5-17.1	13.35	1031	134	0.13	232.1	1.4	1524.5	89.1	25.06	0.4	.1573	1.5	.0949	4.7	
RR06-5-8.1	12.74	1035	114	0.11	401.5	1.7	2179.6	26.0	15.13	0.4	.1565	0.8	.1362	1.5	
RR06-5-3.1	12.76	897	289	0.33	684.5	7.2	2308.5	35.6	8.70	1.1	.1647	1.5	.1467	2.1	
RR06-5-5.1	12.33	671	561	0.86	868.8	2.9	2463.8	12.3	6.87	0.3	.1667	0.5	.1608	0.7	
RR06-5-4.1	11.82	665	244	0.38	1028.6	3.3	2430.0	12.0	5.69	0.3	.1684	0.4	.1575	0.7	
RR06-5-16.1	11.12	661	421	0.66	1153.8	3.8	2510.0	7.0	5.09	0.4	.1669	0.4	.1652	0.4	
RR06-5-7.1	10.43	502	402	0.83	1330.9	4.3	2523.8	8.1	4.35	0.4	.1686	0.4	.1666	0.5	
RR06-5-2.1	4.12	410	215	0.54	2241.6	7.6	2565.9	6.3	2.40	0.4	.1714	0.4	.1708	0.4	
RR06-5-20.1	0.40	186	122	0.68	2547.2	11.9	**2572.3**	**8.3**	2.06	0.6	.1717	0.5	.1715	0.5	
RR06-5-19.1	0.32	271	207	0.79	2550.1	9.7	**2567.5**	**7.0**	2.06	0.5	.1715	0.4	.1710	0.4	
RR06-5-18.1	0.23	186	175	0.97	2554.8	12.2	**2569.9**	**8.3**	2.06	0.6	.1712	0.5	.1713	0.5	
RR06-5-21.1	0.25	264	259	1.01	2564.7	10.4	**2582.3**	**7.1**	2.05	0.5	.1724	0.4	.1725	0.4	

Appendix 2

(continued)

Spot Name	% common ^{206}Pb	U (ppm)	Th (ppm)	$\frac{^{232}Th}{^{238}U}$	^{204}Pb corrected $^{206}Pb/^{238}U$ Age	1 sigma error	**Preferred age***	**1 sigma error**	Total $^{238}U/^{206}Pb$	% error	Total $^{207}Pb/^{206}Pb$	% error	^{204}Pb corrected $^{207}Pb/^{206}Pb$	% error	Reason to exclude
Vipont pluton, leucocratic phase phase, sample06-15. 28.2 ± 0.3 Ma MSWD=0.9															
RR06-5-22.1	-0.13	236	219	0.96	2571.7	10.9	**2560.8**	**7.5**	2.04	0.5	.1707	0.4	.1703	0.4	
RR06-5-15.1	-0.39	164	217	1.36	2580.8	13.6	**2555.7**	**8.0**	2.03	0.6	.1697	0.5	.1698	0.5	
RR06-5-14.1	-0.22	142	151	1.10	2583.9	14.3	**2566.8**	**9.9**	2.03	0.7	.1713	0.6	.1709	0.6	
RR06-5-1.1	5.97	167	136	0.84	3026.8	14.8	3241.4	10.6	1.67	0.6	.2596	0.7	.2591	0.7	

* Preferred age of Tertiary zircons is the ^{207}Pb-corrected, $^{206}Pb/^{238}U$ age. The preferred age for Precambrian zircons is the ^{204}Pb-corrected, $^{207}Pb/^{206}Pb$ age. All ages are shown as Ma. Bold type indicates the analyses that were used to calculate the ages of plutons discussed in the text. Analyses shown in italics were not used. The final column shows the reason to exclude a point from the age determination. 1 = high common Pb content (normally discordant), 2 = Pb loss, 3 = high U (see text for discussion), 4 = reversely discordant, 5 = antecristic zircon that was inherited from an earlier phase in the same magmatic system.

Appendix 3

Oxygen isotope ratios and trace element concentrations in zircon

Comment	U-Pb age	$\delta^{18}O$ VSMOW	2SD	1s err	Li	Na	Mg	Al^{27}	P^{31}	K^{39}	Ca^{40}	Ti^{49}	Fe^{56}	Hf	Th	U	model temp °C*
Middle Mountain gneiss, SampleGG4																	
GG4-9.1	**32.2**	**5.46**	**0.43**	**0.4**	0.1	2.8	0.8	13	180	0.5	3.1	**4.5**	2	**12681**	124	324	706
GG4-10.1r	**31.7**	**5.14**	**0.43**	**0.6**	0.2	2.7	1.0	11	51	0.5	3.2	**1.2**	4	**17950**	12	397	603
GG4-11.1r	**32.8**	**5.48**	**0.43**	**0.6**	0.2	1.3	0.2	4	53	0.4	1.4	**1.9**	3	**8416**	9	192	635
GG4-12.1	**31.1**	**5.34**	**0.43**	**0.6**	0.1	2.9	0.6	8	103	0.5	3.4	**1.5**	2	**12471**	28	292	617
GG4-13.1	**30.8**	**5.76**	**0.43**	**0.8**	0.1	1.8	0.3	6	279	0.4	1.7	**13.5**	1	**9636**	67	96	812
GG4-14.1	**29.4**	**5.39**	**0.16**	**0.6**													
GG4-15.1r	**31.7**	**5.69**	**0.16**	**0.7**													
GG4-16.2r	**32.0**	**5.58**	**0.16**	**0.6**													
GG4-17.1r	**30.6**	**5.76**	**0.16**	**0.9**													
GG4-3.1r	**28.9**	**5.30**	**0.14**	**0.5**	0.1	1.7	0.4	7	123	0.3	1.6	**2.2**	2	**14492**	64	333	649
GG4-4.1r	**32.0**	**5.50**	**0.43**	**0.6**	0.2	2.8	1.4	12	120	0.6	3.3	**2.6**	2	**14530**	41	253	661
GG4-5.1r	**31.6**	**5.20**	**0.43**	**1.1**	0.0	3.5	1.0	24	426	0.6	3.6	**8.7**	1	**9543**	44	58	766
GG4-8.1	**31.7**	**6.00**	**0.43**	**1.0**	0.0	2.8	1.0	13	284	0.6	4.1	**11.9**	2	**9339**	84	133	798
GG4-9.2c	**2509**			**9**	0.0	4.8	0.7	14	186	0.7	3.4	**17.5**	11	**8292**	88	99	840
GG4-11.2c	**2340**	**5.94**	**0.43**	**61**	0.1	3.0	0.4	9	255	0.5	2.3	**31.7**	9	**9356**	56	65	911
GG4-14.2c	**2541**	**6.08**	**0.16**	**7**	0.6	6.6	0.5	22	483	3.3	2.1	**17.0**	21	**11121**	238	316	837
GG4-16.1c	**1722**			**26**	0.2	3.7	0.5	17	128	1.4	3.9	**18.0**	11	**10355**	65	102	843
GG4-2.1c	**1802**	**6.23**	**0.14**	**24**	0.0	2.6	37.9	12	95	0.5	2.6	**14.2**	13	**7682**	15	49	817
GG4-4.2c	**2512**	**5.68**	**0.43**	**5**	1.5	14.8	1.4	44	431	3.9	3.9	**8.5**	132	**13436**	85	387	765
GG4-6.1c	**2457**			**5**	0.7	10.5	3.1	44	154	19.6	46.0	**17.6**	73	**12391**	298	1216	840
Almo pluton, sample05-41																	
05-41-5.1	**35.3**	**5.41**	**0.22**	**0.1**													
05-41-7.1	**34.8**	**5.18**	**0.22**	**0.1**													
05-41-9.1	**32.7**	**5.77**	**0.22**	**0.6**													
05-41-10.1	**31.7**			**0.3**					38.9		0.2	**2.4**	6	**16202**	183.4	822	656
05-41-5.1	**35.3**	**5.41**	**0.22**	**0.1**													
05-41-7	**31.6**	**5.66**	**0.22**	**0.2**													
05-415.1	**31.2**	**5.68**	**0.22**	**0.4**					50.2		0.8	**3.0**	5	**10975**	110.1	399	671
05-41-13.1	**31.2**	**5.87**	**0.10**	**0.2**													
05-41-14.1	**31.1**	**5.15**	**0.10**	**0.3**													
05-41-11.1	**30.9**	**5.82**	**0.10**	**0.6**					43.2		1.6	**4.1**	11	**13120**	118.6	492	699
05-41-11.2	**30.8**	**5.33**	**0.10**	**0.3**													
05-41-15.1	**30.6**	**5.26**	**0.10**	**0.3**													
05-41-16.1	**30.6**	**5.46**	**0.10**	**0.4**													
05-41-17.1	**30.2**	**5.21**	**0.10**	**0.2**													
05-41-18.2 dark rim	**30.1**	**4.80**	**0.15**	**0.6**													
05-41-18.1 light rim	**29.9**	**5.13**	**0.15**	**0.2**													
05-41- 7.1	**29.8**	**6.10**	**0.15**	**0.4**													
05-41- 9.2	**29.7**	**5.19**	**0.15**	**0.3**					42.7		12.0	**3.1**	15	**12789**	368.3	1180	676

Appendix 3
(continued)

Comment	U-Pb age	$\delta^{18}O$ VSMOW	2SD	1s err	Li	Na	Mg	Al^{27}	P^{31}	K^{39}	Ca^{40}	Ti^{49}	Fe^{56}	Hf	Th	U	model temp °C*
Almo pluton, sample05-41																	
05-41-10	**29.7**	**5.32**	**0.15**	**0.4**													
05-41-1.2	**29.3**	**6.24**	**0.28**	**1.0**													
05-41-15	**29.1**	**6.18**	**0.15**	**0.4**													
05-41- 19.1	**27.9**	**5.53**	**0.15**	**1.9**													
05-41-3.1	**2678**	**5.19**	**0.28**	**5**					46.7		0.2	**1.5**	6	**17620**	241.4	1591	618
05-41-8.1	**2699**			**41**					47.7		0.1	**2.7**	6	**10735**	398.9	970	665
05-41-8.2	**2543**	**5.51**	**0.28**	**13**													
05-41-12.1	**2554**	**5.35**	**0.28**	**6**					39.4		0.3	**4.2**	5	**11939**	187.3	414	701
05-41-12.2	**2549**	**6.05**	**0.28**	**8**													
05-41- 1.1	**2532**	**5.22**	**0.22**	**8**					50.3		0.2	**2.9**	4	**10117**	69.9	279	669
05-41- 2.1	**2160**	**5.37**	**0.22**	**51**					45.5		0.4	**2.5**	6	**13340**	140.6	528	658
05-41- 3.1	**1222**	**4.92**	**0.22**	**23**					47.5		0.6	**6.4**	22	**11356**	82.6	309	738
05-41- 2.1 core	**1185**	**9.28**	**0.22**	**28**													
Almo pluton, sample C914F																	
C914F-7.1	**34.1**	**5.08**	**0.28**	**0.4**													
C914F-8.1	**32.2**	**4.94**	**0.28**	**0.4**													
C914F-11.1	**32.1**			**0.4**	0.7	3.6	0.9	11	187	1.0	4.7	**5.9**	4	**10904**	148	397	731
C914F-9	**31.6**	**5.31**	**0.23**	**0.8**													
C914F-12	**31.5**	**5.18**	**0.23**	**0.5**	1.0	3.8	7.4	11	454	1.1	3.8	**5.9**	9	**12138**	327	1080	731
C914F-13.1c	**31.1**	**3.74**	**0.23**	**0.4**	2.6	23.7	3.5	64	127	10.1	10.5	**14.9**	85	**9203**	276	434	822
C914F-14.1 r	**30.8**	**5.34**	**0.23**	**0.4**	10.9	3.8	0.9	11	1499	1.5	3.7	**2.6**	32	**21729**	1863	8235	660
C914F-15.1 c	**30.5**	**6.15**	**0.23**	**0.5**													
C914F-16.1	**30.3**	**5.37**	**0.23**	**0.4**													
C914F-17.1	**30.3**	**5.03**	**0.23**	**0.4**	3.7	2.8	0.7	9	1192	0.8	3.1	**2.2**	16	**20160**	766	5582	647
C914F-18.1	**29.7**	**4.48**	**0.23**	**0.5**													
C914F-3.1	**2566**			**9**	4.5	32.0	2.1	76	109	21.8	12.7	**33.0**	38	**10799**	188	524	916
C914F-4.1	**2529**	**4.91**	**0.28**	**4**	3.1	1.7	0.4	7	394	0.4	1.9	**7.5**	10	**11653**	1414	1984	753
C914F-5.1	**2533**			**8**	0.8	2.9	2.0	11	221	0.9	3.6	**6.1**	5	**10423**	214	395	733
C914F-6.1r	**2520**	**4.45**	**0.28**	**15**	5.5	3.7	1.3	12	516	0.8	3.3	**5.3**	15	**14031**	1600	3466	720
C914F-6.2	**2437**	**5.45**	**0.28**	**15**													
Almo pluton, aplite dike, sample 05-20																	
05-20-1.1r	**32.0**	**5.15**	**0.19**	**0.3**					58.8		19.9	**20.1**	144	**15657**	3053.5	4617	856
05-20-2.1r	**28.5**	**5.86**	**0.19**	**0.2**					52.2		15.5	**8.2**	38	**14227**	2268.8	3871	761
05-20-4.1r	**31.9**	**5.63**	**0.19**	**0.2**					134.0		80.6	**11.8**	82	**11926**	1678.2	4217	797
05-20-5.1r	**34.2**			**0.1**					62.5		6.2	**2.7**	53	**24345**	60.1	1966	664

Appendix 3
(continued)

Comment	U-Pb age	$\delta^{18}O$ VSMOW	2SD	1s err	Li	Na	Mg	Al^{27}	P^{31}	K^{39}	Ca^{40}	Ti^{49}	Fe^{56}	Hf	Th	U	model temp °C*
Almo pluton, aplite dike, sample 05-20																	
05-20-6.1r	**29.2**			**0.2**													
05-20-1.2c	**2035**	**5.19**	**0.19**	**11**					63.9		14.4	**6.8**	166	**15884**	419.8	1699	744
05-20-2.2c	**2545**	**5.64**	**0.19**	**11**													
Vipont pluton, biotite-bearing phase, sample 05-28																	
05-28-1.1	**29.7**	**5.80**	**0.23**	**0.4**													
05-28-2.1 core	**28.4**	**6.12**	**0.23**	**0.4**	0.4	7.7	0.3	40.9	252	15.8	2.7	**12.7**	6.3	**9722**	518	464	805
05-28-2.2 rim	**28.5**	**6.27**	**0.23**	**0.4**	1.0	4.4	0.3	25.5	183	34.2	4.0	**17.1**	1.5	**11711**	301	104	837
05-28-3.1 rim	**28.5**			**0.6**	0.8	74.8	0.4	107.9	351	40.2	4.1	**4.4**	5.2	**14987**	776	1599	705
05-28-5.1core	**28.7**	**6.21**	**0.23**	**0.3**	0.5	25.6	0.7	31.3	374	1.3	4.4	**15.4**	8.3	**13455**	410	718	826
05-28-5.2 rim	**28.9**	**5.38**	**0.23**	**0.6**	1.3	8.7	6.9	93.9	202	55.8	6.9	**15.2**	35	**15658**	180	751	824
05-28-6.1r	**28.9**	**4.95**	**0.28**	**0.5**	0.4	2.7	0.3	13.5	132	0.7	1.9	**3.6**	1.4	**12896**	65	190	687
05-28-7.1r	**28.9**	**5.01**	**0.28**	**0.4**	0.3	4.7	0.5	39.4	138	1.0	4.4	**2.7**	1.6	**14158**	49	218	662
05-28-7.2 core	**28.9**	**6.19**	**0.28**	**0.6**													
05-28-8.1r	**29.1**	**5.21**	**0.28**	**0.4**	1.0	5.6	0.5	17.6	386	1.8	3.9	**10.1**	18.5	**16184**	480	1680	781
05-28-9.1 r	**29.3**	**5.58**	**0.28**	**0.6**													
05-28-9.2 c	**29.5**	**6.08**	**0.28**	**0.4**	1.5	6.3	0.6	42.1	92	8.0	3.7	**18.0**	38	**11438**	408	1627	843
05-28-10.1r	**29.6**	**5.35**	**0.28**	**0.4**													
05-28-11c	**29.6**			**0.3**	0.4	5.3	0.7	22.5	251	1.3	3.8	**15.2**	7.3	**9195**	465	413	825
05-28-12.1r	**2510**	**5.18**	**0.28**	**7**													
05-28-13c	**2550**	**6.66**	**0.28**	**4**	2.7	17.0	0.9	53.9	293	6.5	4.9	**23.2**	49	**14005**	243	2808	872
05-28-13.3r	**2544**	**6.21**	**0.28**	**4**	0.1	5.7	0.5	10.3	142	1.7	3.5	**5.4**	0.9	**12135**	79	155	722
05-28-14.1c	**2542**	**5.88**	**0.28**	**5**	2.9	9.0	1.1	60.9	262	3.2	4.5	**25.8**	68	**13219**	1249	4107	
05-28-16.1c	**2543**	**5.64**	**0.28**	**9**	0.5	4.6	0.6	9.6	1082	2.5	3.7	**5.2**	2.4	**12030**	836	1092	719
05-28-15.1 r	**2551**	**5.27**	**0.28**	**7**													
05-28-18.1c	**2550**	**6.61**	**0.19**	**15**													
05-28-17.1 r	**2585**	**5.34**	**0.19**	**8**	0.4	9.2	0.9	12.7	158	3.5	4.9	**1.4**	1.8	**13619**	26	393	616
05-28-19.1 r	**2599**	**4.90**	**0.19**	**7**	0.7	19.7	1.4	52.4	225	19.1	28.5	**37.4**	67	**13891**	142	783	932
Vipont pluton, garnet + muscovite-bearing phase, sample 06-15																	
06-15-5.1	**36.2**	**5.363**	**0.14**	**0.1**	0.1	1.9	0.4	13.4	241	0.6	2.8	**10.0**	1.4	**11550**	415	332	780
06-15-6.1	**31.2**			**0.2**	0.9	3.5	0.4	19.0	1247	1.2	3.7	**2.4**	9.2	**17681**	130	2145	653
06-15-7.1	**30.3**	**6.480**	**0.21**	**0.3**													
06-15-8.1	**29.0**	**6.274**	**0.21**	**0.2**	0.1	2.0	0.3	10.5	242	0.6	2.0	**15.5**	1.1	**9178**	372	239	826
06-15-10.1	**28.9**			**0.7**	18.9	6.0	0.7	25.8	425	2.2	5.7	**0.8**	12.2	**33557**	42	5584	639
06-15-11.1	**28.6**			**0.6**	0.2	3.2	0.6	15.7	306	1.3	2.8	**14.5**	9.6	**11436**	143	480	819
06-15-12.1	**28.5**	**5.632**	**0.21**	**0.6**													
06-15-14.1	**28.3**	**6.222**	**0.21**	**0.5**	0.1	5.5	0.4	13.2	297	1.2	2.7	**18.0**	1.5	**10630**	425	404	843
06-15-15.1	**28.1**	**6.566**	**0.21**	**0.6**	0.0	2.8	0.4	13.8	199	1.1	3.5	**9.3**	0.7	**10704**	150	154	774
06-15-16.1	**27.5**	**6.850**	**0.21**	**0.7**													
06-15-16.2	**27.4**	**6.725**	**0.21**	**0.8**	0.0	2.3	0.2	10.3	263	0.3	1.6	**13.1**	0.8	**9190**	199	90	809

Appendix 3
(continued)

Comment	**U-Pb age**	**$\delta^{18}O$ VSMOW**	**2SD**	**1s err**	Li	Na	Mg	Al^{27}	P^{31}	K^{39}	Ca^{40}	**Ti^{49}**	Fe^{56}	**Hf**	Th	U	model temp °C*
Vipont pluton, garnet + muscovite-bearing phase, sample 06-15																	
06-15-17.1	**27.1**	**6.888**	**0.21**	**0.6**	0.0	1.8	0.2	9.3	184	0.5	1.8	**10.5**	0.3	**9659**	91	78	785
06-15-18.1	**26.9**	**6.275**	**0.21**	**1.1**													
06-15-21.1	**26.2**	**7.008**	**0.21**	**0.6**													
06-15-1.1	**2565**	**5.432**	**0.14**	**12**	0.1	3.2	0.4	20.4	265	0.8	2.4	**12.4**	0.6	**9122**	168	141	802
06-15-3.1	**2543**	**5.332**	**0.14**	**5**	0.0	2.2	0.3	9.5	190	0.5	1.7	**10.4**	0.6	**10784**	198	176	784
06-15-4.1	**1706**	**5.733**	**0.14**	**12**													
06-15-4.2	**699**	**5.237**	**0.14**	**25**													
Green Creek gneiss																	
RR06-9-1.1R	**2562**	**5.94**	**0.28**	**6**													
RR06-9-2.1C	**2571**	**6.01**	**0.28**	**6**													
RR06-9-3.1C	**2575**	**5.24**	**0.28**	**7**													
RR06-9-4.1R	**2581**	**5.89**	**0.28**	**9**													
RR06-5-20.1	**2424**	**5.58**	**0.49**	**11**	0.5	3.9	0.8	20	439	1.0	3.6	**8.8**	95	**10691**	144	251	768
RR06-5-19.1	**2550**	**5.89**	**0.49**	**8**	1.7	10.2	1.4	34	320	4.6	4.4	**8.9**	181	**11134**	185	404	769
RR06-5-21.1	**2550**	**5.63**	**0.49**	**8**	1.1	10.1	0.7	33	263	3.3	3.7	**12.1**	86	**10781**	188	506	800

References

Annen, C., Blundy, J. D., and Sparks, R. S. J., 2006, The genesis of intermediate and silicic magmas in deep crustal hot zones: Journal of Petrology, v. 47, p. 505–539, doi:10.1093/petrology/egi084.

Armstrong, R. L., 1968, Mantled Gneiss Domes in the Albion Range, Southern Idaho: Geological Society of America Bulletin, v. 79, p. 1295–1314, doi:10.1130/0016-7606(1968)79[1295:MGDITA]2.0.CO;2.

——— 1982, Cordilleran metamorphic core complexes—from Arizona to southern Canada: Annual Reviews Earth Planetary Sciences, v. 10, p. 129–154, doi:10.1146/annurev.ea.10.050182.001021.

Armstrong, R. L., and Hills, F. A., 1967, Rb-Sr and K-Ar geochronologic studies of mantled gneiss domes, Albion Range, Southern Idaho, USA: Earth and Planetary Science Letters, v. 3, p. 114–124, doi:10.1016/0012-821X(67)90021-0.

Armstrong, R. L., and Ward, P., 1991, Evolving geographic patterns of Cenozoic magmatism in the North American Cordilleran: the temporal and spatial association of metamorphic core complexes: Journal of Geophysical Research, v. 96, p. 13,201–13,224, doi:10.1029/91JB00412.

Best, M. G., Christiansen, E. H., and Blank, H. R., Jr., 1989, Oligocene caldera complex and calc-alkaline rocks of the Indian Peak volcanic field, Nevada and Utah: Geological Society of America Bulletin, v. 101, n. 8, p. 1076–1090, doi:10.1130/0016-7606(1989)101⟨1076:OCCACA⟩2.3.CO;2.

Best, M. G., Scott, R. B., Rowley, P. D., Swadley, W. C., Anderson, R. E., Gromme, C. S., Harding, A. E., Deino, A. L., Christiansen, E. H., Tingey, D. G., and Sullivan, K. R., 1993, Oligocene-Miocene caldera complexes, ash-flow sheets, and tectonism in the central and southeastern Great Basin, *in* Lahren, M. M., Trexler, J. H., Jr., and Spinosa, C., editors, Crustal Evolution of the Great Basin and the Sierra Nevada: Reno, University of Nevada, Field Trip Guidebook for Cordilleran/Rocky Mountain Sections of the Geological Society of America, p. 285–312.

Black, L. P., Kamo, S. L., Allen, C. M., Davis, D. W., Aleinikoff, J. N., Valley, J. W., Mundil, R., Campbell, I. H., Korsch, R. J., Williams, I. S., and Foudoulis, C., 2004, Improved $^{206}Pb/^{238}U$ microprobe geochronology by the monitoring of a trace-element-related matrix effect: SHRIMP, ID-TIMS, ELA-ICP-MS and oxygen isotope documentation for a series of zircon standards: Chemical Geology, v. 205, n. 1–2, p. 115–140, doi:10.1016/j.chemgeo.2004.01.003.

Block, L., and Royden, L. H., 1990, Core complex geometries and regional scale flow in the lower crust: Tectonics, v. 9, n. 4, p. 557–567, doi:10.1029/TC009i004p00557.

Breitsprecher, K., Thorkelson, D. J., Groome, W. G., and Dostal, J., 2003, Geochemical confirmation of the Kula-Farallon slab window beneath the Pacific Northwest in Eocene Time: Geology, v. 31, n. 4, p. 351–354, doi:10.1130/0091-7613(2003)031⟨0351:GCOTKF⟩2.0.CO;2.

Brooks, W. E., Thorman, C. H., and Snee, L. W., 1995, The $^{40}Ar/^{39}Ar$ ages and tectonic setting of the middle Eocene northeast Nevada volcanic field: Journal of Geophysical Research, v. 100(B6), p. 10,403–10,416, doi:10.1029/94JB03389.

Christiansen, R. L., Yeats, R. S., Graham, S. A., Niem, W. A., Niem, A. R., and Snavely, P. D., 1992, Post-Laramide geology of the U.S. Cordilleran region, *in* Burchfield, C., Lipman, P. W., and Zoback, M. L., editors, The Cordilleran orogen: Conterminous U.S.: Boulder, Colorado, Geological Society of America, The Geology of North America, v. G-3, p. 261–406.

Claiborne, L. L., Miller, C. F., Walker, B. A., Wooden, J. L., Mazdab, F. K., and Bea, F., 2006, Tracking magmatic processes through Zr/Hf ratios in rocks and Hf and Ti zoning in zircons: An example from the Spirit Mountain batholith, Nevada: Mineralogical Magazine, v. 70, n. 5, p. 517–543, doi:10.1180/0026461067050348.

Claiborne, L. L., Miller, C. F., Flanagan, D. M., Clynne, M. A., and Wooden, J. L., 2010, Zircon reveals protracted magma storage and recycling beneath Mount St. Helens: Geology, v. 38, n. 11, p. 1011–1014, doi:10.1130/G31285.1.

Clement, S. W. J., and Compston, W., 1994, Ion probe parameters for very high resolution without loss of sensitivity: U.S. Geological Survey Circulation, v. 1107, p. 62.

Colgan, J. P., and Henry, C. D., 2009, Rapid middle Miocene collapse of the Mesozoic orogenic plateau in north-central Nevada: International Geology Review, v. 51, p. 920–961, doi:10.1080/00206810903056731.

Colgan, J. P., and Metcalf, J. R., 2006, Rapid Middle Miocene Unroofing of the Southern Ruby Mountains, Nevada: Geological Society of America Abstracts with Programs, v. 38, p. 417.

Compton, R. R., 1972, Geologic map of the Yost quadrangle, Box Elder County, Utah, and Cassia County, Idaho: USGS Miscellaneous Geologic Investigations, Map I-672.

——— 1975, Geologic map of the Park Valley quadrangle, Box Elder County, Utah, and Cassia County, Idaho: USGS Miscellaneous Geologic Investigations, Map I-873.

——— 1983, Displaced Miocene rocks on the west flank of the Raft River–Grouse Creek core complex, Utah, *in* Miller, D. M., Todd, V. R., and Howard, K. A., editors, Tectonic and Stratigraphic studies in the Eastern Great Basin: Geological Society of America Memoir, v. 157, p. 271–279.

Compton, R. R., Todd, V. R., Zartman, R. E., and Naeser, C. W., 1977, Oligocene and Miocene metamorphism, folding, and low-angle faulting in northwestern Utah: Geological Society of America Bulletin, v. 88, n. 9, p. 1237–1250, doi:10.1130/0016-7606(1977)88⟨1237:OAMMFA⟩2.0.CO;2.

Coney, P. J., 1980, Cordilleran metamorphic core complexes: An overview, *in* Crittenden, M. D., Coney, P. J., and Davis, G. H., editors, Cordilleran Metamorphic Core Complexes: Boulder, Colorado, Geological Society of America Memoir, v. 153, p. 7–34.

Coney, P. J., and Harms, T. A., 1984, Cordilleran metamorphic core complexes: Cenozoic extensional relics of Mesozoic compression: Geology, v. 12, n. 9, p. 550–554, doi:10.1130/0091-7613(1984)12⟨550:CMCCCE⟩2.0.CO;2.

Cunningham, C. G., Unruh, D. M., Steven, T. A., Rowley, P. D., Naeser, C. W., Mehnert, H. H., Hedge, C. E., and Ludwig, K. R., 1998a, Geochemistry of volcanic rocks in the Marysvale volcanic field, west-central Utah, *in* Friedman, J. D., and Huffman, A. C., Jr., coordinators, Laccolith complexes of southeastern

Utah—Time of emplacement and tectonic setting—Workshop Proceedings: U.S. Geological Survey Bulletin 2158, p. 223–232.
Davis, G. H., 1980, Structural characteristics of metamorphic core complexes, southern Arizona, *in* Crittenden, M. D., Jr., Coney, J., and Davis, G. H., editors, Cordilleran Metamorphic Core Complexes: Geological Society of America Memoir, v. 153, p. 35–77.
DeCelles, P. G., 2004, Late Jurassic to Eocene evolution of the Cordilleran thrust belt and foreland basin system, western USA.: American Journal of Science v. 304, p. 105–168, doi:10.2475/ajs.304.2.105.
Dixon, J. E., Dixon, T. H., Bell, D. R., and Malservisi, R., 2004, Lateral Variation in Upper Mantle Viscosity: Role of Water: Earth and Planetary Sciences Letters, v. 222, n. 2, p. 451–467, doi:10.1016/j.epsl.2004.03.022.
Dostal, J., Breitsprecher, K., Church, B. N., Thorkelson, D. J., and Hamilton, T. S., 2003, Eocene melting of Precambrian lithospheric mantle: Analcime-bearing volcanic rocks from the Challis-Kamloops Belt of south central British Columbia: Journal of Volcanology and Geothermal Research, v. 126, p. 303–326. doi:10.1016/S0377-0273(03)00153-7.
du Bray, E. A., 2007, Time, space, and composition relations among northern Nevada intrusive rocks and their metallogenic implications: Geosphere, v. 3, n. 5, p. 381–405, doi:10.1130/GES00109.1.
Egger, A. E., Dumitru, T. A., Miller, E. L., and Savage, C. F. I., 2003, Timing and nature of Tertiary plutonism and extension in the Grouse Creek Mountains, Utah: International Geological Review, v. 45, p. 497–532, doi:10.2747/0020-6814.45.6.497.
Fayon, A. K., Whitney, D. L., and Teyssier, C., 2004, Exhumation of orogenic crust: diapiric ascent versus low-angle normal faulting, *in* Whitney, D. L., Teyssier, C., and Siddoway, C. S., editors, Gneiss Domes and Orogeny: Geological Society of America Special Paper, v. 380, p. 129–139, doi:10.1130/0-8137-2380-9.129.
Ferriss, E. D. A., Essene, E. J., and Becker, U., 2008, Computational study of the effect of pressure on the Ti-in-zircon geothermometer: European Journal of Mineralogy, v. 20, n. 5, p. 745–755, doi:10.1127/0935-1221/2008/0020-1860.
Ferry, J. M., and Watson, E. B., 2007, New thermodynamic models and revised calibrations for the Ti-in-zircon and Zr-in rutile thermometers: Contributions to Mineralogy and Petrology, v. 154, n. 4, p. 429–437, doi:10.1007/s00410-007-0201-0.
Foster, D. A., Schafer, C., Fanning, C. M., and Hyndman, D. W., 2001, Relationships between crustal partial melting, plutonism, orogeny, and exhumation: Idaho-Bitterroot batholith: Tectonophysics, v. 342, p. 313–350, doi:10.1016/S0040-1951(01)00169-X.
Fu, B., Page, F. Z., Cavosie, A. J., Fournelle, J., Kita, N. T., Lackey, J.-S., Wilde, S. A., and Valley, J. W., 2008, Ti-in-zircon thermometry: Applications and limitations: Contributions to Mineralogy and Petrology, v. 156, n. 2, p. 197–215, doi:10.1007/s00410-008-0281-5.
Gans, P. B., 1987, An open-system, two-layer crustal stretching model for the Eastern Great Basin: Tectonics, v. 6, n. 1, p. 1–12, doi:10.1029/TC006i001p00001.
Gans, P. B., Mahood, G. A., and Schermer, E., 1989, Synextensional magmatism in the Basin and Range Province: A case study from the eastern Great Basin: Geological Society of America Special Paper, v. 233, 53 p.
Gordon, S. M., Whitney, D. L. Teyssier, C., Grove, M., and Dunlap, W. J., 2008, Timescales of migmatization, melt crystallization, and cooling in a Cordilleran gneiss dome: Valhalla Complex, southeastern British Columbia: Tectonics, v. 27, TC4010, 28 p., doi:10.1029/2007TC002103.
Grice, W. C., Jr., Foster, D. A., and Kalakay, T. J., 2005, Quantifying exhumation and cooling of the Eocene Anaconda metamorphic core complex, western Montana: Abstracts with Programs, Geological Society of America, v. 37, n. 7, p. 230.
Harris, C. R., Hoisch, T. D., and Wells, M. L., 2007, Construction of a composite pressure-temperature path: revealing the synorogenic burial and exhumation history of the Sevier hinterland, U.S.A: Journal of Metamorphic Geology, v. 25, p. 915–934, doi:10.1111/j.1525-1314.2007.00733.x.
Harrison, T. M., Watson, E. B., and Aikman, A. B., 2007, Temperature spectra of zircon crystallization in plutonic rocks: Geology v. 35, n. 7, p. 635–638, doi:10.1130/G23505A.1.
Hayden, L. A., and Watson, E. B., 2007, Rutile saturation in hydrous siliceous melts and its bearing on Ti-thermometry of quartz and zircon: Earth and Planetary Science Letters, v. 258, n. 3–4, p. 561–568, doi:10.1016/j.epsl.2007.04.020.
Hirth, G., and Tullis, J., 1992, Dislocation creep regimes in quartz aggregates: Journal of Structural Geology, v. 14, n. 2, p. 145–159, doi:10.1016/0191-8141(92)90053-Y.
Hodges, K. V., and Walker, J. D., 1992, Extension in the Cretaceous Sevier orogen, North American Cordillera: Geological Society of America Bulletin, v. 104, n. 5, p. 560–569, doi:10.1130/0016-7606(1992)104⟨0560:EITCSO⟩2.3.CO;2.
Hofmann, A. E., Valley, J. W., Watson, E. B., Cavosie, A. J., and Eiler, J. M., 2009, Sub-micron scale distributions of trace elements in zircon: Contributions to Mineralogy and Petrology, v. 158, n. 3, p. 317–335, doi:10.1007/s00410-009-0385-6.
Hoisch, T. D., Wells, M. L., and Hanson, L. M., 2002, Pressure-temperature paths from garnet zoning: Evidence for multiple episodes of thrust burial in the hinterland of the Sevier orogenic belt: American Mineralogist, v. 87, n. 1, p. 115–131.
Hoisch, T. D., Wells, M. L., and Grove, M., 2008, Age trends in garnet-hosted monazite inclusions from upper amphibolite facies schist in the northern Grouse Creek Mountains, Utah: Geochimica et Cosmochimica Acta, v. 72, n. 22, p. 5505–5520, doi:10.1016/j.gca.2008.08.012.
Holdaway, M. J., 1971, Stability of andalusite and the aluminosilicate phase diagram: American Joumal of Science, v. 271, p. 97–l3l, doi:10.2475/ajs.271.2.97.
Howard, K. A., 2003, Crustal structure in the Elko-Carlin region, Nevada, during Eocene gold mineraliza-

tion: Ruby-East Humboldt metamorphic core complex as a guide to the deep crust: Economic Geology, v. 98, p. 249–268, doi:10.2113/gsecongeo.98.2.249.
Humphreys, E. D., 1995, Post-Laramide removal of the Farallon slab, western United States: Geology, v. 23, n. 11, p. 987–990, doi:10.1130/0091-7613(1995)023⟨0987:PLROTF⟩2.3.CO;2.
Humphreys, E., Hessler, E., Dueker, K., Farmer, G. L., Erslev, E., and Atwater, T., 2003, How Laramide-age hydration of North American lithosphere by the Farallon slab controlled subsequent activity in the western U.S., *in* Klemperer, S. L., and Ernst, W. G., editors, The George A. Thompson volume: Boulder, Colorado, Geological Society of America, International Geology Review, v. 45, n. 7, p. 575–595, doi: 10.2747/0020-6814.45.7.575.
Ickert, R. B., Thorkelson, D. J., Marshall, D. D., and Ullrich, T. D., 2009, Eocene adakitic volcanism in southern British Columbia: Remelting of arc basalt above a slab window: Tectonophysics. v. 464, n. 1–4, p. 164–185, doi:10.1016/j.tecto.2007.10.007.
Ireland, T. R., and Williams, I. S., 2003, Considerations in zircon geochronology by SIMS, *in* Hanchar, J., and Hoskin, P., editors, Zircon: Reviews in Mineralogy and Geochemistry, v. 53, n. 1, p. 215–241, doi:10.2113/0530215.
Kita, N. T., Ushikubo, T., Fu, B., and Valley, J. W., 2009, High Precision SIMS Oxygen Isotope Analyses and the Effect of Sample Topography: Chemical Geology, v. 264, p. 43–57, doi:10.1016/j.chemgeo.2009.02.012.
Klemperer, S. L., Hauge, T. A., Hauser, E. C., Oliver, J. E., and Potter, C. J., 1986, The Moho in the northern Basin and Range Province, Nevada, along the COCORP 40°N seismic reflection transect: Geological Society of America Bulletin, v. 97, p. 603–618, doi:10.1130/0016-7606(1986)97⟨603:TMITNB⟩2.0.CO;2.
Lee, C.-T. A., 2005, Trace-element evidence for hydrous metasomatism at the base of the North American lithosphere and possible association with Laramide low angle subduction: The Journal of Geology, v. 113, n. 6, p. 673–685, doi:10.1086/449327.
Link, P. K., and Johnston, S., 2008, Proterozoic paleogeography and stratigraphy of the Snake Range, Eastern Nevada and Albion–Grouse Creek Ranges, Southern Idaho: Detrital zircon constraints and stratigraphic surprises: Geological Society of America Abstracts with Programs, v. 40, n. 6, p. 145.
Ludwig, K. R., 2001, Squid, A user's manual: Berkeley Geochronology Center Special Publication No. 2.
——— 2003, Isoplot 3.00, a geochronological toolkit for Excel: Berkeley Geochronoogy Center Special Publication No. 4.
McGrew, A. J., Peters, M. T., and Wright, J. E., 2000, Thermbarometric constraints on the tectonothermal evolution of the East Humboldt Range metamorphic core complex, Nevada: GSA Bulletin, v. 112, n. 1, p. 45–60, doi:10.1130/0016-7606(2000)112⟨45:TCOTTE⟩2.0.CO;2.
McKenzie, D., Nimmo, F., Jackson, J. A., Gans, P. B., and Miller, E. L., 2000, Characteristics and consequences of flow in the lower crust: Journal of Geophysical Research, v. 105, n. B5, p. 11029–11046, doi:10.1029/1999JB900446.
Miller, D. M., 1980, Structural geology of the northern Albion Mountains, south-central Idaho, *in* Crittenden, M. D., Jr., Coney, P. J., and Davis, G. H., editors, Cordilleran metamorphic core complexes: Geological Society of America Memoir, v. 153, p. 399–423.
——— 1983, Strain on a Gneiss Dome in the Albion Mountains Metamorphic Core Complex, Idaho: American Journal of Science, v. 283, p. 605–632, doi:10.2475/ajs.283.6.605.
Miller, D. M., and Bedford, D. R., 1999, Pluton intrusion styles, roof subsidence and stoping, and timing of extensional shear zones in the City of Rocks National Reserve, Albion Mountains, southern Idaho: Utah Geological Association Publication 27, p. 11–25.
Miller, D. M., Armstrong, R. L., Bedford, D. R., and Davis, M., 2008, Geologic map and digital data base of the Almo Quadrangle and City of Rocks National Reserve, Cassia County, Idaho: U.S. Department of the Interior, U.S. Geological Survey; in cooperation with the National Park Service and the Idaho Department of Parks and Recreation U.S. Geological Survey open-file report, 2008-1103.
Miller, E. L., and Gans, P. B., 1989, Cretaceous crustal structure and metamorphism in the hinterland of the Sevier thrust belt, western U.S. Cordillera: Geology, v. 17, n. 1, p. 59–62, doi:10.1130/0091-7613(1989)017⟨0059:CCSAMI⟩2.3.CO;2.
Miller, E. L., Dumitru, T. A., Brown, R. W., and Gans, P. B., 1999, Rapid Miocene slip on the Snake Range–Deep Creek Range fault system, east-central Nevada: Geological Society of America Bulletin, v. 111, n. 6, p. 886–905, doi:10.1130/0016-7606(1999)111⟨0886:RMSOTS⟩2.3.CO;2.
Miller, J. S., Matzel, J. E. P., Miller, C. F., Burgess, S. D., and Miller, R. B., 2007, Zircon and recycling during the assembly of large, composite arc plutons: Journal of Volcanology and Geothermal Research, v. 167, Issue 1–4, p. 282–299, doi:10.1016/j.jvolgeores.2007.04.019.
Moye, F. J., Hackett, W. R., Blakey, J. D., and Snider, L. G., 1988, Regional geologic setting and volcanic stratigraphy of the Challis volcanic field, central Idaho, *in* Link, P. K., and Hackett, W. R., editors, Guidebook to the Geology of Central and Southern Idaho: Idaho Geological Survey Bulletin 27, p. 87–97.
Mueller, P. A., Wooden, J. L., Henry, D. J., and Bowes, D. R., 1985, Archean crustal evolution of the eastern Beartooth Mountains, Montana-Wyoming, *in* Czamanske, G. K., and Zientek, M. L., editors, The Stillwater Complex: Montana Bureau of Mines and Geology Special Publication, v. 92, p. 9–20.
Nelson, S. T., and Davidson, J. P., 1998, The petrogenesis of the Colorado Plateau laccoliths and their relationship to regional magmatism, *in* Friedman, J. D., and Huffman, A. C., Jr., coordinators, Laccolith complexes of southeastern Utah: Time of emplacement and tectonic setting-workshop proceedings: U.S. Geological Survey Bulletin 2158, p. 85100.
Palmer, H. C., and MacDonald, W. D., 2002, The Northeast Nevada Volcanic Field: Magnetic properties and source implications: Journal of Geophysical Research, v. 107, B11, 2298, 19 p., doi:10.1029/2001JB000690.
Passchier, C. W., and Trouw, R. A. J., 1998, Microtectonics: Berlin, Germany, Springer, 289 p.
Patiño-Douce, A. E., 1999, What do experiments tell us about the relative contributions of crust and mantle

to the origin of granitic magmas?, *in* Castro, A., Fernandez, C., and Vigneresse, J. L., editors, Understanding granites: Integrating new and classical techniques: Geological Society Special Publication, v. 168, p. 55–75, doi:10.1144/GSL.SP.1999.168.01.05.

Petford, N., and Gallagher, K., 2001, Partial melting of mafic (amphibolitic) lower crust by periodic influx of basaltic magma: Earth and Planetary Science Letters, v. 193, p. 483–499, doi:10.1016/S0012-821X(01)00481-2.

Reynolds, S. J., and DeWitt, E., 1991, Proterozoic geology of the Phoenix region, central Arizona, *in* Karlstrom, K. E., editor, Proterozoic Geology and Ore Deposits of Arizona: Arizona Geological Society Digest 19, p. 237–250.

Saltzer, S. D., and Hodges, K. V., 1988, The Middle Mountain shear zone, southern Idaho: Kinematic analysis of an early Tertiary high-temperature detachment: Geological Society of America Bulletin, v. 100, n. 1, p. 96–103, doi:10.1130/0016-7606(1988)100⟨0096:TMMSZS⟩2.3.CO;2.

Spear, F. S., and Cheney, J. T., 1989, A petrogenetic grid for pelitic schists in the system SiO_2-Al_2O_3-FeO-MgO-K_2O-H_2O: Contributions to Mineralogy and Petrology, v. 101, n. 2, p. 149–164, doi:10.1007/BF00375302.

Strickland, A., Miller, E. L., and Wooden, J. W., 2007, Timing of ductile deformation in the Albion–Raft River–Grouse Creek (ARG) metamorphic core complex: Preliminary U-Pb SHRIMP results: Geological Society of America Abstracts with Programs, Cordilleran Section, v. 39, n. 4, p. 5.

——— 2011, The Timing of Tertiary Metamorphism and Deformation in the Albion–Raft River–Grouse Creek Metamorphic Core Complex, Utah and Idaho: The Journal of Geology, v. 119, n. 2, p. 185–206, doi:10.1086/658294.

Sullivan, W. A., and Snoke, A. W., 2007, Comparative anatomy of core-complex development in the northeastern Great Basin, U.S.A.: Rocky Mountain Geology, Spring, v. 42, n. 1, p. 1–29, doi:10.2113/gsrocky.42.1.1.

Teyssier, C., and Whitney, D. L., 2002, Gneiss domes and orogeny: Geology, v. 30, n. 12, p. 1139–1142, doi:10.1130/0091-7613(2002)030⟨1139:GDAO⟩2.0.CO;2.

Teyssier, C., Ferré, E. C., Whitney, D. L., Norlander, B., Vanderhaeghe, O., and Parkinson, D., 2005, Flow of partially molten crust and the origin of detachments during collapse of the Cordilleran Orogen: Geological Society, London, Special Publications, v. 245, p. 39–64, doi:10.1144/GSL.SP.2005.245.01.03.

Thompson, A. B., 1999, Some time-space relationships for crustal melting and granitic intrusion at various depths, *in* Castro, A., Fernández, C., and Vigneresse, J. L., editors, Understanding granites: Integrating new and classical techniques: Geological Society, London, Special Publications, v. 168, p. 7–25, doi: 10.1144/GSL.SP.1999.168.01.02.

Thompson, A. B., and Connolly, J. A., 1995, Melting of the continental crust: Some thermal and petrological constraints on anatexis in continental collision zones and other tectonic settings: Journal of Geophysical Research, v. 100, B8, p. 15565–15579, doi:10.1029/95JB00191.

Todd, V. R., 1980, Structure and petrology of a Tertiary gneiss complex in northwestern Utah: Geological Society of America Memoir, v. 153, p. 349–383.

Valley, J. W., 2003, Oxygen isotopes in zircon, *in* Hanchar, J. M., and Hoskin, P. W. O., editors, Zircon: Reviews in Mineralogy and Geochemistry, v. 53, p. 343–385, doi:10.2113/0530343.

Valley, J. W., and Kita, N. T., 2009, In situ Oxygen Isotope Geochemistry by Ion Microprobe, *in* Fayek, M., editor, MAC Short Course Toronto, May 2009: Secondary Ion Mass Spectrometry in the Earth Sciences, v. 41, p. 19–63.

Valley, J. W., Lackey, J. S., Cavosie, A. J., Clechenko, C. C., Spicuzza, M. J., Basei, M. A. S., Bindeman, I. N., Ferreira, V. P., Sial A. N., King, E. M., Peck, W. H., Sinha, A. K., and Wei, C. S., 2005, 4.4 billion years of crustal maturation: Oxygen isotope ratios of magmatic zircon: Contributions to Mineralogy and Petrology, v. 150, n. 6, p. 561–580, doi:10.1007/s00410-005-0025-8.

Valley, J. W., Graham, C. M., Harte, B., Kinny, P., and Eiler, J. M., 1998, Ion microprobe analysis of oxygen, carbon, and hydrogen isotope ratios, *in* McKibben, M. A., editors, Society of Economic Geology Reviews in Economic Geology, v. 7, p. 73–98.

Vanderhaeghe, O., Teyssier C., McDougall, I., and Dunlap, W. J., 2003, Cooling and exhumation of the Shuswap metamorphic core complex constrained by $^{40}Ar/^{39}Ar$ thermochronology: Geological Society of America Bulletin, v. 115, n. 2, p. 200–216, doi:10.1130/0016-7606(2003)115⟨0200:CAEOTS⟩2.0.CO;2.

Wagner, F. A., III, and Johnson, R. A., 2006, Coupled basin evolution and late-stage metamorphic core complex exhumation in the southern Basin and Range Province, southeastern Arizona: Tectonophysics, v. 420, n. 1–12, p. 141–160, doi:10.1016/j.tecto.2006.01.012.

Wells, M. L., 1997, Alternating contraction and extension in the hinterlands of orogenic belts: An example from the Raft River Mountains, Utah: Geological Society of America Bulletin, v. 109, n. 1, p. 107–126, doi:10.1130/0016-7606(1997)109⟨0107:ACAEIT⟩2.3.CO;2.

——— 2001, Rheological control on the initial geometry of the Raft River detachment fault and shear zone, western United States: Tectonics, v. 20, n. 4, p. 435–457, doi:10.1029/2000TC001202.

Wells, M. L., and Hoisch, T. D., 2008, The role of mantle delamination in widespread Late Cretaceous extension and magmatism in the Cordilleran orogen, western United States: Geological Society of America Bulletin, v. 120, n. 5–6, p. 515–530, doi:10.1130/B26006.1.

Wells, M. L., Dallmeyer, R. D., and Allmendinger, R. W., 1990, Late Cretaceous extension in the hinterland of the Sevier thrust belt, northwestern Utah and southern Idaho: Geology, v. 18, n. 10, p. 929–933, doi:10.1130/0091-7613(1990)018⟨0929:LCEITH⟩2.3.CO;2.

Wells, M. L., Hoisch, T. D., Hanson, L. M., Struthers, J., and Wolff, E. D., 1997, Large magnitude crustal thickening and repeated extensional exhumation in the Raft River, Grouse Creek, and Albion Mountains: Brigham Young University Geological Studies, v. 42, pt. 1, p. 325–340.

Wells, M. L., Hoisch, T. D., Peters, M. T., Miller, D. M., Wolff, E. D., and Hanson, L. M., 1998,The Mahogany

Peaks Fault, a Late Cretaceous-Paleocene normal fault in the hinterland of the Sevier Orogen: The Journal of Geology, v. 106, n. 5, p. 623–634, doi:10.1086/516046.
Wells, M. L., Snee, L. W., and Blythe, A. E., 2000, Dating of major normal fault systems using thermochronology: An example from the Raft River detachment, Basin and Range, western United States: Journal of Geophysical Research, v. 105, n. B7, p. 16303–16327.
Wells, M. L., Spell, T. L., Hoisch, T. D., Arriola, T., and Zanetti, K. A., 2008, Laser-probe $^{40}Ar/^{39}Ar$ dating of strain fringes: Mid-Cretaceous synconvergent orogen-parallel extension in the hinterland of the Sevier orogen: Tectonics, v. 27, TC3012, 20 p., doi:10.1029/2007TC002153.
Whitney, D. L., Teyssier, C., and Vanderhaeghe, O., 2004, Gneiss domes and crustal flow, *in* Whitney, D. L., Teyssier, C., and Siddoway, C. S., editors, Gneiss Domes in Orogeny: Geological Society of America Special Papers, v. 380, p. 15–33, doi:10.1130/0-8137-2380-9.15.
Williams, I. S., 1997, U-Th-Pb geochronology by ion microprobe: not just ages but histories: Society of Economic Geologists Reviews in Economic Geology, v. 7, p. 1–35.
Wooden, J. L., and Barth, A. P., 2010, Geochemistry of minor phases and implications for thermometry and melt evolution in calc-alkalic rocks: Geological Society of America Abstracts with Programs, v. 42, n. 5, p. 626.
Wooden, J. L., and Mueller, P. A., 1988, Pb, Sr, and Nd isotopic compositions of a suite of Late Archean, igneous rocks, eastern Beartooth Mountains: Implications for crust-mantle evolution: Earth and Planetary Science Letters, v. 87, n. 1–2, p. 59–72, doi:10.1016/0012-821X(88)90064-7.
Wooden, J. L., Mazdab, F. K., and Barth, A. P., 2007, Hafnium and temperature (from titanium) variations in zircons: a potential new tool to evaluate petrologic processes in magmas: Geological Society of America, Abstracts with Programs, v. 39, n. 6, p. 406.
Wright, J. E., and Wooden, J. L., 1991, New Sr, Nd, and Pb isotopic data from plutons in the northern Great Basin: Implications for crustal structure and granite petrogenesis in the hinterland of the Sevier thrust belt: Geology, v. 19, n. 5, p. 457–460, doi:10.1130/0091-7613(1991)019⟨0457:NSNAPI⟩2.3.CO;2.